# Gas Turbines for Heat Generation:
## Conceptual Comparison & Design for Stack Loss Reduction

J.W.Tiemensma

Technische Universiteit Delft

TU Delft Delft University of Technology

INNECS innovative energy conversion systems

Challenge the future

# Gas Turbines for Heat Generation:

## Conceptual Comparison & Design for Stack Loss Reduction

by

**J.W.Tiemensma**

in partial fulfillment of the requirements for the degree of

**Master of Science**
in Mechanical Engineering

at the Delft University of Technology,
to be defended publicly on Friday January 11, 2019 at 01:00 PM.



| | | |
|---|---|---|
| Student number: | 4145321 | |
| Project duration: | February 26, 2018 – January 11, 2019 | |
| Supervisor: | Prof. dr. ir. S.A. Klein | |
| Thesis committee: | Prof. dr. ir. B.J. Boersma, | TU Delft |
| | Dr. ir. C.A. Infante Ferreira, | TU Delft |
| | Dr. ir. H.G. Schimmel, | Innecs Power Systems B.V. |

# Preface

This thesis is written in order to fulfill the Masters degree in Mechanical Engineering with a specialization in Energy & Process Technology at the Delft University of Technology. The subject was provided by Innecs Power Systems B.V., located in Ter Aar, the Netherlands. At this location, I conducted the research in the form of an internship from February to November 2018.

In this report, I investigated methods to improve the performance of a cogeneration gas turbine for the production of steam, relative to a classic burner. I selected concepts which were capable of doing so. Based on a thermodynamic and economic analysis, supplementary firing turned out to be the best to do so. Although this is not a new concept, coming up with a design proposal was not easy. But, I think I was able to give it my own twist.

I want to thank everyone at Innecs for the pleasant working environment they provided for the duration of my internship, and for allowing me to work on other side projects. I want to thank Pieter van der Meer and Gijs Schimmel especially, for their supervision, support and for sharing their knowledge on the subject. Furthermore, I would like to thank my supervisor from the TU Delft, Sikke Klein, for his advice and supervision during this project.

Finally, gratitude goes out towards my parents as well. They have been very patient, considerate and helpful during the process of writing my thesis and all my years as a student.

*J.W.Tiemensma*
*Delft, December 2018*

# Abstract


Firing industrial installations, like boilers, with a cogeneration gas turbine instead of a classic burner have several beneficial aspects. A cogeneration system allows for a more efficient utilization of energy and lowered emissions. What makes such a system especially interesting is that the revenue of the generated electrical power can outweigh the extra costs required to operate a gas turbine for producing a specific amount of thermal energy. The technical challenge, covered in this thesis, consists of improving a gas turbine for cogeneration applications relative to a classic burner. The solution can be found in reduction of the high stack losses, as these comprise the main disadvantage of firing a boiler with a gas turbine. Reduction of the stack losses allows the thermal capacity and efficiency of the cogeneration gas turbine to increase. This report focuses specifically on cogeneration with the PowerBurner, a gas turbine developed and manufactured by Innecs Power Systems, located in Ter Aar, the Netherlands.

The goal of this study was to identify, analyze and conceptualize methods that reduce the stack losses of a PowerBurner used for the production of steam. Implementation of such methods should allow the PowerBurner to become a more attractive alternative for steam production compared to employing a conventional burner. The final objective was to develop a conceptual design of the best performing method. From an analysis of available literature, four concepts were selected which could improve operation of a cogeneration gas turbine: Steam injection does not specifically reduce stack losses, but could allow for more revenue by increasing the electrical output. Flue gas recirculation reduces the stack losses by recirculating the flue gases back into the system. Finally, through supplementary firing or implementation of a boiler in the combustion chamber, the Velox boiler, stack losses can be reduced by the combustion of more fuel.

A thermodynamic model of a gas turbine was created in Thermoflex. The model was based on the design point specification of the PowerBurner, from which it deviates less than 1% at any point in the process. In the thermodynamic model, each of the four concepts was implemented in order to determine the thermal- and electrical efficiency at varying thermal outputs, as well as the thermal capacity. Implementation of steam injection was able to induce the largest increase the electrical efficiency, from 10.5% to 20%, whereas flue gas recirculation resulted in the highest increase in total efficiency, from 85% to 95%. Through application of supplementary firing and the Velox-type boiler, the thermal capacity and -efficiency could be increased the most, from 2 MW to 6.8 MW and from 74% to 90%, respectively.

With the outputs of the thermodynamic models the profitability of each setup, compared to making use of a conventional burner for an equal thermal output, was determined. From this analysis followed that the supplementary-fired system allows for the largest range of thermal outputs in which it is more profitable than a conventional burner. A qualitative cost analysis showed that supplementary-fired setup required the least capital expenditures. From a combination of the thermodynamic and economic characteristics, the supplementary-fired PowerBurner turned out to be the best alternative for replacing a conventional burner for the production of steam.

With the selection of supplementary firing as the best performing concept, a conceptual design of a burner for such an application was created in ANSYS Fluent. This design should aid in the future development of a supplementary-fired PowerBurner. The design was able to operate over a range of fuel inputs of at least 0.485 MW up to 4.85 MW. 100% Combustion efficiency was achieved over the full range. From the CFD analysis followed that the pressure losses over the burner are low at 1.6 mbar. Whether the current burner design results in a stable flame cannot be determined from the model. A $NO_x$ analysis in Fluent indicated that the emissions of oxides of nitrogen might be slightly over the Dutch regulation standards for gas turbines, but the accuracy of this result is not known. Therefore, future research is required to determine flame stability and pollutant emissions.

# Nomenclature and list of abbreviations

## Symbols

| | | |
|---|---|---|
| A | Surface area | [$m^2$] |
| Cp | Specific heat | [kJ/kgK] |
| d | Diameter | [m] |
| E | Price | [€/kWh] |
| h | Heat transfer coefficient | [$W/m^2K$] |
| j | Heat transfer factor | [-] |
| k | Thermal conductivity | [W/mK] |
| L | Length | [m] |
| $\dot{m}$ | Mass flow | [kg/s] |
| $\dot{M}$ | Molar flow | [mol/s] |
| N | Amount | [-] |
| Nu | Nusselt number | [-] |
| P | Production rate | [kWh] |
| p | Pressure | [Pa] |
| Pr | Prandtl number | [-] |
| PR | Price ratio | [-] |
| Prof | Profitability | [€/hr] |
| PRR | Pressure ratio | [-] |
| Q | Heat | [W] |
| Re | Reynolds number | [-] |
| T | Temperature | [K] |
| u | Overall heat transfer coefficient | [$W/m^2K$] |
| U | Internal Energy | [W] |
| V | Velocity | [m/s] |
| W | Work | [W] |
| Y | Years of operations | [years] |

## Greek symbols

| | | |
|---|---|---|
| $\eta$ | Efficiency | [-] |
| $\kappa$ | Ratio of specific heats | [-] |
| $\phi$ | Equivalence ratio | [-] |
| $\rho$ | Density | [$kg/m^3$] |
| $\sigma$ | Stefan-Boltzmann constant | [$W/m^2K^4$] |

## Subscripts

| | |
|---|---|
| 02 | Compressor inlet conditions |
| 03 | Compressor outlet conditions |
| 04 | Turbine inlet conditions |
| 05 | Turbine outlet conditions |
| 51 | Conditions at secondary burner inlet |
| a | Ambient Conditions (T = 288 K, P = 1.01325 Pa) |
| c | Compressor |
| cold | Cold side conditions |
| con | Concept |
| conv | Convective |
| Elec | Electricity |
| fg | Flue gas conditions |
| fuel | Fuel conditions |
| hot | Hot-side conditions |
| i | Inner |
| lm | Logarithmic Mean |
| o | Outer |
| pb | Powerburner |
| r | Recirculation |
| rad | Radiative |
| st | Stoichiometric |
| stack | Stack conditions |
| steam | Steam conditions |
| t | Turbine |
| w | Weight |

## Abbreviations

| | |
|---|---|
| AFR | Air-to-Fuel ratio |
| CAPEX | Capital Expenditures |
| FFR | Flue gas-to-Fuel Ratio |
| LHV | Lower Heating Value |
| PPM | Parts Per Million |
| SPOT | Simple PayOut Time |
| TiT | Turbine inlet Temperature |

# Contents

# List of Figures

# List of Tables

# 1

# Introduction

Cogeneration is a common method to increase the overall efficiency of a power utility. Less common is the application of the cogeneration concept in direct fired industrial boilers. With the application of cost effective classic burners that allow an industrial boiler to have a high thermal efficiency, cogeneration is generally not an obvious solution. While cogeneration allows for local power generation, reduced emissions and a high total efficiency, it is still restricted in terms of heat generation compared to a classic burner. In this thesis, solutions are explored through which the negative effect can be compensated for.

## Purpose

The purpose of this research is to identify, analyze and conceptualize methods that allow a cogeneration gas turbine to become a more attractive alternative for a conventional burner to fire industrial installations.

## Background

The energy policy of an industry is subject of political, social and economic trends and events. At this moment, most of the trends are related to the climate issue and energy transition. Due to these trends the need for more cost effective, energy efficient and sustainable solutions is increasing.

Innecs Power Systems, located in Ter Aar, the Netherlands, develops and manufactures energy conversion systems. With these systems, Innecs aims to provide in the need of clients for efficient, cost effective and sustainable energy systems. One of these systems is the so called 'PowerBurner'. This is a gas turbine specifically developed for cogeneration applications, as it simultaneously delivers electrical power and high temperature heat. The system is displayed in figure 1.1.

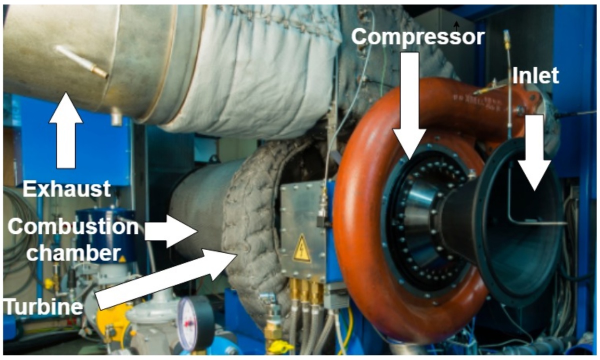


Figure 1.1: The PowerBurner including the combustion chamber, the turbine & exhaust, the compressor and the air inlet.

The unique configuration offers a thermal output of almost 2 MW at a high temperature (>690 °C) as the main product. Compared to other conventional CHP-systems, which have low (<250 °C) exhaust temperatures, this system can be used for more industrial heating applications. It delivers a net electrical power output of 280 kW, which can be used locally or sold back to the grid.

For the production of steam, the PowerBurner replaces a conventional burner. Even though the thermal efficiency of the PowerBurner is lower than that of a conventional boiler-burner setup (74% vs 95%), it can be the favourable option as revenue from the produced electrical power outweighs the extra fuel costs and investments required for the same thermal output.

## 1.1. Problem definition

The main disadvantage of the PowerBurner compared to a conventional burner lies in the less effective production of high temperature heat. Like any other gas turbine, the PowerBurner has a large amount of stack losses caused by an excess in mass flow, which is a result of the necessity for cooling the combustion products to allowable turbine entry temperature levels. If the temperature is above the allowable entry levels, thermal damage to the turbine blade occurs, which results in complete mechanical failure of the system.

The technical challenge of this research lies in improving the PowerBurner for cogeneration applications relative to a conventional burner. Figure 1.2 shows the solution may be found in reduction of the stack losses as these, for the PowerBurner-boiler combination, are a factor 3 times larger than those of a conventional boiler-burner combination that produces an equal amount of steam with a thermal efficiency of 95%.

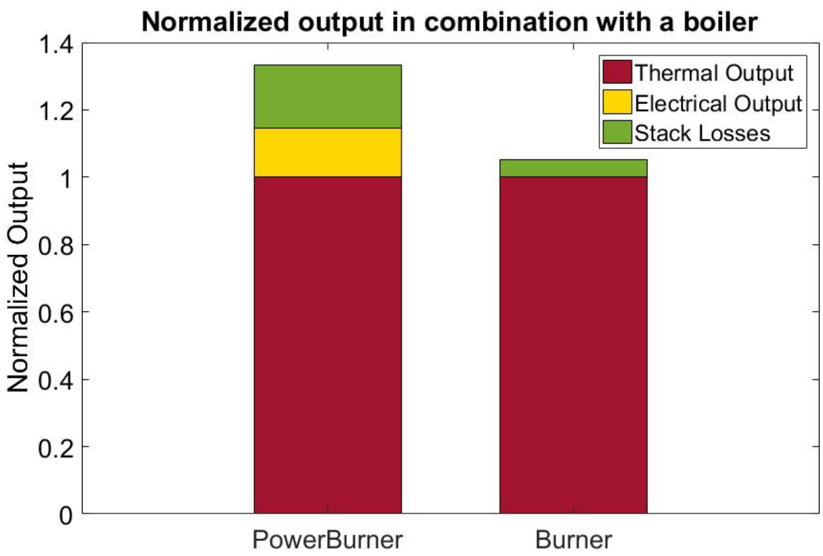


Figure 1.2: Total outputs of a PowerBurner and conventional burner producing an equal amount of steam.

There is a possibility of overcoming the stack loss problem. As the excess air results in excess oxygen in the PowerBurner exhaust (14 vol%), there is a possibility for the combustion of more fuel which could allow for more heat transfer in the boiler. As a result, this increases the thermal capacity and thermal- and total efficiency compared to the current setup. The turbine inlet temperature has to be kept in mind, however.

For the end-user, reduction of the stack losses allows the PowerBurner-boiler setup to become a more attractive alternative for a conventional burner as it results in a profitable system that is more energy efficient and has low emissions compared to the separate generation of heat and power. To realize this, the improved PowerBurner setup is required to retain a high electrical output over a large range of thermal outputs and remain cost-effective. An increased thermal capacity enables the PowerBurner-boiler setup to meet a larger range of thermal demands, which allows Innecs to appeal to a larger market with its product.

Based on the interests of the stakeholders, the following requirements are defined. The improved PowerBurner-boiler setup must be able to achieve:

- A high thermal efficiency;
- A high thermal capacity;
- Low cost;
- Efficient operation over the full operating range;
- A high power output.

With these characteristics in mind, in the next section, the research question is formulated. On top of that, sub-questions are defined which aid in answering the research question by going into more detail on the aforementioned aspects.

### 1.1.1. Research question

In order to investigate the possibilities for improving the PowerBurner system through reduction of the stack losses, the following research- and sub-questions are defined:

- How can the stack losses of the PowerBurner-boiler combination be reduced, and what makes this a better alternative to a conventional burner?
    1. Which concepts are available to improve the performance of a gas turbine-boiler system compared to a conventional burner?
    2. What is the effect of the implementation of such concepts on the PowerBurner-boiler system from a thermodynamic point of view?
    3. What is the effect of the implementation of such concepts on the PowerBurner-boiler system from a economic point of view?
    4. Which aspects have to be considered in the design of such concepts and how can the design influence the performance?
    5. Which aspects should be considered for the practical implementation of the viable concepts?

The goal of this report is to identify, analyze and conceptualize methods that would allow the co-generation PowerBurner to become a more attractive alternative to a conventional burner by increasing the thermal efficiency- and capacity while retaining both cost-effectiveness and a high thermal output. The final objective is to develop a conceptual design of the best performing method. The conceptual design should aid in the preliminary design phase of the concept, possibly performed by Innecs in the future.

### 1.1.2. Scope

As the PowerBurner is primarily designed for the production of steam in a boiler, the system analyzed in this report always consists of a PowerBurner and a boiler. This will be referred to as the PowerBurner-boiler system. More specifically, a boiler of the fire-tube kind is used. Such a boiler can produce steam at pressures of up to 25 bar, which is sufficient for most heating- and process steam applications [13]. All comparisons done between this setup and other systems are based on equal thermal outputs, as this is the main product of the PowerBurner. The PowerBurner-boiler setup is indicated in figure 1.3.

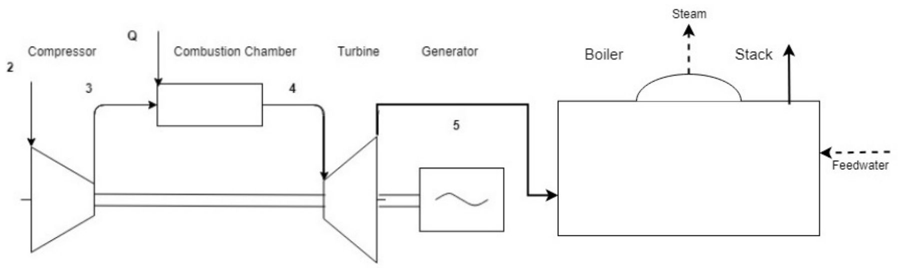


Figure 1.3: Cogeneration system containing both the PowerBurner and a boiler for the production of steam.

### 1.1.3. Outline of the report

In the next chapter, chapter 2, a more detailed background is given on gas turbines and the PowerBurner. This chapter aids in the understanding of the working principle and components of gas turbines and cogeneration.

After that, in chapter 3, concepts which could enable the PowerBurner-boiler setup to become a better alternative to a conventional burner are identified. From this, four concepts with the largest potential are analyzed further. These are:

- Steam injection;
- Flue gas recirculation;
- A Velox-type Boiler, which is a boiler integrated in the gas turbine combustion chamber;
- Supplementary firing.

In that same chapter, the working principle of these concepts is elaborated, as well as the basic design layout.

In chapter 4, a thermodynamic analysis is performed of the PowerBurner-boiler cycle including each concept. From this analysis it is possible to estimate the performance for each concept in terms of the thermal- and electrical requirements. This is compared to the current setup in order to conclude whether or not each concept allows for an improvement of the PowerBurner-boiler cycle from a technical perspective.

Chapter 5 provides an economic analysis. In this analysis, the profitability and CAPEX for each concept is determined. The results of this analysis yield a better idea of which concepts allow the PowerBurner-boiler setup to become a more attractive alternative to a conventional burner from an economic point of view.

From the evaluation of chapters 4 and 5 follows that supplementary firing is the best performing solution. For the implementation of supplementary firing in the PowerBurner-boiler setup, in chapter 6, the design requirements are specified. Based on these, a conceptual design is developed and its performance is validated by comparing a 2D axisymmetric- and 3D model.

Then, in chapter 7, several aspects for the practical implementation of the PowerBurner with supplementary firing are analyzed. This chapter gives insight in the different methods available for part-load operation and the economic viability of using the PowerBurner at a specific locations. Finally, in chapter 8, the conclusions from each chapter are summarized. Also, recommendations for future work on the subject are given.

#### Methodology

A general overview of the process for creating a conceptual design, as followed in this research, is indicated in figure 1.4. This is based on the ”Engineering Design Process”, which offers a methodological approach to create a working product [14]. The steps, performed in this research, are indicated within the red boundary.

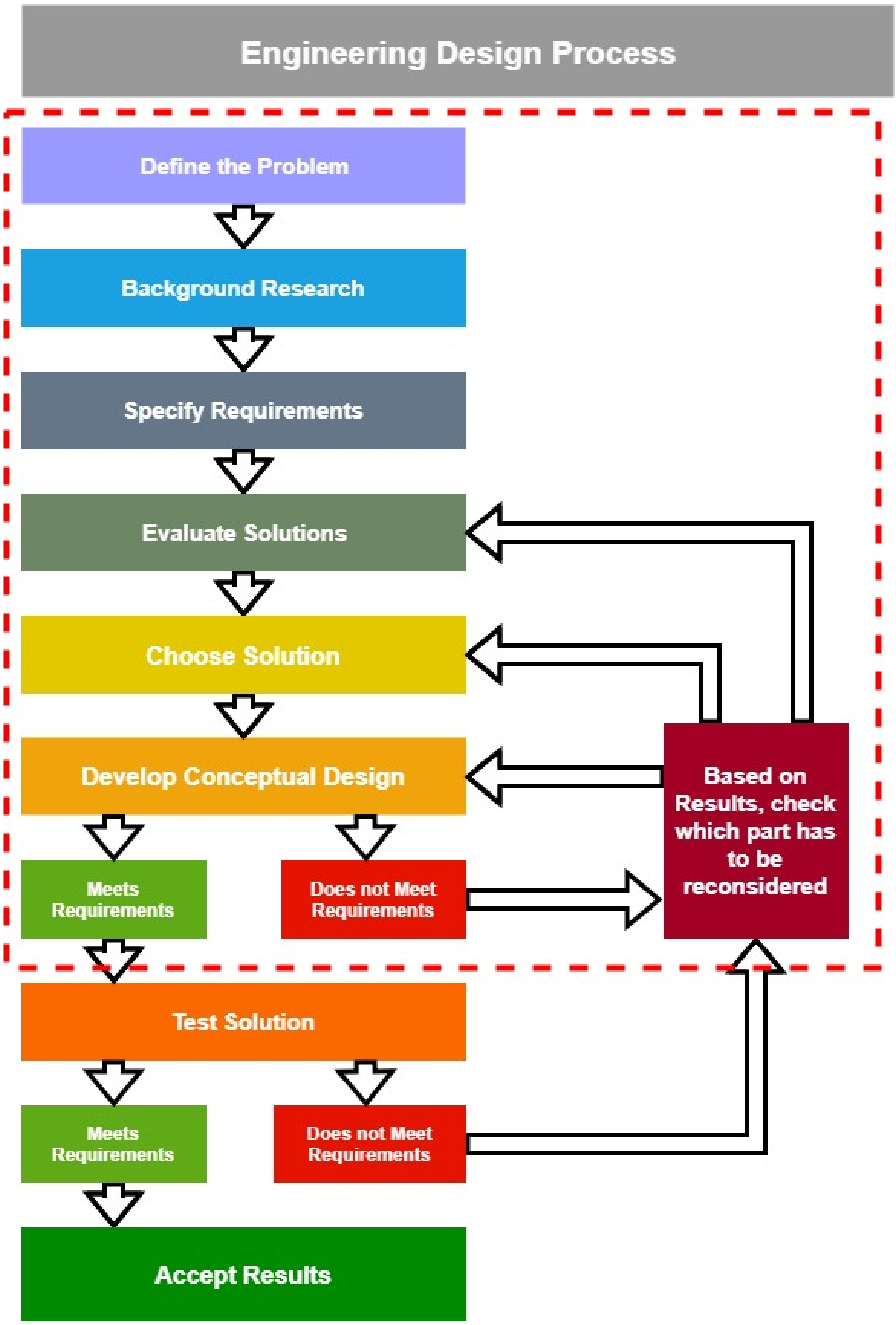


Figure 1.4: Engineering Design Process as used in this report.

# 2

# Theoretical background

This chapter elaborates on the working principle and main components of a gas turbine. On top of that, a more detailed description of the PowerBurner is given. Also, cogeneration and stack losses are elaborated. First, however, some of the history of gas turbines is explained.

## 2.1. Gas turbine history

One of the first devices that could be identified as a gas turbine was the Chimney Jack, created by Leonardo Da Vinci around the year 1500. This device consisted of a fan, hung above a fire pit. Rising gases would drive the fan, which was connected to a series of gears. These gears would turn a roasting skewer.

Since then, attempts have been made on creating devices like this for several purposes. Many failed, mainly because of the very low efficiencies that were achieved. But, with the development of the steam turbine and internal combustion chambers, the possibilities for gas turbines grew. The British engineer H. Riall Sankey (known for the Sankey Diagram) stated in a lecture on heat engines in 1917: "It will also be observed that even now the power developed by the largest steam-turbine is over twelve times greater than that of the largest internal-combustion engine. Notwithstanding, therefore, the considerably higher heat economy of gas- and oil-engines as compared with steam-turbines, the last will hold the field for the large units used for electrical power distribution until a satisfactory gas-turbine is evolved."[15]

### Modern-day gas turbines

The first gas turbine practical for industrial purposes was built by the Swiss company Brown Boveri (now known as ABB) in 1939. Their Neuchatel (figure 2.1) machine was capable of delivering 4 MW of power, at an efficiency of 17.4%.

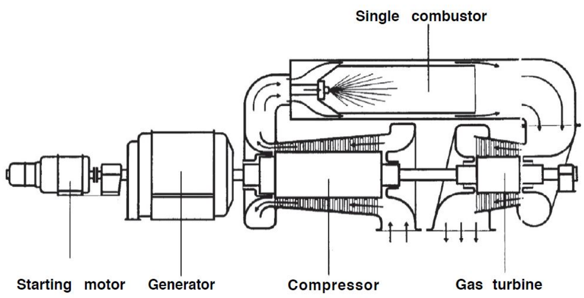


Figure 2.1: The Neuchatel gas turbine Cycle[1].

In the years after the Neuchatel turbine, the power output of conventional gas turbines kept increasing and can currently reach around 300 MW. In 1939, it was already known that the turbine inlet temperature (TiT) has an important role in turbine efficiency. The TiT for the Neuchatel turbine was about 550°C. Over the years, this is increased to 1700 °C because of the development of coatings, new alloys, ceramics and/or new blade designs with internal cooling mechanisms.

It was not until the end of the 1950s that the first gas turbine was used for combined heat and power generation (CHP) or cogeneration. These turbines not only produced electricity, but the exhaust heat is used as well for a variety of purposes like heating, cooling or steam production. Exhaust heat could also be used in a Combined Cycle Gas Turbine (CCGT), where the heat is used to increase the power output of the turbine by producing steam, which is fed through a steam turbine. These Combined Cycle turbines have been operational for about 40 years.

## 2.2. The working principle of gas turbines

Gas turbines, as defined in this report, are based on the (open) ideal Joule-Brayton cycle. The cycle, depicted in figure 2.2, starts from atmospheric air that is continuously sucked up by a compressor. The compressor applies work to the flow, which increases its pressure and temperature. As it is an ideal cycle, no entropy is generated between points 2 and 3.

In the combustion chamber, additional energy in the form of heat is added to the compressed air through the combustion of fuel. This is done between points 3 and 4. In the ideal cycle, this happens at constant pressure. In order to protect the turbine from thermal damage, the temperature of the flow is controlled and capped by adding excess air to the combustion chamber.

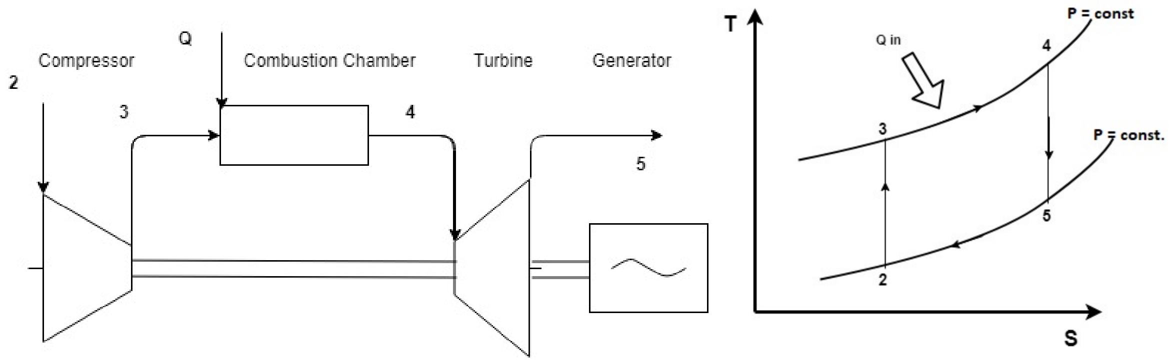


(a) Components of a gas turbine as the ideal Joule-Brayton cycle. (b) TS-diagram of the ideal Joule-Brayton cycle

Figure 2.2: Components and TS-diagram of the ideal Joule-Brayton cycle.

The turbine converts the high pressure- and temperature combustion products into shaftwork. Due to the expansion process during the conversion in the turbine, the temperature of the flow decreases. Again, as this is an ideal cycle, no entropy is generated between points 4 and 5. For this cycle, containing only a single shaft, the shaftwork from the turbine also drives the compressor. The leftover work in the shaft is used to generate electricity in the generator.

### The Actual Cycle & the PowerBurner

The PowerBurner is a gas turbine for cogeneration applications. Like any other gas turbine, it consists of four main components which are indicated in figure 2.3. The PowerBurner can take over the function of a regular burner for (for example) steam production, while having the power output as an extra. Basically, any process that requires heating, cooling or drying like in the food or agricultural industry or production processes, can employ this gas turbine. It has some other advantages over conventional methods for these processes. $NO_x$ emissions are relatively low. As a single shaft turbine, it does not have many rotating parts, so not much maintenance is required [16].

An overview of the PowerBurner characteristics is indicated in table 2.1.

The compressor in the PowerBurner is a so-called centrifugal compressor, as indicated in figure 2.4. Air is sucked in from the axial direction continuously. Momentum is added to the flow through the impeller, which is driven by the shaft. The flow is turned in the radial direction, after which the velocity is converted to pressure in the diffuser. Air is collected in the volute and flows through the outlet towards the combustion chamber.

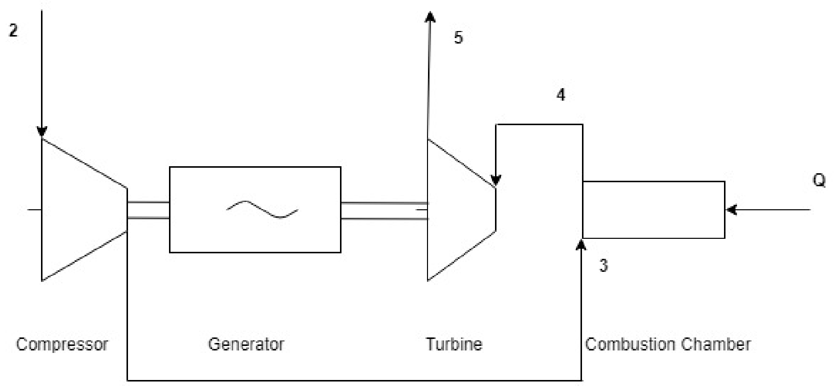


Figure 2.3: Setup of the PowerBurner.

Table 2.1: In- and output characteristics of the PowerBurner.

| **Parameter** | **Value** | **Remarks** |
|---|---|---|
| Electrical output | 280 kWe | $\eta_{elec}$ = 10.6 % |
| Thermal output | 2370 kW | $\eta_{th}$ = 89.4 % |
| Fuel input | 2650 kW | |
| Turbine inlet temperature | 900 °C | |
| Exhaust temperature | 690 °C | 14 vol % $O_2$ available |

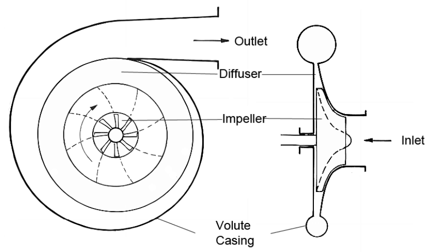


Figure 2.4: Centrifugal compressor including inlet, rotor (impeller), stator (diffuser) and exit[2].

Centrifugal compressors are more suitable for smaller gas turbines, as they perform better at handling small-volume flows, have a shorter length and have better resistance to damage from foreign objects and depositions on the blade surfaces compared to axial-flow compressors [17].

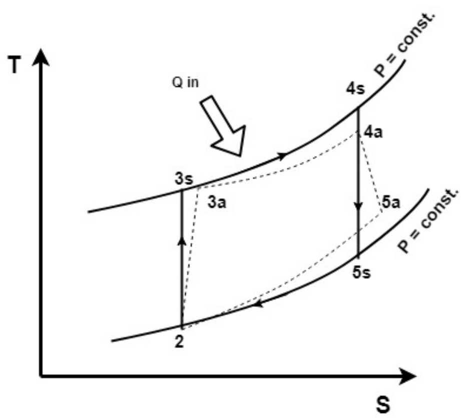


Figure 2.5: TS-diagram of the ideal Joule-Brayton cycle (s) and for an actual gas turbine cycle cycle (a).

Figure 2.5 indicates the difference between the ideal and actual compressor cycle between points 2, 3s (ideal) and 3a (actual). In the actual cycle, due to isentropic inefficiencies, the temperature must be higher in order to achieve an equal pressure as the ideal cycle. Because of this, the compressor requires more work, which results in less work that is available to be converted to electrical power.

After being compressed, the air enters the combustion chamber. A gas turbine combustion chamber is displayed in figure 2.6. Only part of the air is used for the actual combustion process, as the other part is required to cool down the combustion products. The turbine blades have to withstand very high thermal and physical loads. Since the combustion temperature is much higher than what the blades can endure, the gases requires cooling. For this purpose, combustion chambers are designed to have a dilution zone in which the combustion products are diluted with compressed air to reach allowable entry temperatures.

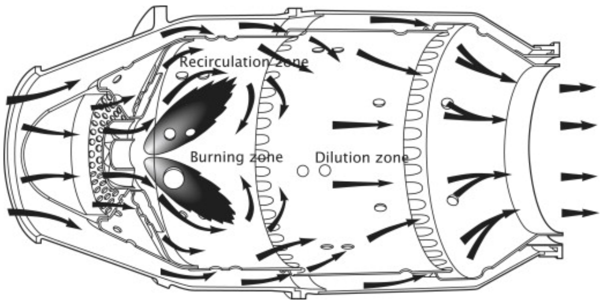


Figure 2.6: Combustion chamber with dilution holes [3].

Dilution of the combustion products affects pollutant emissions, as well. Most important combustion products, in terms of pollution, are nitrogen oxides ($NO_x$), unburned hydrocarbons (UHC) and carbon monoxide/dioxide ($CO/CO_2$)[17]. A well-designed combustor with a stable flame can reduce these emissions. A flame in such a combustor is self-sufficient and allows for complete combustion of the fuel.

Another important parameter of the combustion chamber is the pressure loss of the flow. Combustion generally leads to a static pressure drop of 2-10%. The electrical efficiency will be reduced by almost the same amount[3], as the combustion chamber pressure drop reduces the turbine pressure ratio. This is indicated in figure 2.5, in which a lower temperature and pressure is achieved at the turbine inlet for the actual cycle (4a) compared to the ideal cycle (4s).

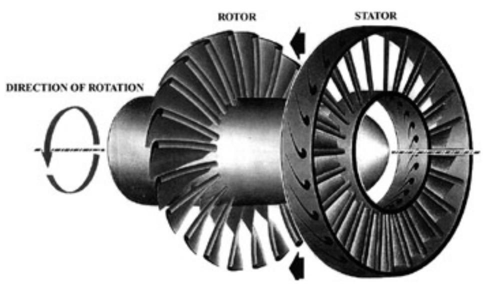


Figure 2.7: Axial Turbine including the stator and rotor[4].

After the combustion products have reached the allowable turbine inlet temperature, they enter the turbine. For a PowerBurner, this is an axial turbine. The combustion gas enters the turbine axially through a series of stator vanes around the shaft. Through these vanes, part of the pressure is converted to momentum. Then, at the rotor, the momentum is converted to shaftwork. The shaft drives both the compressor and a generator. Figure 2.5 indicates that, compared to the ideal cycle, the turbine outlet temperature is higher (5a). Due to isentropic inefficiencies part of the momentum is not converted to shaftwork, but to heat. Therefore, the turbine power output of the actual cycle is lower than that of the ideal cycle.

## 2.3. Gas turbine outputs and efficiencies

The outputs of gas turbines for cogeneration consists of two elements: The electrical power and the thermal energy. The available thermal energy ($Q_{av}$) is defined in equation 2.1 as the amount of energy released when cooling down the flue gases from the exhaust temperature ($T_{exh}$) to the ambient temperature ($T_a$). In this equation, $\dot{m}_{fg}$ is the mass flow of the flue gases, and $C_{p,fg}$ is the specific heat, which is assumed to be constant.

$$Q_{av} = \dot{m}_{fg} C_{p,fg} (T_{exh} - T_a) \tag{2.1}$$

This is not the amount of usable thermal energy that can be employed in subsequent processes, however. For application with a boiler, for example, a minimum flue gas temperature is required to enable heat transfer in the right direction. The flue gas temperature has to be higher than the temperature of water or steam anywhere in the boiler. This minimum flue gas temperature is defined as the stack temperature ($T_{stack}$).

The available thermal energy is split-up in two parts: The usable thermal energy ($Q_{out}$), which is the energy released by cooling the flue gases from the exhaust- to the stack temperature, and the stack losses. The latter ($Q_{stack}$) is the amount of energy which cannot be employed, and is therefore regarded as a loss. Both are indicated in equation 2.2.

$$Q_{out} = \dot{m}_{fg} C_{p,fg} (T_{exh} - T_{stack}) \quad Q_{stack} = \dot{m}_{fg} C_{p,fg} (T_{stack} - T_a) \tag{2.2}$$

The efficiencies of the cogeneration gas turbine are defined as the amount of usable energy as a fraction of the energy put in the system through fuel ($Q_{in}$). In this report, $Q_{in}$ is based on the LHV (Lower Heating Value) of a fuel. The thermal- ($\eta_{th}$), electrical- ($\eta_{elec}$) and total efficiency ($\eta_{total}$) are defined in equation 2.3.

$$\eta_{th} = \frac{Q_{out}}{Q_{in}} \quad \eta_{elec} = \frac{P_{elec}}{Q_{in}} \quad \eta_{total} = \frac{P_{elec} + Q_{out}}{Q_{in}} \tag{2.3}$$

In equation 2.3, the electrical power output ($P_{elec}$) is assumed to be the electrical power available after reduction of the conversion losses and power used by auxiliary equipment.

### Stack losses

By comparing the cooling process in the turbine to that in a conventional burner (figure 2.8) it can be observed that the temperature reduction of the PowerBurner is much more cascaded. The addition of excess air for dilution and the expansion process in the turbine result in a reduction of the available boiler inlet temperature.

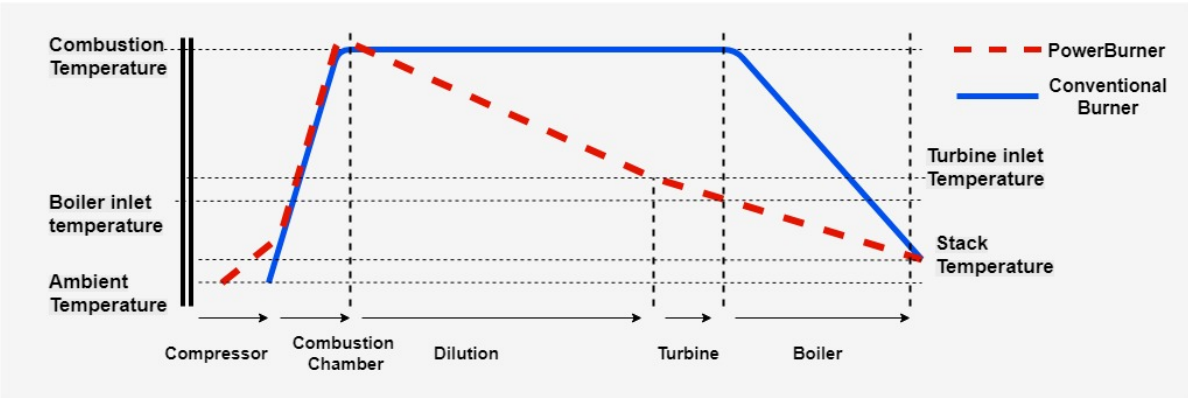


Figure 2.8: Temperature reduction process for a burner versus PowerBurner in combination with a heat-exchanging device.

From the equation for usable heat (equation 2.2) it follows that, since the ΔT over the boiler is much lower for the PowerBurner, the required mass flow for the conventional burner can be much lower in order for such burner to have a thermal output equal to that of the PowerBurner. Assuming that the stack temperature (in $Q_{stack}$ from that same equation) is equal for both the PowerBurner and a conventional burner, the stack losses of the PowerBurner are much higher due to the larger mass flow.

### Off-design operation

Gas turbines are designed to operate at a single most efficient combination of shaft speed, mass flow and pressure ratio. Deviating from this specific point can result in quickly reduced outputs and efficiencies. Figure 2.9a indicates a compressor map from which the general effect of off-design operation can be observed. The x- and y-axis indicates the deviation from the design operating mass flow and pressure. The red lines indicate lines of the deviation from the design shaft speed and the dotted lines indicate the efficiency of the compressor. Maximum efficiency is achieved in the center of the smallest closed surface formed by such a line.

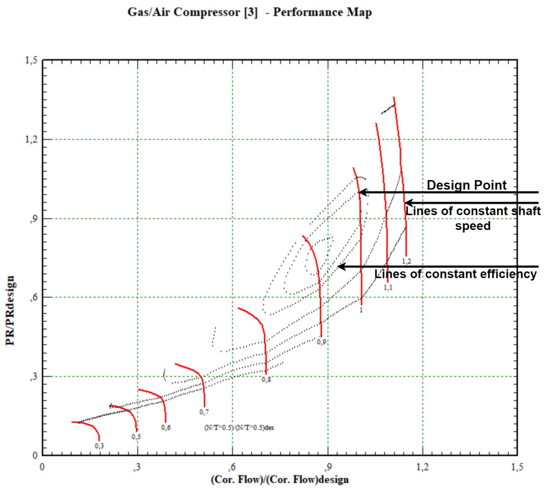


(a) General compressor map

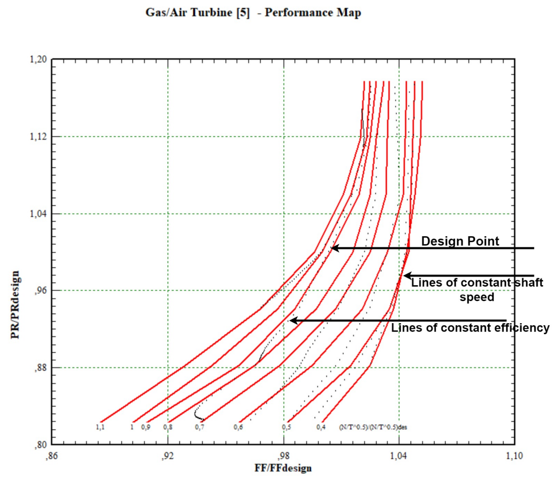


(b) General turbine map

Figure 2.9: Maps of the turbomachinery equipment in a gas turbine indicating part-load performance.

Figure 2.9a indicates that whenever the shaft speed is reduced, the mass flow in the system is lowered as well. Reduction of the pressure ratio at constant shaft speeds generally results in a lowered compressor efficiency. Lowering the mass flow rate at constant shaft speeds beyond the minimum as indicated by the red line results in compressor stall. The turbine map (figure 2.9b) also indicates deviation from the design mass flow and pressure ratio on the x- and y axis. Lowering the shaft speed also results in a lowered mass flow rate. Reduction of the mass flow rate at constant shaft speeds leads to a reduction in pressure ratio over the turbine, and thus in the turbine work output.

## 2.4. Cogeneration & steam production

For many gas turbines, the exhaust temperatures are still high enough to be used in subsequent processes. If part of the available thermal energy of the exhaust is extracted, the gas turbine is used for cogeneration. With such a system, a relatively small amount of extra fuel is required in order to produce both heat and electrical power. A comparison between a cogeneration plant and a plant requiring separate generation for an equal production of heat (at 95% efficiency) and power (40% efficiency) is depicted in figure 2.10.

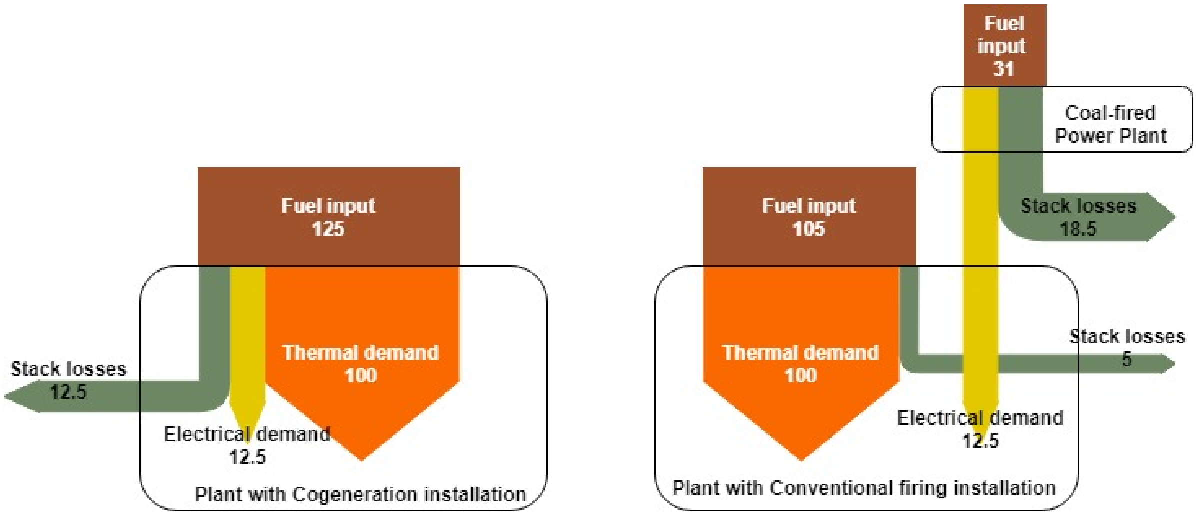


Figure 2.10: Schematic energetic requirements for a cogeneration plant and a plant that makes use of separate generation for an equal amount of heat and power.

Figure 2.11a indicates the ideal TS-diagram of a gas turbine including cogeneration. Heat is extracted between points 5 and 2. This occurs at constant pressure for the ideal cycle. With this process, energy can be transferred to another medium like air or water, which is indicated in figure 2.11b. For the actual cycle, pressure losses occur during the heat transfer process. As the ambient conditions (point 2) are equal for the ideal and actual cycle of figure 2.5, pressure losses from the exhaust gasses result in a lower turbine outlet temperature (5a) and thus a lower pressure ratio.

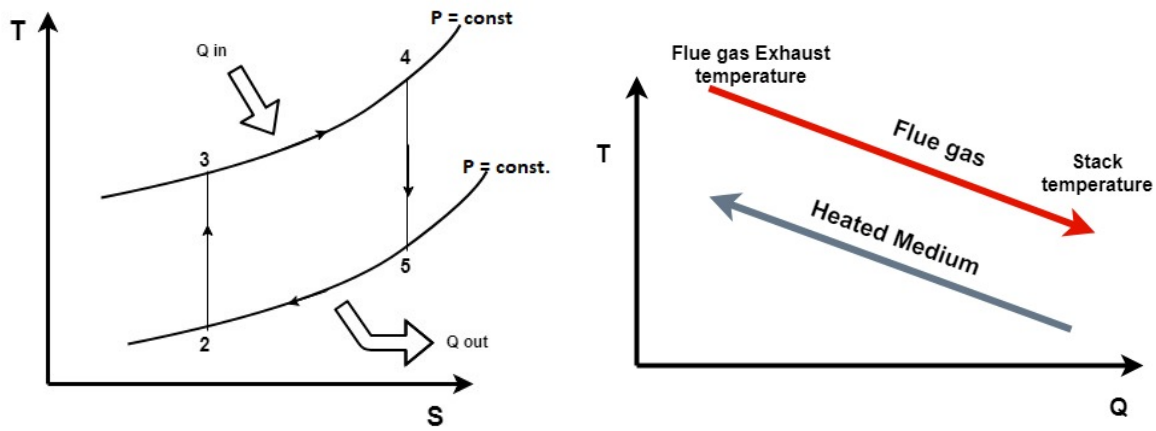


(a) TS-diagram of the gas turbine cycle including cogeneration

(b) QT-diagram for a cogeneration process.

Figure 2.11: Utilization of gas turbine exhaust heat for cogeneration.

### Heat transfer

Heat transfer is propagated via 2 phenomena: Radiation and convection. The governing equation for radiative heat transfer is given in equation 2.4

$$Q_r = \sigma A(T_h^4 - T_c^4) \tag{2.4}$$

Here, $\sigma$ is the Stefan-Boltzmann constant, A is the surface area surrounding the source and $T_h$ and $T_c$ are the temperatures of the hot source and cold sink in Kelvin, respectively. As the transferred energy changes with temperature to the $4^{th}$ power, small temperature changes can lead to large changes to the amount of energy that is transferred in the boiler.

The governing equation for convective (and conductive) heat transfer in boilers is displayed in equation 2.5. Here, $Q_c$ is the amount of heat transferred from gas to water, $A$ is the contact area between the flows and $U$ is the overall heat transfer coefficient. This parameter is a combination of convective and conductive heat transfer based on the materials and velocities of both flows and the piping material. Finally, $\Delta T_{lm}$ is the logarithmic mean temperature difference between the two flows.

$$Q_c = UA\Delta T_{lm} \tag{2.5}$$

Generally, two types of boiler can be distinguished based on the medium flowing through the pipes and what flows on the shell-side. For lower pressures (< 25 bar), *fire-tube boilers* are used (left image of figure 2.12). In these types of boilers, the combustion products flow through the tubes and a water/steam mixture is present on the shell-side.

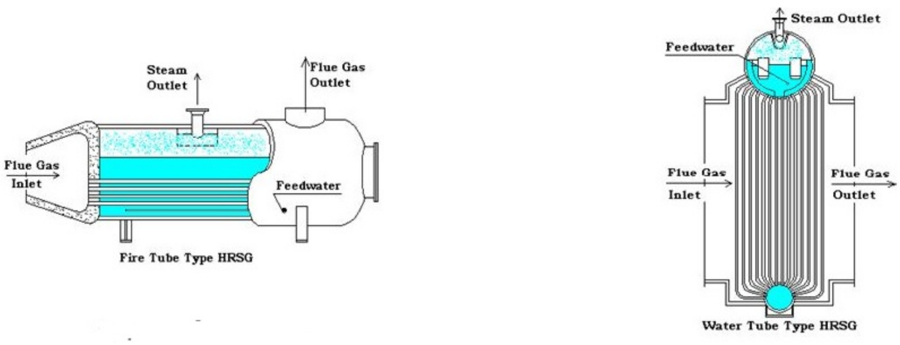


Figure 2.12: Fire tube- (left) and Water tube boiler (right)[5]

*Water-tube boilers* have the combustion products flowing on the shell-side. Such a system is depicted on the left of figure 2.12. This allows the water on the tube-side to reach much higher pressures and steam production rates compared to a fire-tube boiler. Whereas for the fire-tube boiler the shell acts as a drum for water, in the water-tube boiler, a separate drum is required.

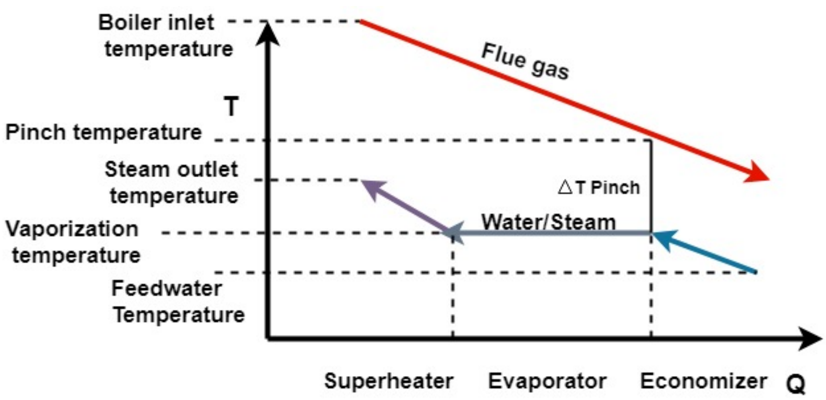


Figure 2.13: QT-diagram for heat transfer in a boiler including an evaporator, economizer and superheater.

The main component of any boiler is the evaporator. On the water-side of the evaporator, a vapor-liquid mixture is present. Despite heat being transferred to the mixture, the temperature remains constant as water undergoes phase-change. The amount of steam that can be produced is limited as there is a minimum temperature difference required between the flue gas and vapor-liquid mixture to enable efficient heat transfer. The minimum required flue gas temperature is the pinch temperature and is generally 10-20 K higher than the vaporization temperature of the water. The pinch temperature difference can be observed in the QT-diagram of figure 2.13. If only an evaporator is applied, the stack losses consist of the heat that can be subtracted from the flue gases by cooling them down from the pinch point to the ambient temperature.

Depending on the required steam temperature and supplied feedwater temperature, a superheater and economizer can be included in the boiler. In the superheater, fully evaporated steam is heated beyond the temperature of vaporization. With this can be made sure that the steam does not condense if heat is extracted during subsequent processes.

An economizer can be applied to heat water from the feedwater temperature up to the vaporization temperature. Including an economizer allows for a higher thermal efficiency in a boiler, as the flue gases can be cooled below the pinch temperature.

# 3

# Evaluation of available concepts

## 3.1. Introduction

In this chapter several concepts for improving the PowerBurner-boiler setup are evaluated. From the evaluation, four concepts are chosen. A preliminary design of each concept is proposed.

The different concepts are analyzed in the following section, based on available literature. These concepts are not chosen for the ability to specifically reduce stack losses, but for the possibility to improve the PowerBurner system compared to a conventional burner to directly fire industrial installations in terms of the following characteristics:

- High thermal efficiency;
- High thermal capacity;
- Low cost;
- Efficient operation over full operating range;
- High power output.

This allows for a broad scope, which is narrowed down by selecting four concepts. These concepts are elaborated further in the final section of this chapter.

## 3.2. Evaluation of concepts

In this section, 7 improvements to the PowerBurner cycle are shortly described and elaborated. Also, the effect of each improvement on the requirements is identified from literature.

### 3.2.1. Steam injection

In a Steam-injected gas turbine (STIG), heat from the turbine exhaust gas is used to produce steam, which is then partly injected back into the system. With such a system, a higher electrical efficiency and output can be reached [18]. Also, $NO_x$ emissions are reduced in the exhaust [19].

Although the stack losses for a steam-injected system are larger due to the increased mass flow in the turbine, this method could improve the PowerBurner cycle in terms of a high power output, which it could achieve over a large range of thermal outputs. Therefore, this concept is chosen to be developed further. The energetic flows of the application of steam injection in a PowerBurner-boiler combination is indicated in figure 3.1. As the PowerBurner setup already incorporates a boiler, steam can be taken from that directly.

Figure 3.2 shows that extra piping is required to transport steam from the boiler to the combustion chamber. An injection system inside the combustion chamber is also required.

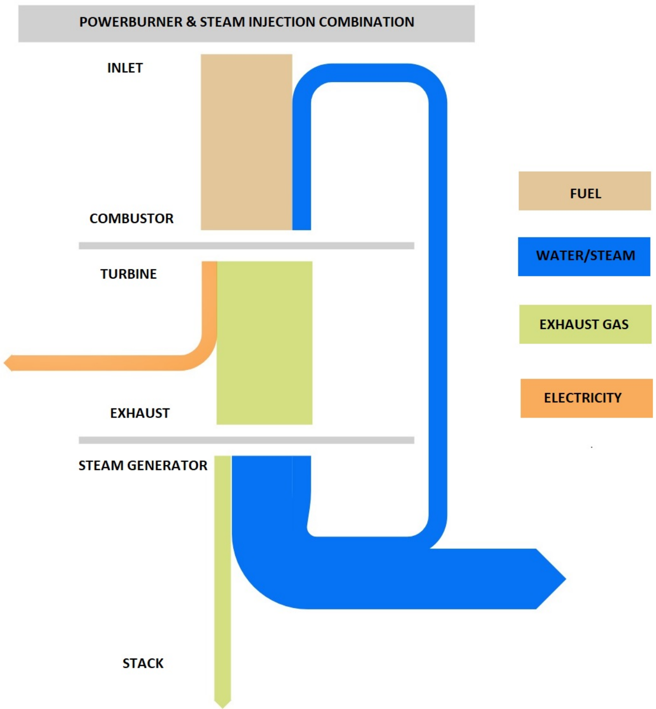


Figure 3.1: Energetic flows for steam injection in the PowerBurner-boiler setup.

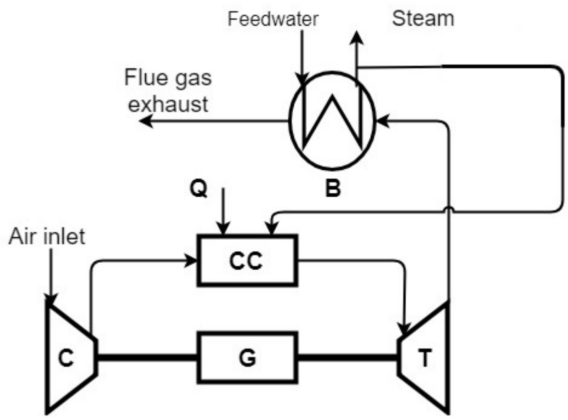


Figure 3.2: PowerBurner cycle including steam injection. Letters indicate the following components: C) compressor CC) combustion chamber T) turbine G) generator B) boiler Q) fuel input.

### 3.2.2. PowerBurner internal improvements

A redesign of the compressor can have some positive effect on the total efficiency. Redesigning for an increase in isentropic efficiency at lower loads could result in more efficient operation, but the impact is most likely limited. As it is preferred to keep the turbomachinery equipment as-is, this is not elaborated further.

For the turbine, the same goes as for the compressor. A redesign might have positive effects on the efficiencies. But, a lot of effort would be required for a small change in efficiency, and it is preferred to keep the turbine as-is. Therefore, this method is not developed further.

The turbine blades have large effect on gas turbine performance through the allowable turbine inlet temperature. The blades have to be designed to be creep-, rupture-, hot corrosion- and oxidation resistant [17]. Furthermore, the material should have low thermal expansion. By increasing the turbine inlet temperature, the stack losses can be reduced. On top of that, the thermal- and electrical outputs are improved. Several methods are available to achieve a higher turbine inlet temperature.

Internal cooling is a method to increase the blade metal temperature limit [3]. Examples are film- or convective cooling methods. Another method to increase the limit, is through the the application of Thermal Barrier Coatings (TBC). These coatings are made of ceramics and provide thermal insulation to the blades, as well as minimizing thermal stresses and reflection of radiant heat from the gas. Application of TBC's can improve inlet temperatures by 70 K[20]. This is only the case when inner blade cooling is implemented, as well.

Coatings and cooled blades have a very large potential for increasing the efficiency and exhaust temperature. The problem for the PowerBurner is the fact that the turbine blades are very small. For such small blades, manufacturing of cooling holes or tubes inside the geometry and the application of coatings is very costly and time-consuming [21]. Therefore, this is not an viable solution.

### 3.2.3. Compressor inlet cooling

Compressor inlet cooling involves reducing the inlet air temperature to improve the electrical output at higher ambient temperatures [22]. This results in a larger fuel input and reduced efficiencies. Inlet cooling works well for improving the performance in high temperature low humidity areas [23], but does not provide specific improvements to the current PowerBurner setup. Therefore, this method is not developed further.

### 3.2.4. Recuperation

In a recuperated cycle, the exhaust heat is partially used to heat air downstream of the compressor. Through recuperation, the electrical efficiency of the system is improved [24] while the thermal output is lowered. This could allow for the efficient generation of electrical power over the operating range. However, the costs of such a system are very high. Innecs has already done research on the viability of this cycle. The marginal increase of the electrical efficiency through recuperation did not outweigh the extra costs of the recuperator [25].

### 3.2.5. Flue gas recirculation

In flue gas recirculation, part of the (hot) exhaust gases are fed back to the compressor inlet. For a flue gas recirculated gas turbine, less flow is available in the system [26] which results in lowered stack losses. As a result, the electrical power output of a gas turbine continuously decreases with increasing recirculation ratios [27]. It could improve the flexibility and total efficiency of the system. This method also allows for a reduction in $NO_x$ emissions [28], which could aid the system from an environmental perspective.

The ratio between the mass flows is the recirculation ratio (equation 3.1). In this equation, $\dot{m}_{fg}$ is the mass flow of flue gas entering the compressor, and $\dot{m}_{com}$ is the total mass flow entering the compressor.

$$R_r = \frac{\dot{m}_{fg}}{\dot{m}_{com}} \tag{3.1}$$

As flue gas recirculation could prove useful for several requirements, this method is chosen to be analyzed in the subsequent chapters. For the PowerBurner-boiler setup, flue gases are already cooled by the boiler. The gases are mixed at the stack temperature with ambient air, before being supplied to the compressor. This process is shown in figure 3.3, in which the flue gases are recirculated from the boiler exhaust back to the inlet.

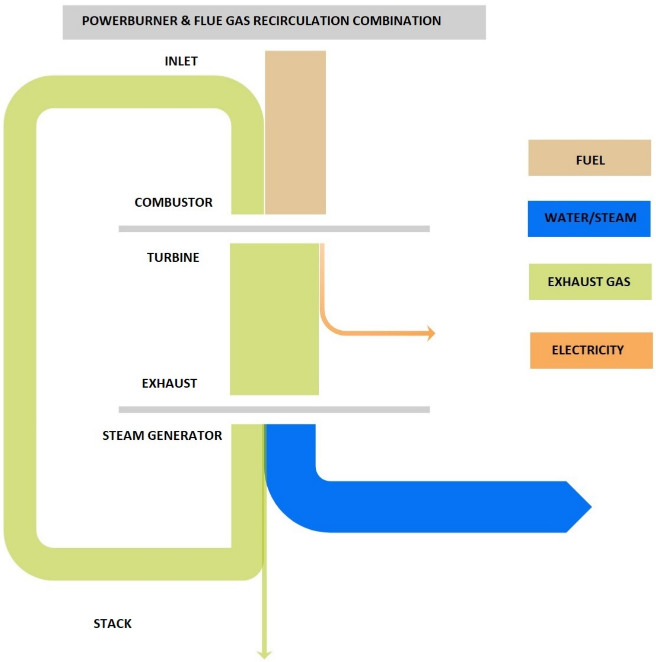


Figure 3.3: Energetic flows for the flue-gas recirculated PowerBurner.

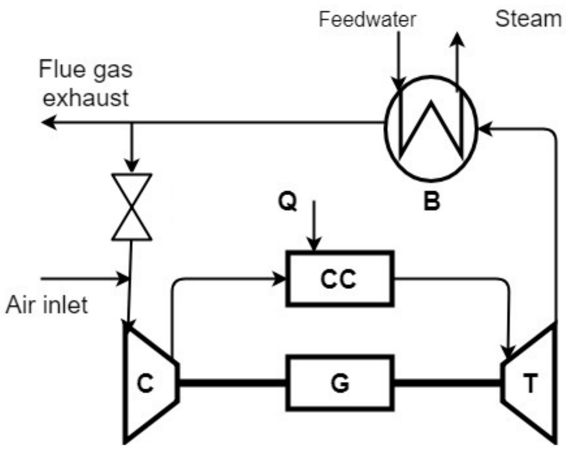


Figure 3.4: PowerBurner cycle flue gas recirculation. Letters indicate the following components: C) compressor CC) combustion chamber T) turbine G) generator B) boiler Q) fuel input.

### 3.2.6. Supplementary firing

In supplementary firing, fuel is burned with the excess oxygen from the exhaust of a gas turbine. This allows for a reduction in stack losses, increase in thermal capacity and elevated boiler inlet temperatures. On top of that, natural gas produces little $NO_x$ when combusted in gas turbine exhausts, as a reduced amount of oxygen is available [29].

As this method could help in many requirements for improving the PowerBurner-boiler setup, and would only require an extra burner to be implemented, it is chosen to be developed further. Figure 3.5 indicates the energetic flows of the supplementary-fired PowerBurner. Extra fuel is added to the exhaust gases, through which more steam can be produced in the boiler.

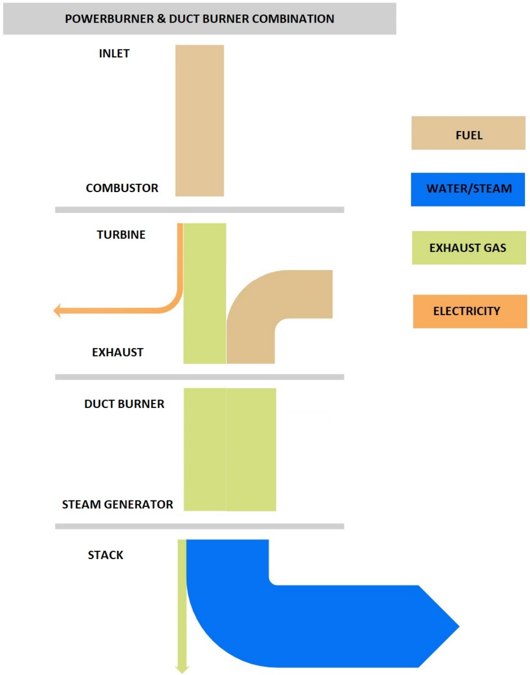


Figure 3.5: Energetic flows for the Supplementary-fired PowerBurner system.

An extra combustor is required for the implementation of supplementary firing in the PowerBurner-boiler setup. The location of the burner can be observed in figure 3.6, in which **CC2** is the location where the secondary combustion stage occurs. Often, this can be done inside the exhaust duct, as long as the burner is positioned close to the boiler. So-called duct burners are available for the combustion of fuel with flue gases.

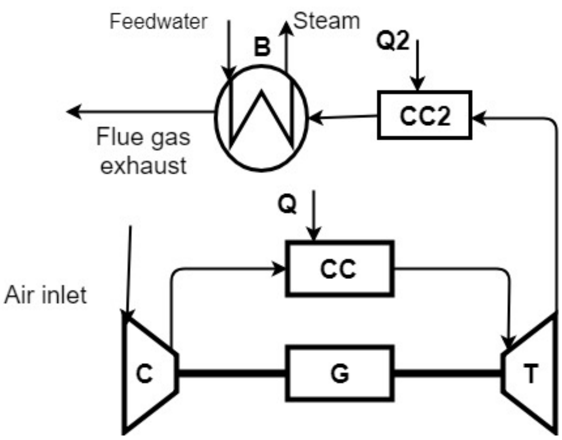


Figure 3.6: PowerBurner cycle including supplementary firing. Letters indicate the following components: C) compressor CC) combustion chamber T) turbine G) generator B) boiler Q) fuel input and CC2) and Q2) the secondary combustion chamber and -fuel input.

Figure 3.4 shows the extension of the PowerBurner setup with flue gas recirculation. Extra piping is required from the boiler exhaust to the compressor inlet, as well as a valve to control the recirculation ratio.

### 3.2.7. The Velox-type boiler

A Velox-type boiler is a boiler which is integrated within the combustion chamber of a gas turbine. In this boiler, heat is transferred from the combustion products to water, through convection and radiation.

This allows for the combustion of more fuel. The targeted turbine blade temperature is then achieved not only due to dilution with excess air, but also through heat transfer in the boiler section. An example of such a Velox-type boiler is shown in figure 3.7. Here, heat is transferred in an evaporator and superheater between the combustion chamber and gas turbine. The steam is then employed in a steam turbine for the generation of extra electricity.

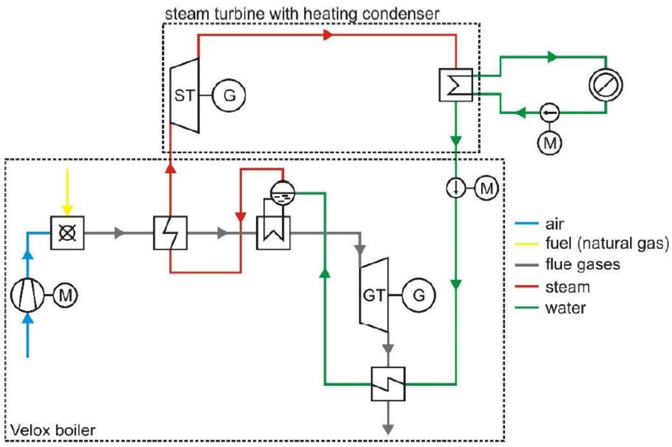


Figure 3.7: Combined Velox-steam cycle [6].

Implementation of this system reduces the stack losses and increases the thermal capacity. For cogeneration applications, the Velox cycle has a higher overall efficiency than a classical gas-steam cycle. A gas turbine, incorporating the Velox-type boiler, is capable of achieving good flexibility and fast changes in loads [6]. On top of that, it requires only 50% of the heat transfer surface area compared to a regular waste-heat boiler and could produce steam at higher temperatures [30]. This method

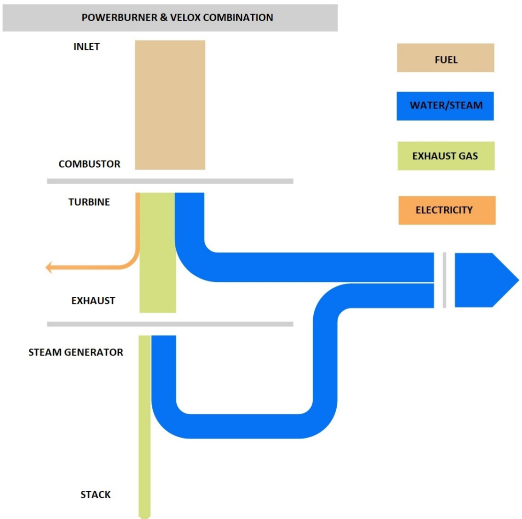


Figure 3.8: Energetic flows for the PowerBurner with a Velox-type boiler.

could improve the setup in terms of the total efficiency, thermal capacity and could result in flexible and efficient operation. Also, there is space available for the implementation, as the combustion section (see figure 1.1) can be moved without moving other components. Therefore, implementation of a Velox-type boiler in the PowerBurner-boiler cycle is developed further. A schematic representation of the energetic flows of application of the Velox-type boiler in the PowerBurner setup is shown in figure 3.8. The thermal output of the system consists of the thermal output of both boilers.

Figure 3.9 shows the layout of the PowerBurner-boiler setup with Velox-type boiler, indicated with **B2**. The size, or heat transfer surface area A in $m^2$, of this boiler, depends on three properties: The amount of heat that is to be transferred to steam, $Q_{thermal}$, the overall heat transfer coefficient $U_0$ and the logarithmic mean temperature difference $\Delta T_{lm}$. This results in the following equation, and only includes convective- and conductive heat transfer.

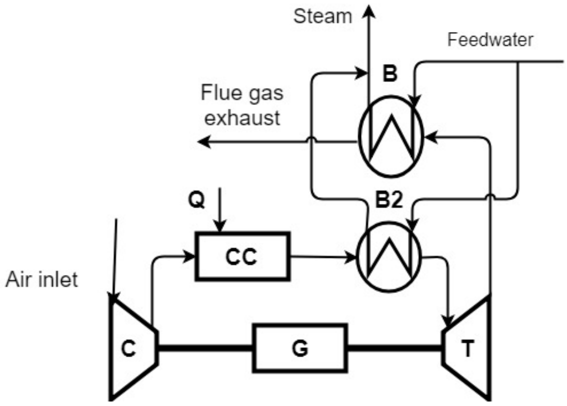


Figure 3.9: PowerBurner cycle including Velox-type boiler Letters indicate the following components: C) compressor CC) combustion chamber T) turbine G) generator B) boiler Q) fuel input and B2) the Velox boiler.

$$Q_{thermal} = U_0 A \Delta T_{lm} \tag{3.2}$$

The boiler size must be large enough to transfer heat over the full operating range. Considering the PowerBurner has a thermal output of close to 2 MW through reduction of the oxygen content from 21 vol% to 14 vol%, it is assumed the Velox-type boiler has a maximum duty of 5 MW. Furthermore, the values indicated in table 3.1 are assumed for the design of the boiler inside the PowerBurner combustion chamber.

Table 3.1: Properties and duty of the gas- and steam paths of the Velox-type Boiler.

| **Gas Path** | **Property** | **Steam Path** |
|---|---|---|
| 2290 | Inlet Temperature [K] | 368 |
| 1173 | Outlet Temperature [K] | 368 |
| 3.18 | Pressure [bar] | 10 |
| 5 | Duty [MW] | 5 |
| 3.25 | Mass flow [kg/s] | 2.11 |

With the in- and outlet temperatures, the logarithmic mean temperature difference can be calculated. The cooling process is depicted in the QT diagram of figure 3.10.

$$\Delta T_{LM} = \frac{(2290 - 368) - (1173 - 368)}{ln\frac{2290-368}{1173-368}} = 1200[K] \tag{3.3}$$

The outlet flue gas temperature of the boiler is equal to the turbine inlet temperature in this case.

With a method supplied by Towler and Sinnott [10], the size of the Velox boiler can be estimated. For this, an overall heat transfer coefficient is assumed first. From table 19.1 of Towler and Sinnott [31], a value of 100 $W/m^2K$ for a flue gas-steam heater is used.

By using the assumed overall heat transfer coefficient, boiler duty and the result from equation 3.3, the heat transfer surface area of equation 3.2 is determined to be 39 $m^2$.

Because of the the increased pressure on the flue gas side, it is beneficial to let the flue gas flow on the shell side [30]. A square tube arrangement is used for reduced pressure drop over the shell side [32].

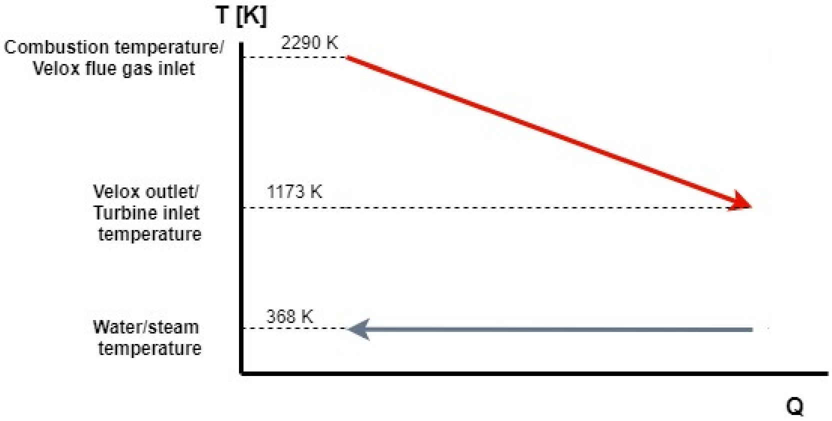


Figure 3.10: Flue gas cooling (red line)- and water heating (blue line) process in the Velox boiler.

With the area known, a more accurate boiler size is determined by assuming specific sizing parameters indicated in table 3.2. With the tube diameter , the amount of tubes required for a total heat transfer area of 39 $m^2$ can be determined. Furthermore, $d_o$ is the standard outside tube diameter and L is the assumed tube length. With these tube dimensions, the steam velocity can be calculated. In order to achieve reasonable values, a recirculation ratio of 10 is assumed, as well as 4 tube passes.

Table 3.2: Standard tube dimensions, with resulting number of tubes and steam velocity.

| Property | Value |
|---|---|
| Outside tube diam. [mm] | 19 |
| wall thickness [mm] | 2.1 |
| Tube length [m] | 2.44 |
| Number of Tubes | 268 |
| Tube Velocity [m/s] | 2 |

With the velocity available, the final parameters required to determine the tube site transfer coefficient $h_i$, can be determined. These are indicated in table 3.3.

Table 3.3: Parameters and results for calculating the tube-side (steam) heat transfer coefficient.

| Property | Value |
|---|---|
| Re | $9.4*10^4$ |
| Pr | 1.85 |
| Nu | 463.6 |
| $h_i$ | $2.1*10^4$ |

The same can be done for the shell-side flow. The results are indicated in table 3.4. Here, $h_o$ is the shell-side transfer coefficient. The shell-side flow area is a result from a method supplied by Towler and Sinnott [10].

Table 3.4: Dimensions and flow velocity of flue gas on the shell side.

| Property | Value |
|---|---|
| Shell-side flow area [$mm^2$] | 213127 |
| Shell-side flow velocity [m/s] | 21.6 |
| Inner shell diameter [mm] | 1032 |
| Re | 5230 |
| Pr | 0.777 |
| Nu | 33.7 |
| $h_o$ [$W/m^2K$] | 174.1 |

With this known, the overall heat transfer coefficient for the current setup can be calculated. The result is tested against the assumed value. If the calculated value deviates less than 30 % from the assumed value, the sizing can be accepted according to Towler and Sinnott [10]. In this case, the calculated coefficient was 121 $W/m^2K$. Therefore, the aforementioned sizing is accepted. A schematic overview of the Velox-type boiler within the PowerBurner setup is depicted in figure 3.11.

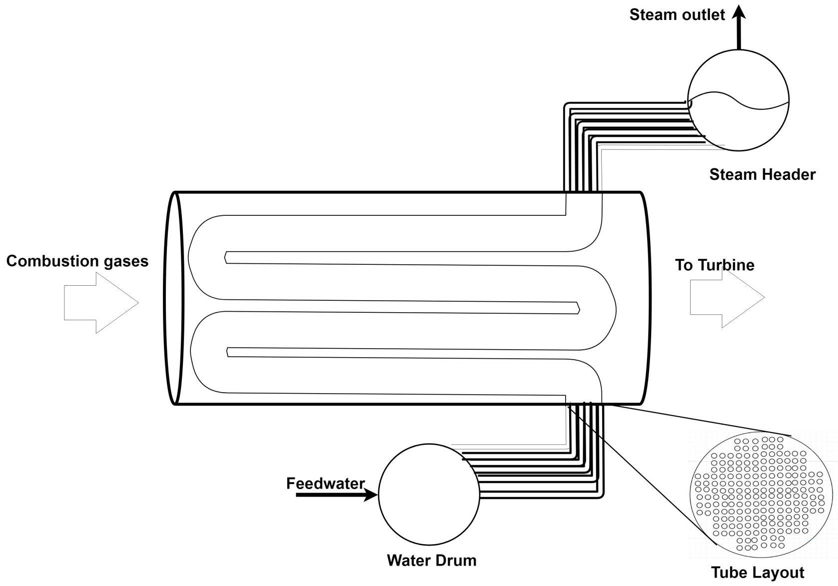


Figure 3.11: Schematic overview of the Velox-type boiler in the PowerBurner setup.

## 3.3. Results

Table 3.5 shows each of the five aforementioned requirements upon which each analyzed concept may have an effect. The concepts in bold indicate the ones that are developed further. A **+** indicates the concept has a positive effect on the requirement, a **-** indicates a negative effect. If there is no indicator, no data was available from literature.

| **Requirement/ Method** | **High thermal efficiency** | **High thermal capacity** | **Low cost** | **Efficient over operating range** | **High power output** | **Remark** |
|---|---|---|---|---|---|---|
| **Steam injection** | | | | + | + | - |
| Compressor inlet cooling | | | | | | Applicable in varying climates |
| Internal improvements | | | | | | Marginal improvements |
| Recuperation | | - | - | + | + | Previous research done |
| **Flue gas recirculation** | + | | | + | | - |
| **Velox-type boiler** | + | + | | + | | - |
| **Supplementary firing** | + | + | + | | | - |

Table 3.5: Overview of the analyzed concepts and requirements they affect based on the analyzed literature.

## 3.4. Conclusion

In this chapter, 7 methods which could improve the PowerBurner-boiler setup are compared in terms of the requirements as described in chapter 1. Based on available literature, four concepts are chosen to be developed further. These are:

- Steam injection;
- Flue gas recirculation;
- A Velox-type boiler;
- Supplementary firing.

In the next chapters, the performance of these concepts in terms of the requirements is analyzed through a thermodynamic and economic analysis. Based on the results of the analyses, the best performing concept is determined.

# 4

# Thermodynamic analysis

In this chapter, the effects of adding each of the four concepts, introduced in the previous chapter, to the PowerBurner setup are analyzed in turn. The four PowerBurner extensions are:

- Steam injection;
- Flue gas recirculation;
- The Velox-type boiler;
- Supplementary firing.

For each system, the performance is analyzed by determining the following parameters:

- Thermal output & efficiency;
- Electrical output & efficiency;
- Thermal capacity;
- Total efficiency.

The results for each setup are compared at specific thermal outputs, as this is the main product. For comparison with the current setup, the performance of the PowerBurner at specific thermal outputs through reduction of the firing rate and shaft speed are included, as well.

## 4.1. Thermoflex and PowerBurner model verification

To determine the in- and output parameters, a model of each setup is built in Thermoflex. In Thermoflex, predefined components can be combined to model gas turbines or complete power plants. It is capable of solving mass- and energy balances, heat transfer and can calculate pressure losses over each component. On top of that, it includes the possibility to simulate off-design operation of compressors and turbines.

All models created for this analysis include three main components: A model of the PowerBurner, of a boiler and of the components required for extension of the cycle with each of the four concepts. A more detailed description of each model can be found in appendix B.

The boiler is modeled in Thermoflex in order to simulate the effect of the varying thermal output on the production of steam. Each model includes the exact same boiler containing an economizer, evaporator and superheater, producing steam at 10 bar. An overview of the basic PowerBurner-boiler setup is indicated in figure 4.1.

As no test data of the PowerBurner was available, in order to get an accurate representation in Thermoflex, the performance of the model is verified with an existing Design Point Specification. This specification contains a detailed description of several PowerBurner characteristics like pressures, temperatures and mass flows at specific points in the cycle during standard operation.

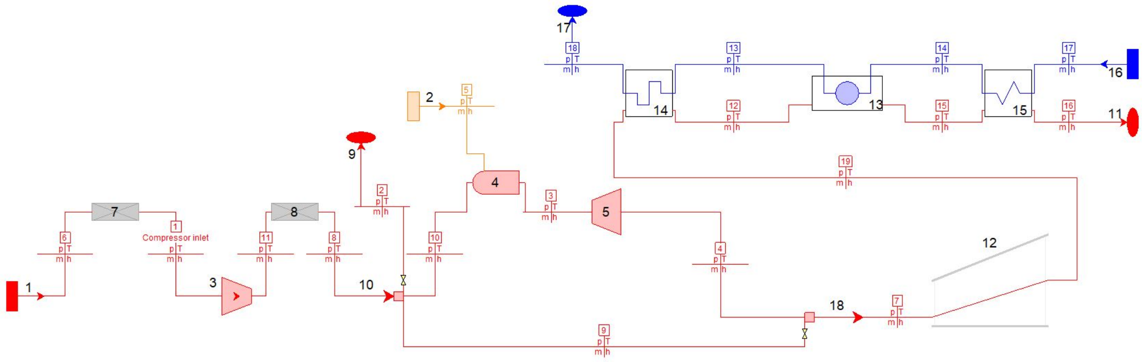


Figure 4.1: Basic Thermoflex model of the PowerBurner, including a boiler connected to the exhaust.

The comparison is indicated in table 4.1. In this table, the third column shows the data from the design point at specific locations. The fourth column indicates the corresponding result from Thermoflex. Column 5 shows by which component number in Thermoflex this data is computed, and column 6 shows the deviation between the Design Point Specification and the Thermoflex model, but only for the parameters which have been calculated by Thermoflex.

From column 6 in table 4.1, only very small deviations between the Design Point Specification and the Thermoflex model can be observed. As the deviations are all smaller than 0.3 %, it can be concluded that the Thermoflex model represents the Design Point Specification accurately enough for this analysis.

To model off-design operation of the compressor and turbine, standard maps are used for both components in Thermoflex. These maps scale based on the basic design parameters like shaft speed, mass flow, efficiency and pressure ratio. The standard maps are shown in figure 4.2. As the actual off-design performance of the PowerBurner is not available, the accuracy of these maps is not known. But, a qualitative analysis of the off-design performance is possible with these maps.

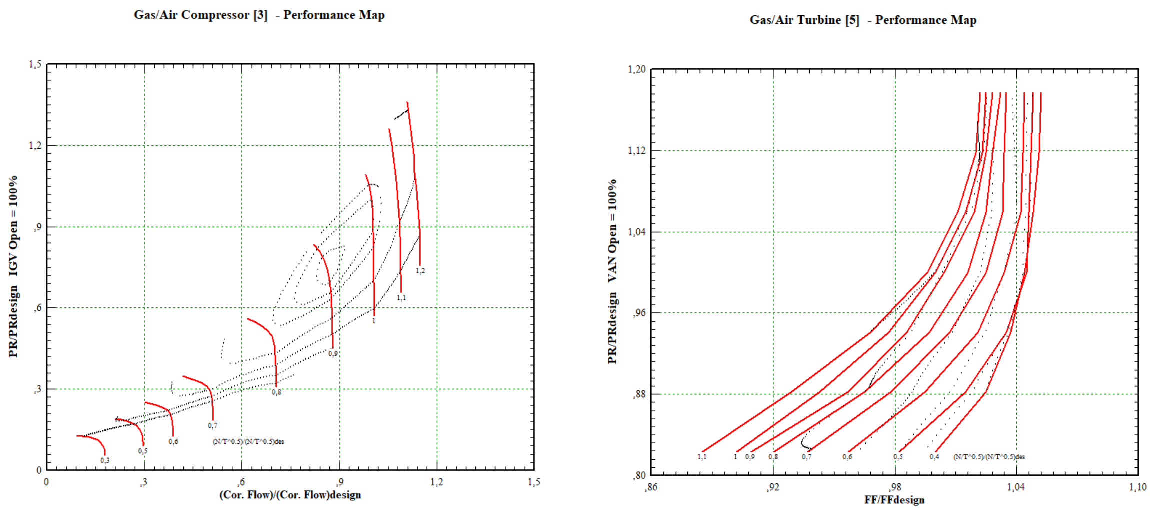


Figure 4.2: Basic compressor- and turbine maps generated in Thermoflex and used for off-design operation in certain models.

Table 4.1: Design point specification and Thermoflex results. Part of the data has not been disclosed on purpose.

| Description | Unit | Design Point | Thermoflex In/output | Comp.No. | deviation |
|---|---|---|---|---|---|
| Ambient temperature | [K] | 288 | 288 | 1 | |
| Ambient pressure | [bar] | 1.013 | 1.013 | 1 | |
| Air mass flow | [g/s] | - | - | 1 | |
| Compressor inlet temperature | [K] | 288 | 288 | 3 | |
| Compressor inlet pressure | [bar] | - | - | 7 | 0.00% |
| Compressor mass flow | [g/s] | - | - | 7 | |
| Compressor exit temperature | [K] | - | - | 3 | -0.23% |
| Compressor exit pressure | [bar] | - | - | 3 | -0.03% |
| Mass flow rate after bleed | [g/s] | - | - | 10 | 0.00% |
| Compressor exit velocity | [m/s] | - | - | - | |
| Combustor inlet temperature | [K] | - | - | 10 | -0.23% |
| Combustor inlet pressure | [bar] | - | - | 10 | -0.09% |
| Compressor pressure ratio | [-] | - | - | 5 | 0.03% |
| Compressor leakage | [g/s] | - | - | 10 | |
| Compensator air | [g/s] | - | - | 10 | |
| Turbine rotor and dome cooling flow | [g/s] | - | - | 10 | |
| Rotorspeed | [rpm] | 28.000 | 28.000 | 5 | |
| Normalized rotorspeed | [%] | 100 | 100 | 5 | |
| Compressor power consumption | [kW] | 480 | 479.4 | 3 | -0.13% |
| Isentropic compressor efficiency | [-] | - | - | 3 | 0.34% |
| Compressor torque | [N m] | - | | - | |
| Turbine inlet temperature | [K] | 1173 | 1173 | 4 | 0.00% |
| Turbine inlet pressure | [bar] | - | - | 4 | 0.16% |
| Turbine inlet mass flow rate | [g/s] | - | - | 4 | |
| LHV fuel | [kJ/kg] | 38,041 | 38,041 | 2 | |
| Equivalence ratio | [-] | - | - | - | |
| Stage exit temperature | [K] | - | - | 5 | 0.30% |
| Stage exit pressure | [bar] | - | - | 5 | 0.09% |
| Stage static exit pressure | [bar] | - | - | - | |
| Stage exit mass flow | [g/s] | - | - | 18 | |
| Volute exit temperature | [K] | - | - | 18 | -0.01% |
| Volute exit pressure | [bar] | - | - | 18 | 0.00% |
| Pressure ratio turbine | [-] | - | - | 5 & 11 | |
| Turbine power | [kW] | 800 | 800 | 5 | 0.00% |
| Isentropic turbine Stage efficiency | [%] | - | - | 5 | -0.11% |
| Turbine disk cooling flow | [g/s] | - | - | 10 | |
| Stator exit mass flow rate | [g/s] | - | - | | |
| Mechanical efficiency | [%] | - | - | 5 | |
| Exit temperature | [K] | 959 | 958.7 | 12 | -0.03% |
| Specific heat exhaust gas flow | [J/kg K] | - | - | | |
| Exit pressure | [bar] | 1.066 | 1.066 | 12 | |
| Exit static pressure | [bar] | - | - | - | |
| Exit mass flow rate | [g/s] | - | - | 18 | |
| Fuel flow rate Groningen NG | [g/s] | - | - | 4 | 0% |
| Gross shaft power | [kW] | - | - | 3 & 5 | |
| Friction losses | [kW] | - | - | 5 | |
| Electrical losses | [kW] | - | - | 5 | |
| Power cons. by auxiliaries | [kW] | - | - | 5 | |
| Gross specific fuel consumption | [kg/kW h] | - | - | - | |
| Electrical power output | [kW] | 279 | 280 | 3 & 5 | 0.36% |
| Electrical efficiency | [%] | 10.6 | 10.56 | 5 | -0.38% |
| Cycle thermal efficiency | [%] | - | | | |

## 4.2. Results of the thermodynamic analysis

In this section, the analytic results of the standard PowerBurner configuration are shown first. This is the reference case and includes operation through variation of the firing rate and shaft speed. After that, the performance of the cycles with implementation of the four concepts is covered. Also, the effect of the concept variables on the thermal output is indicated.

### 4.2.1. Reference case

For variation of the shaft speed, the model turbine inlet temperature is kept constant, while the compressor and turbine are operated in off-design. This allows the model to calculate new fuel inputs. For the model in which the firing rate is varied, the shaft speed is kept constant and the compressor and turbine are operated in off-design, as well.

The performance of varying the shaft speed and firing rate for the standard PowerBurner-boiler setup is indicated in figures 4.3a and 4.3b. More specifically, figure 4.3a shows that the thermal efficiency of the setup is higher at lower thermal outputs, which is at decreased shaft speeds. The electrical efficiency shows a slight decrease.

Both observations can be explained by the fact that the reduced shaft speed lowers the flow through the system. This, in turn, lowers the operating pressure inside the system. Lower pressure ratios over the turbine result in a decreased electrical output. The lowered flow results in lower stack losses relative to the fuel input. Therefore, the thermal efficiency is increased.

Reduction of the firing rate in figure 4.3b leads to a large decrease in the performance. A constant flow over the compressor in combination with a lowered fuel input result in a drop in the turbine inlet temperature, large stack losses and a reduced electrical power output.

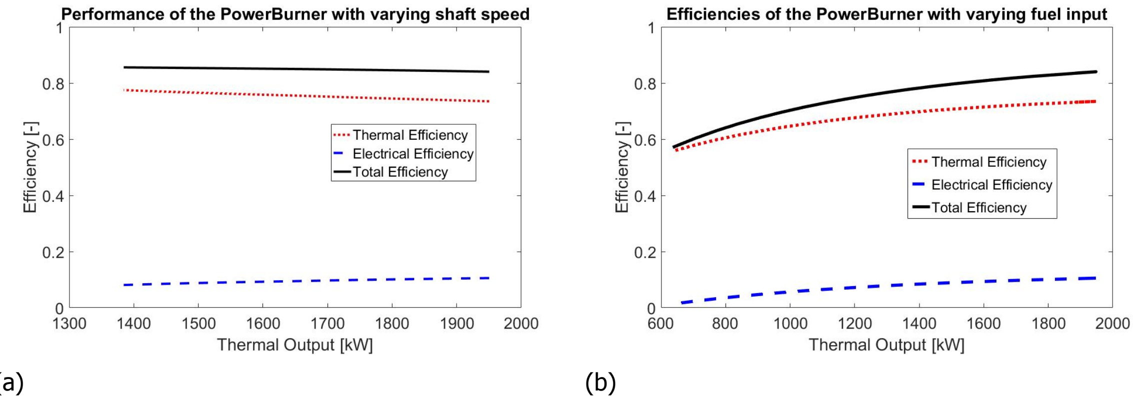


Figure 4.3: Performance of the standard PowerBurner-boiler setup with varying shaft speed (a) and varying firing rate (b)

### 4.2.2. Steam-injected PowerBurner-boiler setup

For this setup, steam from the boiler exhaust is injected in the combustion chamber. Figure 4.4b shows that the thermal output of the steam-injected setup decreases linearly with increasing injection rates. This is obvious, as the amount of steam injected in the combustion chamber is directly taken from the boiler output. The steam injection rate is varied from 0 to 1 kg/s. Thermoflex does not allow higher injection rates.

In this model, the turbine inlet temperature is kept constant at a turbine inlet temperature of 1173 K. Also, the shaft speed is kept constant. At specific steam injection rates, Thermoflex calculates the amount of fuel required to reach the turbine inlet temperature. This results in new mass- and energy balances over the system. By setting the compressor and turbine to off-design, the performances at different injection rates is defined as Thermoflex reads the according values from the compressor- and turbine maps.

In terms of performance, figure 4.4a shows the efficiencies at varying thermal outputs. Here it can be observed that, at lower thermal outputs (and thus higher injection rates), an increase in electrical efficiency occurs, as well as a large decrease in thermal efficiency.

More fuel is required to reach the turbine inlet temperature, as the injected steam cools down the products in the combustion chamber. The combination of a larger fuel input and the reduced thermal output results in a rapid decrease of the thermal efficiency. Although the combustion of more fuel allows for the reduction of excess air, the stack losses of this setup are still large due to the extra mass flow of the injected steam.

The constant compressor flow, in combination with the injected steam, results in a larger flow inside the system. This increases the pressure between the compressor and turbine. Therefore, the compressor uses more work. The extra work that can be extracted from the turbine due to the higher pressure ratio outweighs this, and thus a larger net electrical output can be achieved.

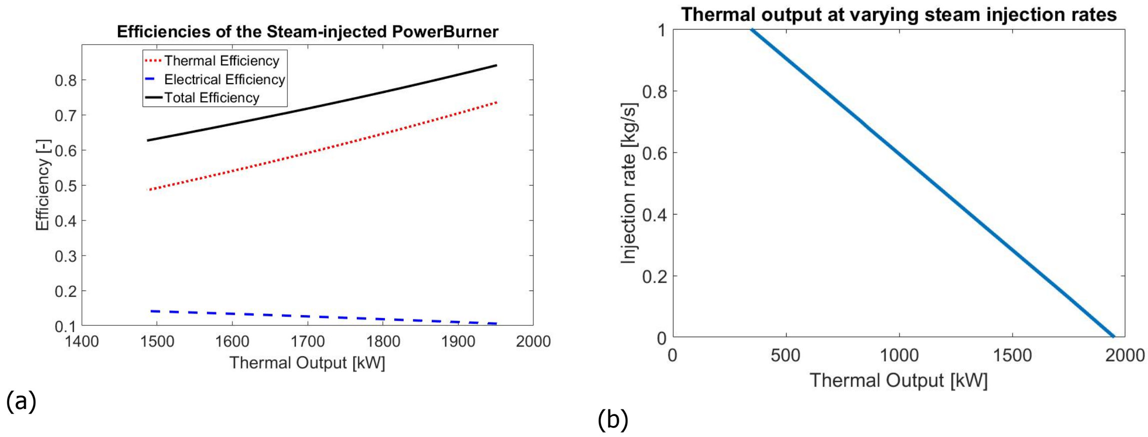


Figure 4.4: Performance of the steam-injected PowerBurner-boiler setup at specific thermal outputs (a) and thermal output as a function of the injection rate (b).

### 4.2.3. Flue-gas recirculated PowerBurner-boiler setup

In flue gas recirculation, exhaust gases are fed back to the compressor inlet. For this setup, the turbine inlet temperature and shaft speed are held constant. At varying recirculation ratios, Thermoflex calculates the amount of fuel required to reach the turbine inlet temperature. With this, the mass- and energy balances over the system can be calculated. The compressor- and turbine modes are set to off-design, which results in the performance being calculated from the respective maps.

Increased recirculation ratios result in higher inlet temperatures, and thus in lower thermal outputs. This can be observed in figure 4.5b. The recirculation ratio is varied from 0 to 68%. Varying the ratio beyond 68% will result in a deficiency in oxygen in the combustion chamber. Because of this deficiency, not enough fuel can be burned to achieve the turbine inlet temperature.

Due to the higher compressor outlet temperature, less fuel is required to reach the turbine inlet temperature. This has a positive effect on both the thermal- and electrical efficiency. But, figure 4.5a shows that the electrical efficiency is decreased. The reduced mass flow in the system results in a lower operating pressure. Both the turbine- and compressor work are reduced but the reduction in turbine work is larger than the reduction in required compressor work. Therefore, the electrical output and -efficiency are reduced at increased recirculation ratios. As the amount of flow over the system is reduced the stack losses are lowered as well. This results in a higher thermal efficiency.

### 4.2.4. PowerBurner-boiler setup with Velox-type boiler

In the Velox-type boiler of the PowerBurner setup extra fuel is burned. The increased temperature in the combustion chamber is lowered by transferring heat to a boiler, of which the tubes surround the chamber. As the heat is directly used to produce steam, the thermal output increases with increasing extra fuel inputs, as is indicated in figure 4.6b. For this system, the extra fuel input is varied from 0 to a maximum of 4.8 MW based on the LHV of natural gas, as at this point, the exhaust oxygen content is reduced to 3 vol%.

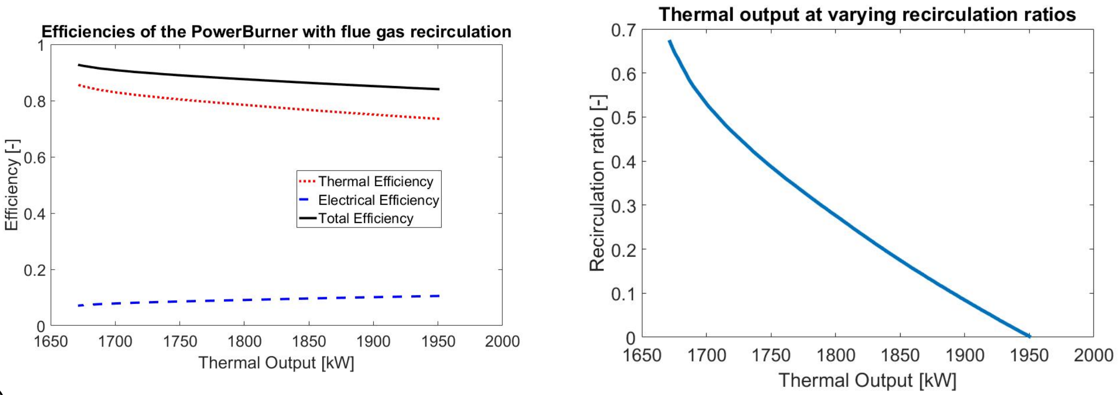


(a) (b)

Figure 4.5: Performance of the flue-gas recirculated PowerBurner-boiler setup at varying thermal outputs (a) and thermal output as a function of the recirculation ratio (b).

In the model, the shaft speed is held constant. The gas-side outlet temperature of the Velox-boiler is set at 1173 K, which is the turbine inlet temperature. By varying the combustor outlet temperature to values higher than the TiT, the surplus of heat is transferred to water in the Velox boiler. As this affects the mass flow and pressure inside the system, the turbine and compressor are modeled in off-design and their performance follows from the maps.

The flow in the compressor remains constant so the combustion of extra fuel reduces the excess air in the exhaust, which lowers the stack losses. This can be observed in figure 4.6a, where the thermal efficiency is increased at higher thermal outputs. The additional fuel results in a slight increase in mass flow in the combustion chamber and thus in the operating pressure. This results in a very small increase in electrical output, but as the fuel input is also increased, a decrease in electrical efficiency is observed in figure 4.6a. Overall, the increase in thermal efficiency is larger than the decrease in electrical efficiency, as the total efficiency is improved.

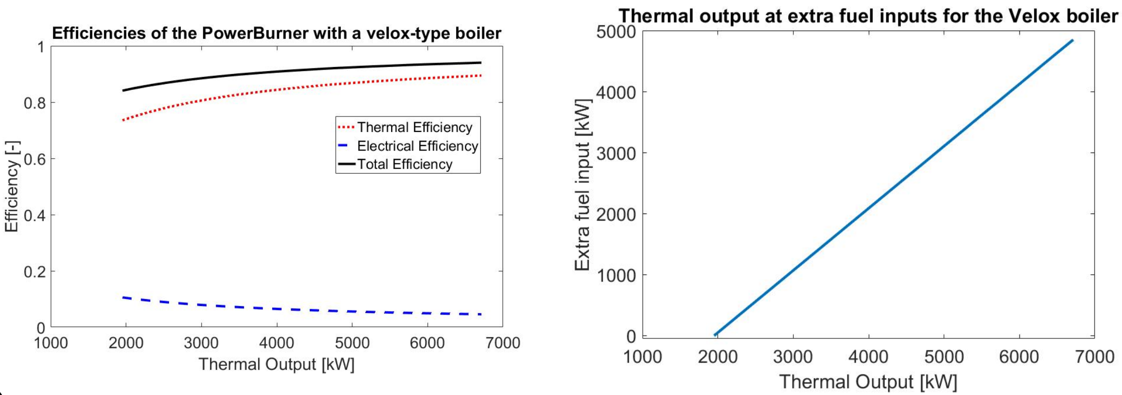


(a) (b)

Figure 4.6: Performance of the PowerBurner-boiler setup with Velox-type boiler (a) and thermal output as a function of the extra fuel added (b).

### 4.2.5. Supplementary-fired PowerBurner-boiler setup

For the supplementary-fired system, extra fuel is combusted with exhaust gases from the gas turbine. This allows for an increase in the thermal output of the boiler, as indicated in figure 4.7b. The extra fuel input is varied from 0 to a maximum of 4.8 MW based on the LHV of natural gas, as this results in 3 vol% oxygen in the exhaust.

The whole PowerBurner setup can be kept constant in Thermoflex, except for the turbine- and compressor performance, which are set to off-design. These vary, as a larger fuel injection in the exhaust result in larger pressure losses in the exhaust. Therefore, the turbine outlet pressure is lowered and a new pressure ratio over both components is required.

The excess air is reduced through the combustion of more fuel. This results in a decrease in stack losses and an increase in the thermal efficiency. Pressure losses over the burner in the duct in combination with the extra fuel input result in a reduction in the electrical efficiency.

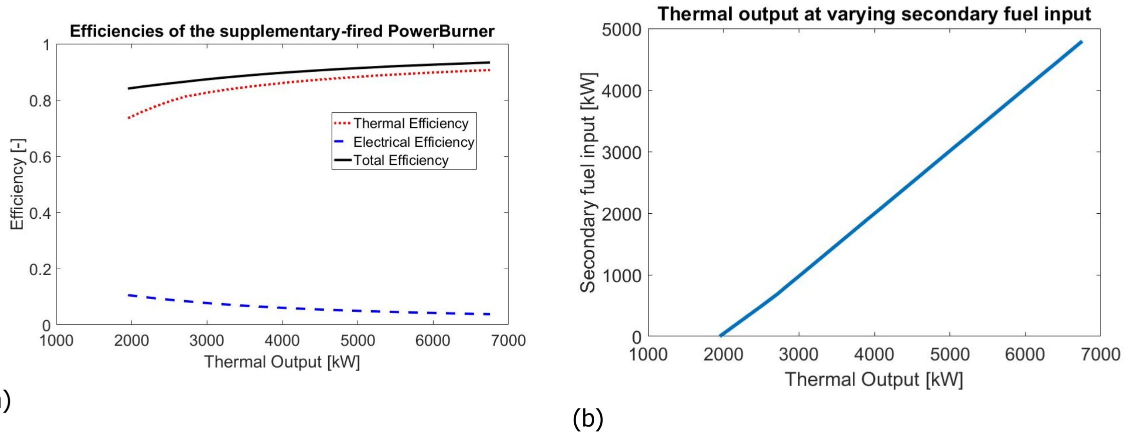


Figure 4.7: Performance of the supplementary-fired PowerBurner-boiler setup at varying thermal outputs (a) and thermal output as a function of the secondary fuel input (b).

## 4.3. Comparison of the results

From the analyzed setups, all methods but lowering of the firing rate induce a reduction in the excess air in the system. Two general effects on the thermal output of the PowerBurner-boiler setup are observed:

- Reduction of the thermal output;
- Increase of the thermal output.

Reduction of the shaft speed and firing rate, as well as flue gas recirculation and steam injection all lower the thermal output of the system. Implementation of supplementary firing and a Velox-type boiler allow for an increase in the thermal capacity on the other hand.

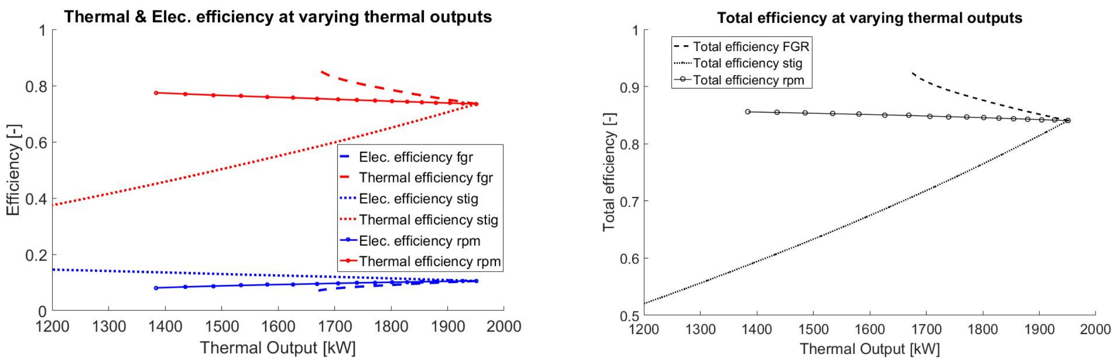


(a) Thermal- and electrical efficiency (b) Total efficiency

Figure 4.8: Efficiencies versus thermal output for flue gas recirculation (FGR), steam injection (STiG) and shaft speed variation (rpm) of the PowerBurner-boiler setup.

An overview of the methods that decrease the thermal output of the PowerBurner-boiler setup is indicated in figure 4.8. In order to achieve a thermal output which is larger than that of the PowerBurner-boiler setup at standard operation, several of these systems are to be employed. Variation of the firing rate is left out of this figure, as from figure 4.3b follows that it is never a better option than variation of the shaft speed.

From this figure it follows that, at any required thermal demand, steam injection offers the lowest thermal- and total efficiency, but the highest electrical efficiency. Also, this option is scalable in thermal output over the largest range, which allows for the best operational flexibility. The injected steam cannot be retrieved from the exhaust, however, which increases the operational expenses of this system.

Extension of the PowerBurner-boiler setup with flue gas recirculation offers the largest thermal- and total efficiency but at the lowest electrical efficiency at any given thermal output. On top of that, it is not possible to scale down the thermal output of the flue-gas recirculated system as much as the steam injection cycle or the cycle with varying shaft speeds. But, as the total efficiency is largest over its operating range, implementation of flue gas recirculation results in the lowest stack losses.

Through variation of the the shaft speed, the current PowerBurner-boiler setup offers a balanced solution between the other two concepts, as it provides neither the best nor the worst thermal-, electrical-, and total efficiency and scale down capacity over the operating range.

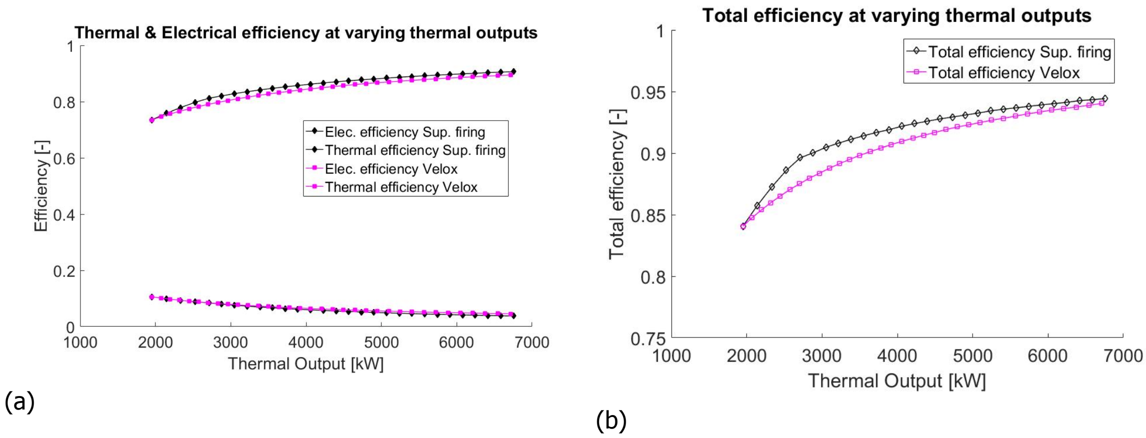


Figure 4.9: Thermal & Electrical efficiency (a) and total efficiency (b) at varying thermal outputs for supplementary firing (Sup. firing) and the Velox-type (Velox) boiler extensions of the PowerBurner-boiler setup.

Figure 4.9 shows the efficiencies at specific thermal outputs of the methods that increase the thermal capacity. From this figure follows that the thermal efficiency of the supplementary-fired system is better at any thermal output, as well as the total efficiency compared to the Velox-setup. Therefore, stack losses are lower at any thermal output for the supplementary-fired system. The electrical efficiency is comparable for both systems.

The higher thermal efficiency of the supplementary-fired system is a result of the implementation of the economizer at the boiler outlet. The burner in the exhaust allows for a higher boiler inlet temperature. This results in a lower stack temperature of the flue gases due to the pinch point. This process is displayed in figure 4.10. Due to the lowered stack temperature, the stack losses are lower and the thermal efficiency is higher. Therefore, if the boiler at the PowerBurner exhaust includes an economizer, the cycle extended with supplementary firing has the highest thermal efficiency. This effect will not be present if there is no economizer.

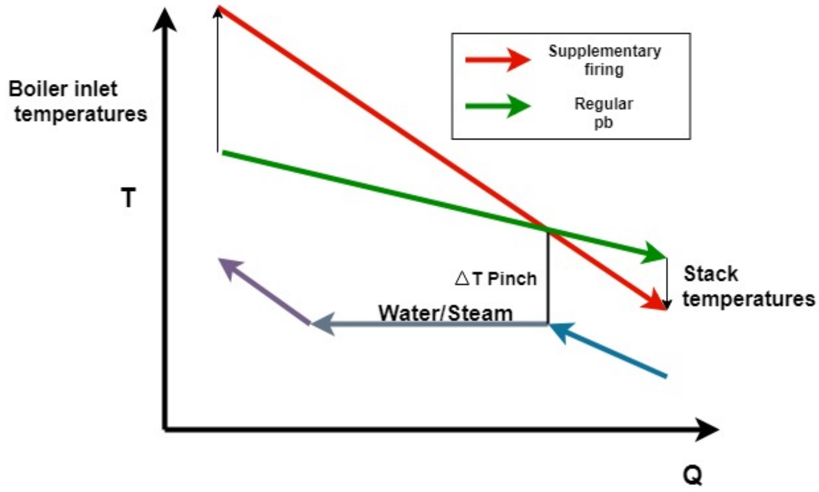


Figure 4.10: QT-diagram indicating the difference in stack temperatures with implementation of an economizer.

An overview of the variation in the PowerBurner operating ranges, caused by the implementation of each concept, is indicated in figure 4.11. Under the assumption that only a single improvement is implemented, operation of the Velox-setup or supplementary-fired system at thermal outputs below 1950 kW is done through reduction of the shaft speed. For the other methods to achieve a thermal output larger than that of a single PowerBurner-boiler setup, multiple systems are required.

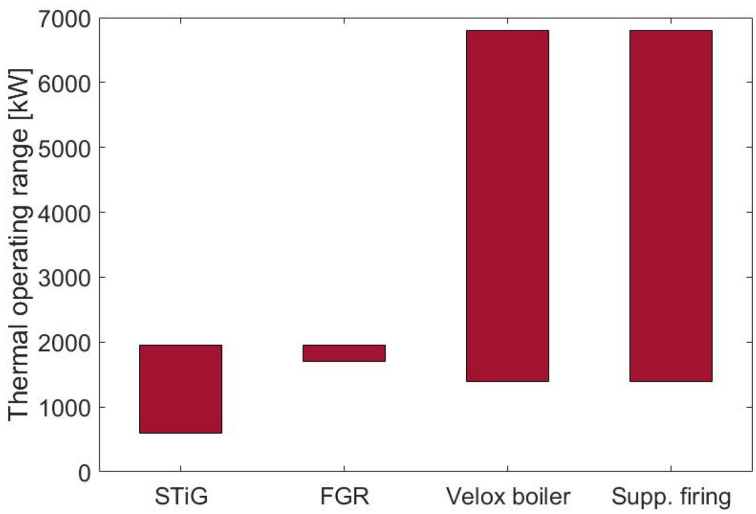


Figure 4.11: Thermal operating range for each extension of the PowerBurner-boiler setup.

## 4.4. Conclusion

The effect of each setup on the thermal- and electrical output is displayed in table 4.2.

| Method | Effect on thermal output | Effect on stack losses | Excess air reduction through | Effect on thermal efficiency | Effect on electrical efficiency |
|---|---|---|---|---|---|
| Shaft speed reduction | ⇓ | ⇓ | Less air required | ⇑ | ⇓ |
| Firing rate reduction | ⇓ | ⇑ | - | ⇓ | ⇓ |
| Steam injection | ⇓ | ⇑ | Larger fuel input | ⇓ | ⇑ |
| Flue gas recirculation | ⇓ | ⇓ | Less air required | ⇑ | ⇓ |
| Velox-type boiler | ⇑ | ⇓ | Larger fuel input | ⇑ | ⇓ |
| Supplementary firing | ⇑ | ⇓ | Larger fuel input | ⇑ | ⇓ |

Table 4.2: Results of the thermodynamic analysis of each extension of the PowerBurner-boiler cycle. Upwards arrow indicates an increase in the specific aspect.

Based on the results of this chapter, a conclusion can be drawn on which concept performs best in the following characteristics:

- Thermal output & efficiency;
- Electrical output & efficiency;
- Thermal capacity;
- Total efficiency.

In terms of the thermal capacity, only the supplementary-fired system and the Velox-type boiler allow for an increase compared to the current PowerBurner setup. Both can increase the thermal output by up to 4.8 MW at 3 vol% oxygen in the exhaust. These systems allow for the largest increase in thermal capacity. Through application of steam injection, the lowest thermal outputs can be achieved. Flue gas recirculation impacts the thermal capacity the least.

In terms of total efficiency, for the methods that allow for operation at lower thermal outputs, flue gas recirculation has the highest total efficiency and thus the lowest stack losses. Second is the current PowerBurner-boiler setup, in which the thermal output is lowered through reduction of the shaft speed. Steam injection performs worst in terms of total efficiency at any thermal output.

For the methods that allow for an increase in the thermal capacity, implementation of supplementary firing allows for a slightly higher total efficiency and lower stack losses than the Velox-type boiler at any thermal output.

Implementation of supplementary firing to the PowerBurner-boiler setup allows for the largest increase in thermal efficiency, closely followed by the system with the Velox-type boiler. Flue gas recirculation allows for high thermal efficiencies at lowered thermal outputs, whereas steam injection results in the lowest thermal efficiency.

The steam-injected system does allow for the highest electrical efficiency at any thermal output below that of the standard PowerBurner-boiler setup. The current setup achieves the second best electrical efficiencies through variation of the shaft speed, whereas flue gas recirculation has the lowest electrical efficiency at any thermal output. The system with the Velox-type boiler has a slightly higher electrical efficiency than the supplementary-fired setup.

With the resulting inputs and outputs of each improvement to the PowerBurner-boiler setup available, it is possible to perform a more detailed economic analysis, which is treated in the next chapter. The best concept was chosen based upon the results of both this and the next chapter.

# 5

# Economic analysis

In this chapter, the economic performance of the four extensions to the PowerBurner-boiler system are analyzed. These extensions are:

- Steam injection (STiG);
- Flue gas recirculation (FGR);
- The Velox-type boiler (Velox);
- Supplementary firing (Sup. Firing).

From the analysis of this chapter, the performance in three of the following characteristics can be determined:

- Increased profitability compared to a conventional Burner;
- Low system cost;
- Profitable over a large operating range.

The thermal- and electrical output and the fuel input, following from the thermodynamic analysis of chapter 4 are used to determine the profitability. The profitability for each cycle can then compared at specific thermal outputs in order to determine which cycle offers the best economic viability. On top of that, a qualitative analysis of the CAPEX (Capital Expenditures) is performed.

In the first section of this chapter, the profitability is defined. Next, the results are indicated and elaborated for each concept. After that, the results are compared. Finally, an analysis of the required CAPEX for each concept follows, along with the selection of the best performing concept.

## 5.1. Definition of the profitability for the end-user

The profitability of a PowerBurner-boiler setup at any specific thermal output is defined as the revenue of the generated electricity minus the expenses of fuel:

$$Prof_{pb} = P_{elec}E_{elec} - Q_{fuel}E_{fuel} \tag{5.1}$$

In this equation, $P_{elec}$ is the electricity production in kW in an hour. $E_{elec}$ and $Q_{fuel,pb}$ are the electricity- and fuel price per kW, respectively. $Q_{fuel}$ is the amount of fuel used in one hour, in kW, required by the PowerBurner-boiler setup to achieve a specific thermal output $Q_{out}$. With these parameters, the profitability ($Prof_{pb}$ in € per hour) is determined.

A price ratio is introduced. With this price ratio, it is possible to determine the profitability of a system in different cases. This is defined as the ratio of electricity price over the fuel price.

$$PR = \frac{E_{elec}}{E_{fuel}} \tag{5.2}$$

The prices and price ratios for different countries in the EU are defined in table 5.1. The source of the price data is indicated for each location and company size. Both the electricity- and gas price include the full price which is to be paid for the consumption by a company. This includes the costs of transportation, delivery and taxes. A more elaborate breakdown of these prices is supplied in appendix A.

Table 5.1: Overview of 2017 prices and price ratios for different-sized industrial consumers of gas and electricity in the EU.

| Country | Company Size | Gas Price €/kWh | Electricity Price €/kWh | Price Ratio |
|---|---|---|---|---|
| Netherlands | S [33] | 0.022 | 0.069 | 3.14 |
| Netherlands | M [33] | 0.02 | 0.041 | 2.05 |
| Netherlands | L [33] | 0.019 | 0.039 | 2.05 |
| Belgium | S [33] | 0.021 | 0.078 | 3.7 |
| Belgium | L [33] | 0.02 | 0.046 | 2.3 |
| Germany | S [33] | 0.027 | 0.0123 | 4.56 |
| Germany | L [33] | 0.023 | 0.065 | 2.83 |
| France | S [33] | 0.033 | 0.09 | 2.73 |
| France | L [33] | 0.025 | 0.03 | 1.73 |
| Italy | M [34, 35] | 0.0253 | 0.142 | 5.6 |

Applying the price ratio to equation 5.1 results in:

$$Prof_{pb} = (P_{elec}PR - Q_{fuel,pb})E_{fuel} \tag{5.3}$$

In order to determine the added value of the implementation of the improved PowerBurner-boiler setup for the end-user, the profitability is compared to making use of a burner for the production of an equal amount of steam. This takes into account the revenue from electricity of the PowerBurner system and the lower thermal efficiency compared to a classic boiler-burner setup. The boiler with conventional burner is assumed to have a thermal efficiency of 95 %. The profitability of the improved PowerBurner-boiler setup compared to making use of a burner to fire a boiler is indicated in equation 5.4.

$$Prof_{pb} = E_{fuel}(P_{elec}PR - (Q_{fuel,pb} - \frac{Q_{out}}{0.95})) \tag{5.4}$$

With this equation, the profitability of the implementation of the four concepts is determined in the next section.

## 5.2. Analysis of the profitability for the end-user

In the following plots, for each extension to the PowerBurner-boiler setup, the profitability is indicated at different thermal outputs and price ratios in order to asses the performance in different locations and at different thermal demands. The price ratio is varied from 0.5-6, which covers every case of table 5.1. After that, the effect of each case is explained in more detail. For the gas price, a standard of €0.02 per kWh is used in every case to simulate operation in a Dutch environment.

### 5.2.1. Profitability of the steam-injected PowerBurner

Figure 5.1 indicates the profitability of the steam-injected PowerBurner-boiler combination. This figure demonstrates that the profitability compared to a conventional burner for an equal thermal output is generally below 0.

At reduced thermal outputs, the thermal efficiency is very low for this system (see figure 4.4a). So in most cases, the revenue from the increased electrical output does not outweigh the cost for the extra fuel which is required to produce a specific thermal output. Only in the cases where the price of electricity is high (at high price ratios) it is more profitable to employ this system.

### 5.2.2. Profitability of the flue-gas recirculated PowerBurner

Profitability of the PowerBurner-boiler setup with flue gas recirculation is indicated in figure 5.2. This figure shows that the profitability of the system at specific thermal outputs compared to making use

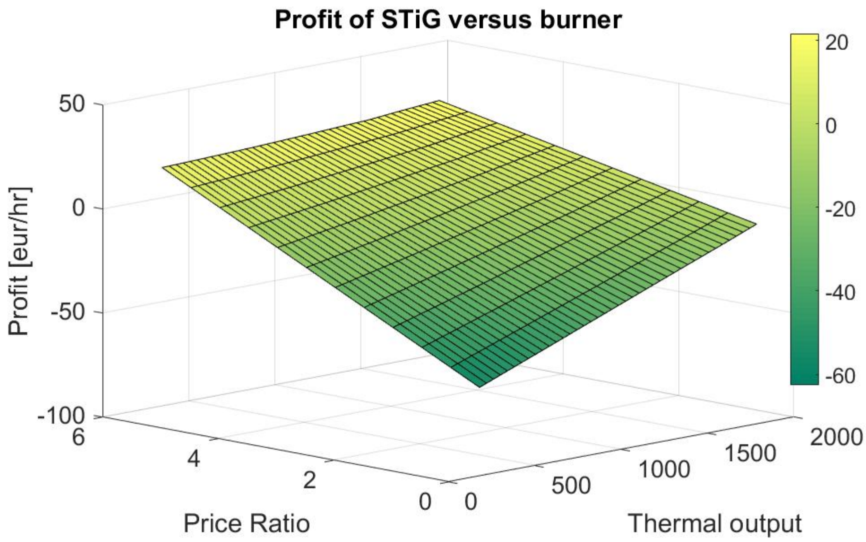


Figure 5.1: Profitability of the PowerBurner setup with steam injection at varying price ratios.

of a conventional burner, is always larger than 0 at price ratios over 2.

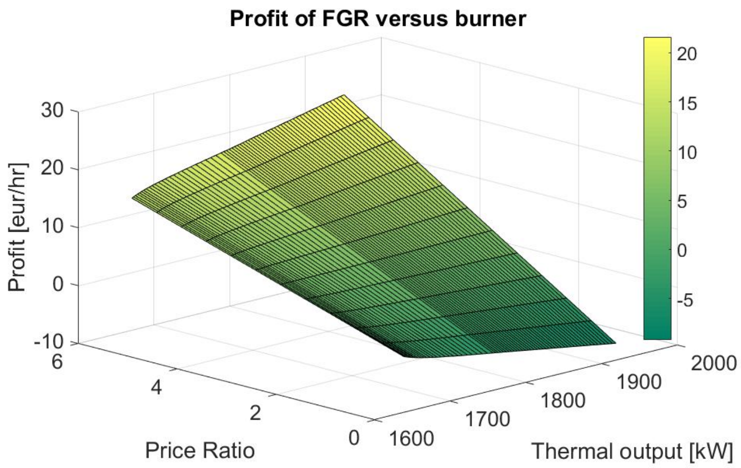


Figure 5.2: Profitability of the PowerBurner setup with flue gas recirculation at varying price ratios.

Decreasing the thermal output by increasing the flue gas recirculation ratio results in a higher thermal, and lower electrical efficiency (see figure 4.5a). At low price ratios, the profitability is dominated by the difference between the fuel usage of the system and of a burner. Therefore, the profitability increases at lower thermal outputs and price ratios, as the difference in fuel usage is reduced.

On the other hand, as the profitability is dominated by the revenue from electricity at high price ratios, the profitability is reduced when the recirculation ratios is decreased. This is a result of the lowered electrical efficiency.

### 5.2.3. Profitability of the PowerBurner setup with Velox-type boiler

Figure 5.3 indicates the profitability of the Velox setup at varying price ratios and thermal outputs. From figure 4.6a followed that the thermal efficiency of the system increases with at higher thermal outputs, whereas the electrical efficiency decreases.

Figure 5.3 shows that at increased thermal outputs, the profitability is increased. This is due to the decrease in extra fuel required, compared to a conventional burner for an equal thermal output. The effect is more profound at higher price ratios, where the revenue from electricity dominates the profitability. The increased electrical output has a larger effect on the profitability in this situation.

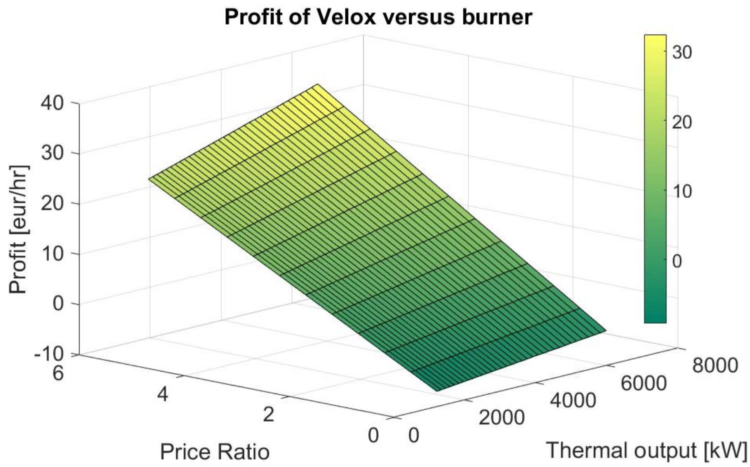


Figure 5.3: Profitability of the PowerBurner setup with a Velox-type boiler at varying price ratios.

### 5.2.4. Profitability of the supplementary-fired PowerBurner setup

In figure 5.4, an increase in profitability can be observed for the supplementary-fired system at higher thermal outputs. Figures 4.7a and 4.7b show an increase in thermal efficiency and -output and a decrease in electrical efficiency at increased secondary fuel inputs. This results in a larger profitability at higher thermal outputs. As the electrical efficiency decreases, the increase is a result of the lowered extra fuel requirement compared to a conventional burner at equal thermal outputs.

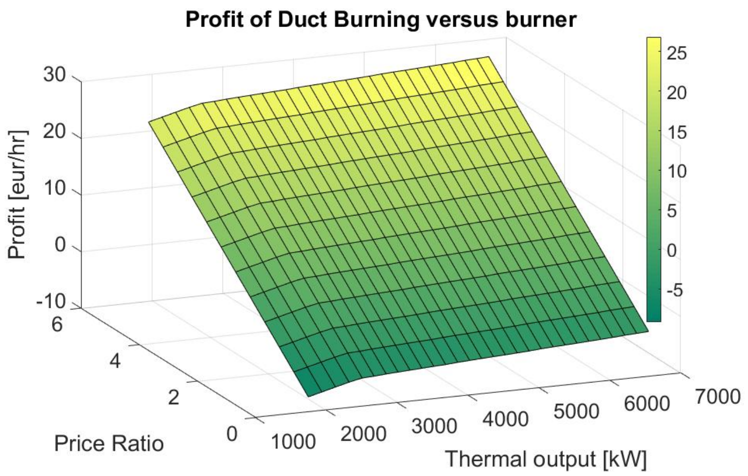


Figure 5.4: Profitability of the PowerBurner setup with supplementary firing at varying price ratios.

Up until a thermal output of about 2500 kW, an extra steep increase in profitability can be observed. This is due to the economizer, present in the boiler. As the flue gas temperature rises most at the lower secondary fuel flows, the effect of the increased boiler inlet temperature on the economizer outlet is the largest.

## 5.3. Comparison of the results

In this section, the results of the profitability analysis for the four PowerBurner-boiler improvement concepts are compared. This is done at a price ratio of 3, which is the average from table 5.1, and a price ratio of 2, to determine the effect of lower electricity prices.

Figure 5.5 indicates the profitability of the flue gas recirculated system, steam injection and shaft speed variation. The flue gas recirculated system has the highest profitability over its full thermal operating range. Variation of the shaft speed shows a much higher profitability than the steam injected system at equal outputs.

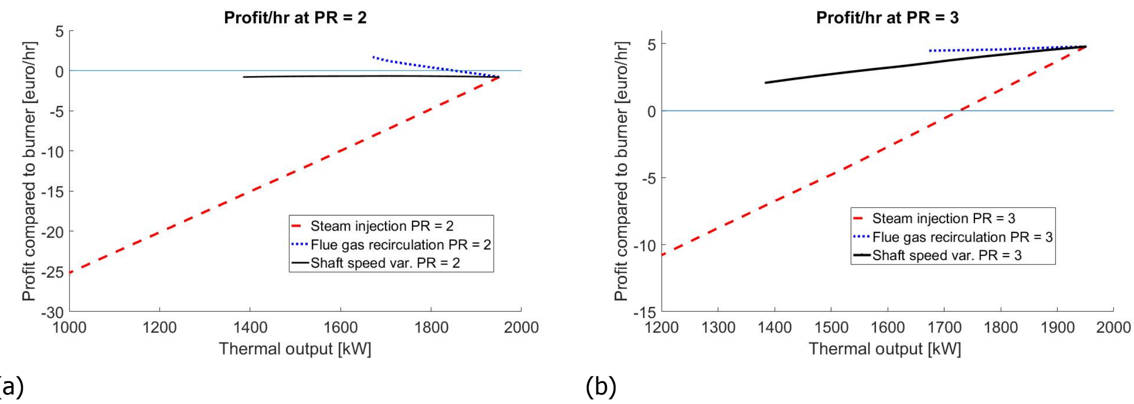


Figure 5.5: Profit/hr at varying thermal outputs for ratios of 2 (a) and 3 (b) of the PowerBurner including steam injection, flue gas recirculation and shaft-speed variation.

From figure 5.5 it can be seen that the system must be implemented in a case in which the price ratio is larger than 2, before shaft speed variation is more profitable than a conventional burner over the full range of thermal outputs. Flue gas recirculation allows for a profitable case at price ratios of 2 and lower.

At increased price ratios, the PowerBurner itself becomes more profitable than a conventional burner for the generation of steam, as the profitability at a thermal output of 1950 kW is larger than 0. The difference in profitability between flue gas recirculation and shaft speed variation reduces because at high price ratios, the profitability is dominated by the revenue from electricity. As the electrical efficiency is lower at lower thermal outputs for the system with flue gas recirculation, the profitability difference is reduced.

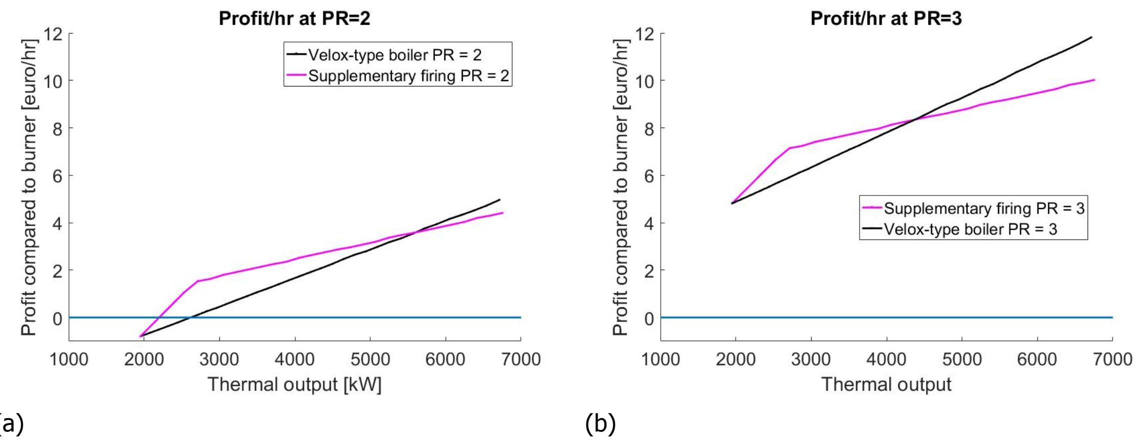


Figure 5.6: Profit/hr at varying thermal outputs for ratios of 2 (a) and 3 (b) of the PowerBurner including the Velox-type boiler and Supplementary firing.

Figure 5.6 indicates the profitability of the supplementary-fired PowerBurner- boiler and the setup with the Velox-type boiler, compared to a conventional burner for an equal thermal output. The supplementary-fired setup has a larger profitability at lower thermal outputs. This is due to the effect of the economizer on the thermal efficiency, as elaborated with figure 4.7a. At higher thermal outputs, the figure shows that the Velox has a higher profitability, which is due to the increased power output.

The range of thermal outputs over which it is more profitable to operate a certain setup, compared to a conventional burner, is indicated in figure 5.7, for price ratios varying from 1-5. This figure indicates that the supplementary-fired setup is profitable over the largest range of outputs and price ratios.

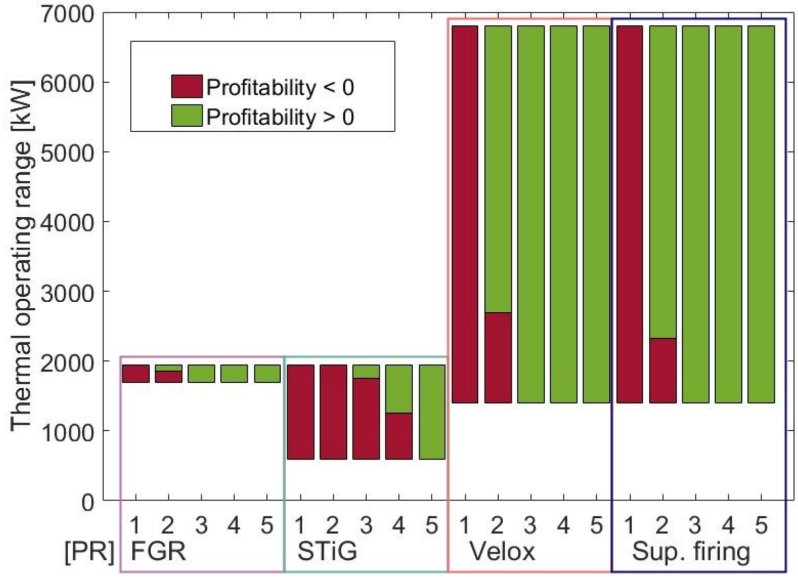


Figure 5.7: Range of thermal outputs with positive profitability at varying price ratios.

## 5.4. System costs analysis

The costs required for the improved PowerBurner-boiler setup are an important factor for both the end-user and Innecs. Whether or not the end-user employs such a system, depends on the payback time. This directly relates to the CAPEX (Capital Expenditures), required for the purchase of the system, in the following manner (equation 5.5).

$$Y_{pb} = \frac{CAPEX_{pb}}{Prof_{pb,year}} \tag{5.5}$$

In this equation, $Y_{pb}$ is the payback time in years and $Prof_{pb,year}$ is the total profit gained from operating the system in a year. Payback times for systems like the PowerBurner generally have to be below 5 years before the implementation is even considered. Therefore, by maintaining the CAPEX low, it is possible to address a large market.

As it is not possible in this stage of the process to provide accurate estimates of the cost for the extension of the PowerBurner setup with each concept, the costs are compared qualitatively. For this, two cases are distinguished: One where the required output is below that of a single PowerBurner-boiler setup operating regularly ($\leq$ 2 MW), and one larger than that of the single setup.

The required CAPEX for each system is rated as "low", "medium" or "high" as compared to the others. The results for each case are captured in table 5.2.

| **Concept/ Output** | **Steam injection** | **Flue gas recirculation** | **Velox-type boiler** | **Supplementary firing** |
|---|---|---|---|---|
| **$\leq$ 2 MW** | Low | Low | High | Medium |
| **$>$ 2 MW** | High | High | High | Low |

Table 5.2: Overview of the expected CAPEX required for the extension of the PowerBurner-boiler setup with a specific concept.

For the case in which the thermal output is equal to- or below that of a single PowerBurner-boiler setup at normal operation, the concepts of steam injection and flue gas recirculation require extra piping (see chapter 3) and some minor extra components. Therefore, the required CAPEX of these systems is marked as "low".

For the Velox-type boiler, a complete boiler with a thermal capacity of around 5 MW is to be implemented. Such an extension is most likely very expensive, and therefore the required CAPEX are marked as "high". In supplementary firing, an exhaust gas burner is required. This is most likely more expensive than the extensions required for steam injection or flue gas recirculation, but does not require as much CAPEX as the Velox boiler. Therefore, this is marked as ”medium”.

To reach a thermal output larger than 1950 kW with a PowerBurner including steam injection or flue gas recirculation, several systems are required to achieve such a thermal output. Therefore, the CAPEX required for these systems is marked as ”high”.

The setup with Velox-type boiler and supplementary firing do not need any alteration up until a thermal output of around 6.8 MW. As extension of the PowerBurner setup with supplementary firing requires much less CAPEX than for the Velox-boiler, the supplementary-fired system is marked as ”low” and the Velox, again, as ”high”.

## 5.5. Conclusions and concept selection

With the results of the economic analysis available, the performance of each concept in terms of three characteristics can be assessed. The characteristics are:

- Increased profitability compared to a conventional burner;
- Profitable over a large operating range;
- Low system cost

In terms of the profitability compared to a conventional burner at equal thermal outputs, application of the Velox-type boiler and supplementary firing to the PowerBurner-boiler setup allow for the largest increase. Figure 5.6 indicates that, at lower price ratios, supplementary firing is generally the most profitable solution, while at higher price ratios, the Velox-type boiler performs best.

At thermal outputs lower than that oft the PowerBurner-boiler setup at standard operation, flue gas recirculation allows for the most profitable operation. Steam injection is only a profitable solution at very high price ratios, whereas reduction of the shaft speed allows for positive profitability at price ratios over 2, which is indicated in figure 5.6.

Figure 5.7 indicates that the supplementary fired setup allows for the largest profitable operating range, followed closely by the Velox setup. This does include part-load performance through reduction of the shaft speed.

In terms of CAPEX required for each system, table 5.2 indicates that the supplementary-fired system is the most optimal when large thermal outputs are required. At such outputs, the cost of the flue gas recirculated and steam-injected system are high as multiple systems are required. The high expected CAPEX requirements of the Velox setup makes it the most undesirable option at lower thermal outputs.

### Concept selection

Table 5.3 depicts an overview of the performance characteristics and includes a ranking of the performance for each PowerBurner-boiler improvement based on the results from the previous 2 chapters.

| **Thermal Capacity** | **Total Efficiency** | **Thermal Efficiency** | **Electrical Output** | **CAPEX** |
|---|---|---|---|---|
| **1. Supp. firing** | 1. Flue gas recirculation | **1. Supp. firing** | 1. Steam injection | **1. Supp. firing** |
| 1. Velox-type boiler | **2. Supp. firing** | 2. Velox-type boiler | 2. Velox-type boiler | 2. Flue gas recirculation |
| 3. Steam injection | 3. Velox-type boiler | 3. Flue gas recirculation | **3. Supp. firing** | 2. Steam injection |
| 4. Flue gas recirculation | 4. Steam injection | 4. Steam injection | 4. Flue gas recirculation | 4. Velox-type boiler |

Table 5.3: Rating of the performance for each concept applied to the PowerBurner-boiler setup, based on 5 characteristics.

The ranking shows that the supplementary-fired system scores best in three out of five requirements. In terms of thermal capacity, the performance is equal to that of the setup with a Velox-type boiler. The flue-gas recirculated system has a slightly higher total efficiency, but can only achieve this at very low thermal outputs. In terms of thermal- and total efficiency, the supplementary-fired system performs slightly better than the Velox-type boiler.

The electrical output is clearly the highest for a steam-injected system, but it is only capable of achieving this at low thermal outputs. On top of that, from chapter 5 it follows that it is, in most cases, not a viable solution for replacing a conventional burner to produce steam in terms of profitability.

The PowerBurner-boiler system with supplementary firing performs similarly to the setup with Velox-type boiler in most aspects. The reason to choose the supplementary-fired system over the Velox-system follows from the system cost. As the Velox-type boiler requires much more CAPEX, while having a profitability similar to the supplementary-fired setup, it has a much larger payback time which prevents the end-user from employing such a system.

# 6

# Conceptual design of the supplementary burner

The analysis of the previous chapters showed that supplementary firing is the best concept that can be applied to the PowerBurner in terms of thermodynamic and economic performance. The aim of this chapter is to provide a conceptual design of such a burner. In order to do this, first, some theoretical background on burners and combustion is given. Based on the background, a set of requirements for the secondary burner for implementation in the PowerBurner-boiler setup indicated.

The choice of the burner type was made within the framework of the requirements. This is done based on data supplied by manufacturers of existing burners. After that, a 2D model of the burner is created and CFD (Computational Fluid Dynamics) is performed with ANSYS Fluent in order to determine its performance in terms of the requirements

Next, a suggestion for the design of the burner is given, by translating the 2D to a 3D model in Solidworks. In order to find out how well the translation from 2D to 3D is done and how this 3D geometry performs in terms of the requirements is determined in another CFD analysis. Finally, the 2D- and 3D models are compared to determine the accuracy of the results.

## 6.1. Background on combustion and burners

In combustion, a fuel and oxidant have an exothermic reaction. The oxidizer is air for most gas turbine applications, whereas the fuel can be many sorts of liquids or gases. Generally, a flame is present in the combustion process. The flame can be defined as a rapid chemical change in a thin layer of fluid with steep gradients of temperature and species concentration, accompanied by luminescence [7]. The flame front is is the interface between the burned- and unburned mixture.

Flames can be divided in two main categories: Premixed flames and non-premixed or diffusion flames. Premixed flames indicate that the fuel and oxidizer have been mixed before the combustion reaction takes place, as indicated in figure 6.1b. For a diffusion flame, they mix through diffusion of the oxidizer into the flame zone, as indicated in figure 6.1a.

For premixed flames, the rate of mixing occurs fast in comparison to the chemical reaction rate of the oxidation reaction. Therefore, the reaction rate determines the combustion rate. In diffusion flames, on the other hand, the mixing is slow compared to the chemical reaction rate. The mixing rate is therefore the controlling rate.

Depending on flow velocities, the flames can either be laminar or turbulent. The flame being laminar or turbulent has a large effect on the flame speed of premixed flames. This is the speed at which the flame propagates over the flammable mixture of air and fuel and is generally around 0.4 m/s for stoichiometric combustion of hydrocarbon fuels [8], whereas turbulent flame speeds can be a factor 100 times larger, which affects flame stability.

Stoichiometric combustion is combustion in which the exact amount of oxygen is available so that all fuel is oxidized. For the combustion of methane, this results in the following reaction:

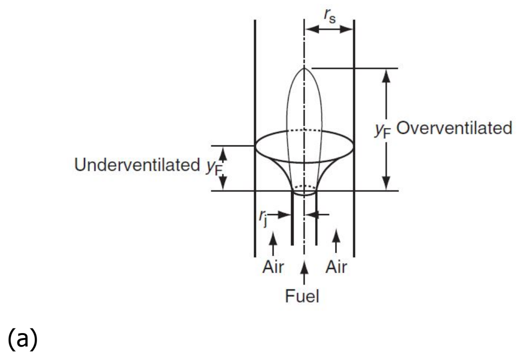


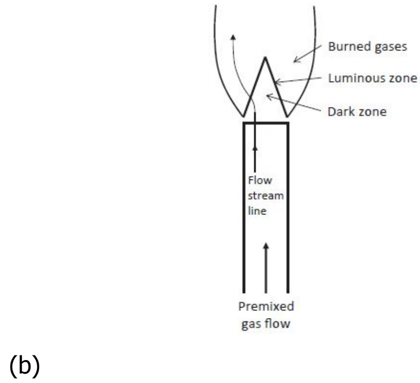


Figure 6.1: Two flame types: A Laminar diffusion flame [7] (a) and a Laminar premixed flame [8] (b).

$$CH_4 + 2O_2 \rightarrow CO_2 + 2H_2O \tag{6.1}$$

For the combustion of methane with ambient air containing 21 vol% oxygen, a stoichiometric air-to-fuel ratio can be defined (AFR$_{st}$), which indicates the mass flow of air required for the combustion of 1 kg of methane. This is defined in equation 6.2.

$$AFR_{st} = \frac{\dot{m}_{air}}{\dot{m}_{methane}} = 17.2 \tag{6.2}$$

Based on the air-to-fuel ratio, the equivalence ratio $\phi$ is defined as the ratio of the actual air-to-fuel ratio to the stoichiometric air-to-fuel ratio (equation 6.3).

$$\phi = \frac{AFR}{AFR_{st}} \tag{6.3}$$

For $\phi > 1$, the mixture is rich in air i.e. more air is available than can be oxidized with the amount of fuel available. On the other hand, if $\phi < 1$, the mixture is lean in air, which indicates not all fuel can be oxidized due to the lack of oxygen.

Lefebvre and Ballal [7] suggests several aspects which are important in the design of a combustor for gas turbines. Of these, the following five can directly be translated to design considerations for an exhaust gas burner. This section aims to elaborate on these aspects and indicate how the burner design can influence its performance.

- High efficiency;
- Reliable ignition;
- Wide stability limits;
- Low Pressure losses;
- Low emissions.

### 6.1.1. Combustion efficiency

The combustion efficiency defined as the heat released through combustion over the heat available in the fuel (equation 6.4).

$$\eta_c = \frac{Q_{released}}{Q_{available}} \tag{6.4}$$

Not only does a low combustion efficiency represent waste of fuel, it also contribute to the emission of pollutants like carbon monoxide and unburned hydrocarbons (UHC's) [7]. Therefore, combustion efficiencies of over 99% are often required and it is important that the burner design allows for the complete combustion of fuel over the whole operating range.

### 6.1.2. Ignition

Ignition of a fuel-air mixture can be done through forced ignition and spontaneous ignition. In forced ignition, a minimum amount of ignition energy is required to ignite the flow. This is supplied through a spark plug, pilot flame or various other methods.

Spontaneous ignition occurs if enough energy is available. For different types of fuels, this occurs at specific autoignition temperatures. Below this temperature, no ignition occurs even after an extended period of time [8]. If the autoignition temperature is achieved, a specific amount of time is required before the ignition occurs. This is the autoignition delay time.

### 6.1.3. Flame stability

In order to maximize the thermal capacity over which a burner can operate, it is necessary for the burner to be able to produce a stable flame. A stable flame can indicate two things: The flame has stable operation over a large range of air-to-fuel ratios, or the blowout velocity is high.

Based on the air-to-fuel ratio, extinction can occur as ”lean extinction” in which there is not enough fuel available for a flame to be present, or ”rich extinction”, in which there is an excess of fuel so large that no flame can persist. The air-to-fuel ratios at which this occurs are the lower- and upper flammability limits. Increasing the pressure or temperature results in a reduction in the lower flammability limit and an increase in the upper limit.

A downside of premixed flames is that a flashback can occur: The flame travels backwards to the source of the fuel and oxidizer mixture. In figure 6.1b this would mean the flame travels in the opposite direction of the premixed flow. This is possible if the flame speed exceeds the gas flow velocity and occurs if the velocity of the fuel-air mixture is lower than the flow velocity or in locations of low velocity caused by boundary layers.

For a premixed flame, if the mixture flow velocity exceeds the flame speed, the flame front is carried away by the gas mixture and can stabilize downstream of the ignition zone. Due to the decrease of the mixture velocity away from the source, it is possible for the flame to flash back again and settle at the initial condition. If the flow velocity keeps exceeding the flame velocity beyond the end of the stability limits, blowout occurs [8]. The velocity at which this occurs is the blowout velocity.

Beside operating outside the flammability limits, extinction of a flame also occurs when the time available for the chemical reaction becomes less than the time required for the generation of enough heat required for ignition [36]. This is in the case no continuous ignition (like through a pilot flame) is applied.

Methods are available to reduce the flow velocity or time available for the chemical reactions to occur. By locally slowing down the flow, a flame can be anchored at a specific location. This could result in a stable flame at the specific location over a large operating range.

One of the possibilities is by introducing a bluff body in the flow. This is depicted in figure 6.2a. The

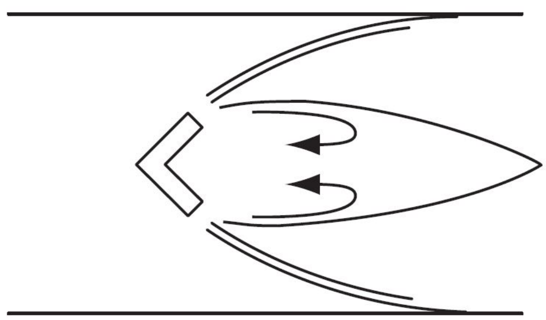

(a) Low-velocity zone by a bluff-body[37].

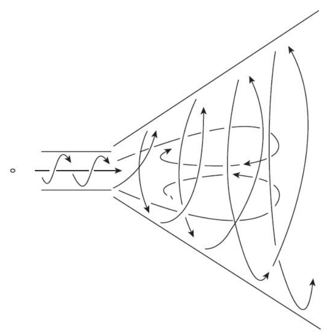

(b) Low-velocity recirculation zone through swirling [8].

Figure 6.2: Two methods to introduce a low-velocity zone for better combustion stability.

wake behind the body should allow the combustion products to have enough time to react, through which the adjacent mixture can be ignited continuously. Also, it ensures the flow velocity is never larger than the blowout velocity. Therefore, the flame is anchored at the low velocity location.

Another method to introduce a recirculating area is through swirling of the flow as indicated in figure 6.2b. The resulting vortex breakdown causes a recirculation zone in the core region of the flow. This provides better mixing than achieved by bluff bodies as the swirl components introduce strong shear regions [37] and allows for enough reaction time or a low local velocity of the flow.

### 6.1.4. Pressure losses

It is important for the exhaust gas burner geometry have a minimized loss due to friction, turbulence and the combustion process, as these influence the performance of the turbine. Large pressure losses over an exhaust gas burner result in a higher turbine outlet pressure which, in turn, result in a reduction of the turbine pressure ratio and thus in a lower power output.

### 6.1.5. Emission

The most concerning components of exhaust gases in terms of pollution are carbon monoxide (CO), Carbon dioxide ($CO_2$), unburned hydrocarbons (UHC) and oxides of nitrogen ($NO_x$).

Carbon monoxide is mainly formed at fuel-rich conditions, in which there is a lack of sufficient oxygen to form carbon dioxide. Also, at temperatures higher than 1800 K, carbon monoxide forms due to the disassociation of $CO_2$. Unburned hydrocarbons exit the exhaust as drops of unburned fuel. The presence of both is a result of incomplete combustion. Reduction of UHC's, CO and of $CO_2$ can be achieved by increasing the combustion efficiency and through good fuel-air mixing in the combustor. This section mainly focuses on the production and reduction of $NO_x$, as any change made in operating conditions to reduce these generally result in a reduction in CO and UHC [7].

$NO_x$ is the general name for all nitrogen oxides. In terms of emission or pollution, NO and $NO_2$ are the most common and are formed by the reaction between oxygen and nitrogen. There are three methods by which $NO_x$ is produced in the gas turbine exhaust:

1. Thermal $NO_x$;
2. Prompt $NO_x$;
3. Fuel $NO_x$.

*Thermal $NO_x$* is formed by oxidation of atmospheric nitrogen in high temperature regions, i.e. close to a flame. *Prompt $NO_x$* is formed under specific conditions by the reaction between nitrogen and certain hydrocarbons which are present in the fuel. This reaction happens very early in the combustion process. *Fuel $NO_x$* is nitrogen present in the fuel. During the combustion process, this nitrogen also oxidizes.

From the three aforementioned methods, thermal $NO_x$ is the most important one, as it accounts for most of the pollution (up to 70% of all $NO_x$), especially at higher temperatures [7].

As $NO_x$ is a very polluting greenhouse gas, very strict limitations have been set up throughout the world, to reduce the emission of $NO_x$. These regulations are different from region to region and also depend on the purpose of the combustion process, i.e. for the generation of electricity or transportation. For example, a boiler setup with a thermal output of over 1 MW can emit a maximum of 70 mg/Nm$^3$ $NO_x$ in the Netherlands, at an exhaust oxygen content of 3 vol%. A gas turbine can emit a maximum of 50 mg/Nm$^3$ $NO_x$ at 15 vol% exhaust oxygen content. This data is acquired from Artikel 3.10 Activiteitenbesluit milieubeheer.

The oxidation of nitrogen for the formation of thermal $NO_x$ happens according to the Zeldovich Mechanism:

$$N_2 + O \Rightarrow NO + N \tag{6.5}$$

$$O_2 + N \Rightarrow NO + O \tag{6.6}$$

$$N + OH \Rightarrow NO + H \tag{6.7}$$

Temperature has a very significant effect on the formation of thermal $NO_x$. The formation is an endothermic reaction and really takes off at temperatures above 1600 °C. This is also shown in figure 6.3.

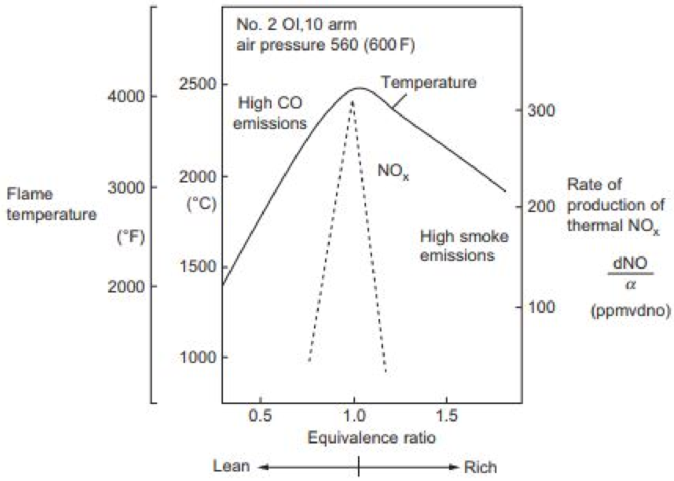


Figure 6.3: Production rate of nitrogen oxides as a function of the flame temperature/ equivalence ratio [3].

Mixing of the fuel and oxidizing fluid is a very important aspect in the formation of nitrogen oxides. If they are not thoroughly mixed, there are be some areas in which the mixture is very lean, while in other areas the equivalence ratio reaches 1. It is in those areas that the $NO_x$ formation rate becomes very large, as is shown in figure 6.3.

There are several ways to control the $NO_x$ formation rate. First and foremost is keeping the flame temperature low, generally below 1850 K. This can be achieved by low air inlet temperatures and decent mixing of the fuel and air.

There is also potential in the reduction of the reaction rate (equations 6.5-6.7). By lowering the chance any of these reactions take place, the formation of nitrogen oxides is reduced. An example for this is the addition of water or steam. This lowers the flame temperature and reduces oxygen atoms, which are required for the reaction in equation 6.5:

$$O + H_2O \Rightarrow 2OH \tag{6.8}$$

Another option to reduce the reaction rate through this mechanism is by staging the combustion process. Splitting the combustor up in 2 sections reduces the $NO_x$ formation, as in the second stage, oxygen depletion in the oxidizer occurs and the flame temperature is lower. As oxygen has a preferential reaction with the fuel, less $NO_x$ is formed compared to non-staged combustion.

## 6.2. Burner requirements

With some background on burners and combustion available, a set of requirements for the conceptual burner design is proposed. The requirements are ones which could be accounted for in the conceptual design of the burner and directly affect the technical performance of the whole supplementary-fired PowerBurner-boiler setup. Other aspects like costs, material selection and manufacturability are left out of the scope of this section, as these do not affect the technical performance directly.

The first requirement is based on the firing rate. The upper limit has been defined previously at the amount of fuel which results in 3 vol% oxygen in the exhaust to make sure complete combustion takes place. The lower flammability limit is decreased due to the high operating temperature, but increased by the deficiency in available oxygen. The true limit is not known, therefore, a minimum fuel input requirement of 10% of the maximum is assumed.

In order to minimize the amount of UHC's and CO in the exhaust, the combustion efficiency is required to be 99 % over the full thermal operating range. Therefore, at any point, 99 % of the fuel put into the system must have reacted in the exhaust.

The PowerBurner is designed with a backpressure of 50 mbar. This indicates that the static pressure loss in the flue gases beyond the PowerBurner exhaust can decrease by a maximum of 50 mbar, before the performance of the turbine is below that of the design point. A common boiler generally has a pressure loss of 10-20 mbar [11]. Therefore, assuming pressure losses in ducts and the stack are high, the static pressure loss over the burner and through combustion is required to be lower than 25 mbar to ensure performance is never below the design point.

The final requirement is with respect to $NO_x$ emissions from a Dutch point of view. It is not clear whether or not the supplementary-fired PowerBurner-boiler setup falls under the category of "boiler burner with a thermal output > 1 MW" or if it can be classified as a "gas turbine". As the PowerBurner on its own is probably not able to comply with the regulations of the first category (< 70 mg/Nm$^3$ at 3 vol% oxygen), it is assumed the system is required to comply with the second category (< 50 mg/Nm$^3$ at 15 vol% oxygen).

With these requirements in mind, in the next section, a specific type of burner is selected on which the concept version of the secondary burner for the PowerBurner-boiler setup is based.

## 6.3. Burner type selection

For this analysis, three types of burners have been considered: A swirl burner, a grid-type duct burner and an Ultra-low $NO_x$ (ULN-) burner. An overview of these burners and their basic working principle is given in table 6.1. Burners from a total of 15 manufacturers have been compared based on three criteria in order to determine which type of burner would fit the best for supplementary firing of the PowerBurner. The data used in this analysis is shown in appendix D.1. The criteria by which they compared are $NO_x$ emission, pressure loss and flame stability.

Table 6.1: Overview of 3 burner types and their working principle.

| Burner Type | Image | Working Principle |
|---|---|---|
| **Grid-type Burner** | 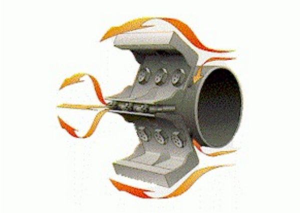 [38] | Recirculation zone through bluff body; Non-premixed flame; Low pressure drop. |
| **Ultra-low $NO_x$ Burner** |  [39] | Swirler for recirculation zone; Premixed combustion; High pressure loss by swirler; Flame settles on socket; Low flame stability for flue gases as oxidizer; Smaller operating range. |
| **Swirl-type Burner** | 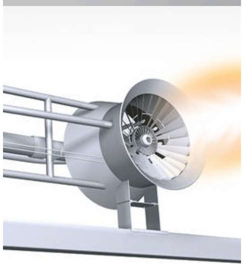 [40] | Swirler to create recirculation zone; Non-premixed flame; Swirler induces high pressure drop over the burner. |

The $NO_x$ emissions supplied by the manufacturer have been captured in figure 6.4b. From this figure is seen that the ULN-burner generally has the lowest emissions of nitrogen oxides. Also, the $NO_x$ emission of grid-type burners is generally equal to- or lower than that of a swirl-type burner.

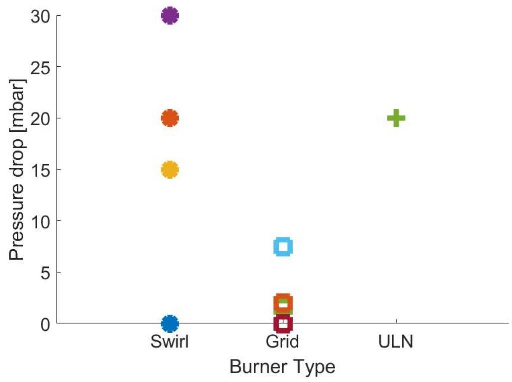


(a) Pressure losses over different burner types.

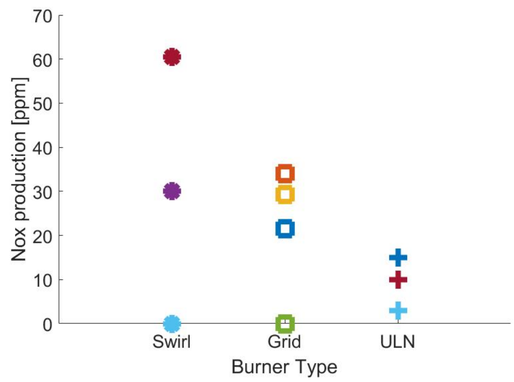


(b) Comparison of $NO_x$ emission of different types of burners.

Figure 6.4: Comparison of different burner types. Data follows from table 6.2.

A comparable analysis is done for the pressure loss over the three types of burners. The results of this analysis is shown in table 6.4a. From this figure can be concluded that the grid-type burner always has a much lower pressure loss than the Swirl-type burner. The pressure loss of an ULN burner is estimated based on the pressure losses of the Swirl-type burner. This is due to the fact that the section that causes the largest pressure loss in the swirl type burner, the swirling vanes, are also present in conventional ULN burners. This means the pressure loss over an ULN burner is comparable to that of a swirl burner, and never lower than that of a duct-type burner.

Quantifying the flame stability for each type is difficult. As both swirl- and duct-type burner achieve flame stability through recirculation of the oxidizer flow, these most likely perform equally well if taken into account in the design. For the ULN-type burner, using flue gas instead of air could result in lowered flame stability, as the local oxygen concentration on the socket surface can be low, resulting in no combustion. Therefore, the ULN-type burner is rated lowest on this criterion.

The results of the comparison have been captured in table 6.2, in which each burner is rated based on $NO_x$ emissions, flame stability and pressure losses from 3 (best) down to 1 (worst). Total score follows from the addition of scores for each criteria, where the highest score indicates that burner type performs best over the three criteria. From this follows that a duct-type burner has the best performance in terms of a combination of $NO_x$ emissions, flame stability and pressure loss. Therefore, a grid-type burner is used as the basis for designing a supplementary burner for the PowerBurner.

Table 6.2: Comparison of three types of burners.

| **Burner Type** | **$NO_x$** | **Pressure Drop** | **Flame Stability** | **Total Score** |
|---|---|---|---|---|
| **Swirl Burner** | 1 | 2 | 3 | 6 |
| **Ultra-Low NOx Fiber Burner** | 3 | 1 | 1 | 5 |
| **Duct Burner** | 2 | 3 | 3 | **8** |

## 6.4. 2D Design of the burner

In this section, a suggestion for the 2D geometry of a supplementary burner is given. The characteristics of this geometry is defined by four factors: Complete combustion, maximized operating range in terms of thermal output, low $NO_x$ emissions and pressure losses within limitations. A brief summary of the design process is given in figure 6.5 and is elaborated in appendix E.

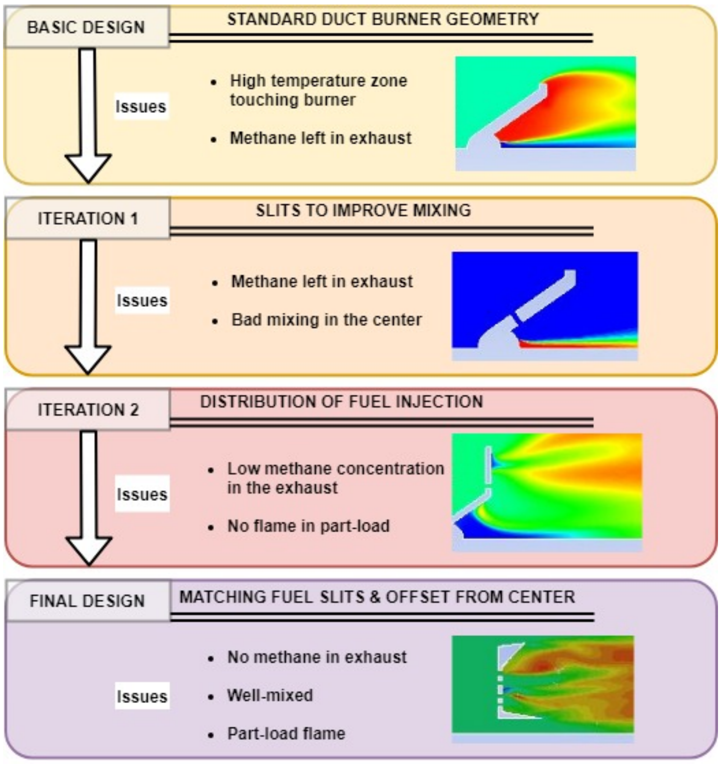


Figure 6.5: Design process of the 2D burner geometry.

### 6.4.1. Overview of the model & parameters used in ANSYS Fluent

The 2D burner model that is created is shown in figure 6.6. This is a 2D axisymmetric model. Dimensions of the flow field are based on the Viessmann Vitomax boiler [11], i.e. the inlet diameter is 0.91 m and the fire-tube diameter is 1.36 m.

The model contains a grid-type burner (indicated with number 2) for supplementary firing of the PowerBurner. This geometry acts as the bluff-body. Flue gas enters the gray flow domain normal to the left boundary (1) and leaves at the rightmost boundary (3). The lower line of the boundary (4) acts as the center axis for the axisymmetric geometry. The upper bound(5) is the wall of the cylindrical fire-tube of a boiler.

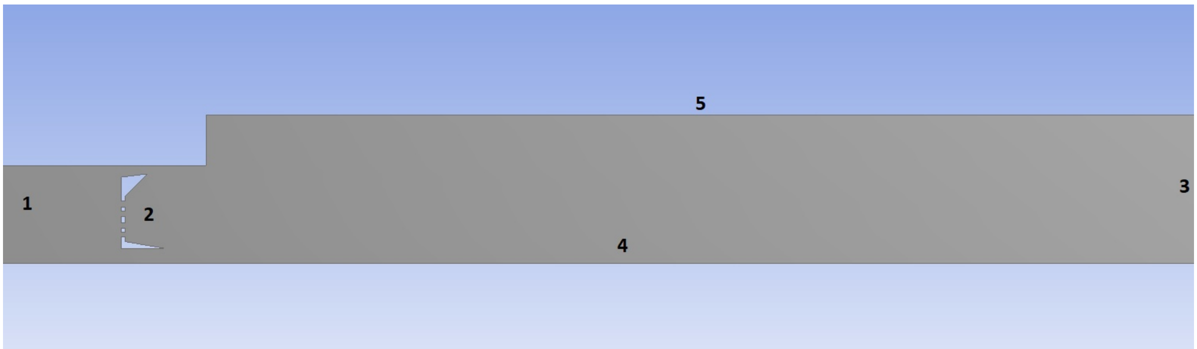


Figure 6.6: 2D burner model and flow domain including five boundaries indicated in talbe 6.5.

Table 6.3: Models used in ANSYS Fluent for the CFD analysis

| Parameter | Model | Remarks |
|---|---|---|
| Viscosity | Realizable k-$\epsilon$ | |
| Species | Non-premixed combustion | Non-adiabatic |
| Energy | On | |

With this geometry, CFD is performed with ANSYS Fluent to determine how the geometry influences the four aforementioned factors. The models that are used in the CFD analysis follow from comparable studies related to diffusion flames [41, 42], and are displayed in table 6.3. However, instead of the standard k-$\epsilon$ viscosity model, the *Realizable k-$\epsilon$* model is used, as it performs better for recirculating flows [43]. Pure methane is supplied as a fuel, at 300 K. The oxidizer composition follows from the basic Thermoflex model (appendix B.1) and is shown in table 6.4. The oxidizer is supplied at 973 K.

Table 6.4: Content of the Oxidizer (flue gas) stream used in ANSYS Fluent.

| Substance | Mole fraction (-) |
|---|---|
| $N_2$ | 0.7509 |
| $O_2$ | 0.1403 |
| $CO_2$ | 0.031 |
| Ar | 0.0090 |
| $H_2O$ | 0.0688 |

The boundary conditions that are used in the Fluent model at specific locations of figure 6.6 are shown in table 6.5:

Table 6.5: Overview of the boundary conditions used in ANSYS Fluent.

| Boundary | # in figure 6.6 | Type of B.C. | Value (if applicable) | Remarks |
|---|---|---|---|---|
| Flue Gas Inlet | 1 | Mass Flow Inlet | 3.14 kg/s | • Composition from table 6.4 |
| Burner Wall | 2 | Wall | - | • No-slip conditions for shear<br>• No heat transfer to burner |
| Flue Gas Outlet | 3 | Pressure Outlet | 0 barg | • Sets pressure loss |
| Lower Fluid Bound | 4 | axis | - | • Central axis for axisymmetric problem |
| Upper Fluid Bound (Boiler/Duct Wall) | 5 | Wall | 450 K | • Wall temperature for heat transfer<br>• No-slip conditions for shear |
| Fuel Inlet | (On burner wall) | Mass Flow Inlet | 0.0097 kg/s (min. load)<br>0.097 kg/s (max. load) | - |

### 6.4.2. Upper limit of the operating range

The operating range is defined as the range of fuel inputs at which the burner can operate. The maximum amount of fuel that can be burned, is reached when the exhaust oxygen content is reduced from 14 to 0 vol%. For the combustion reaction of methane, every mole reacts with 2 moles of oxygen (see equation 6.9):

$$CH_4 + 2O_2 \Leftrightarrow CO_2 + 2H_2O \tag{6.9}$$

The required mass flow of fuel for stoichiometric combustion with the flue gas follows from equation 6.10, in which $\dot{M}_{\ oxygen}$ is the molar flow of oxygen in the flue gas, the factor 2 follows from equation 6.9 and $M_{w,CH4}$ is the molar weight of methane:

$$\dot{m}_{CH4} = \frac{\dot{M}_{oxygen}}{2} M_{w,CH4} = \frac{0.01547}{2} * 32 = 0.123[kg/s] \tag{6.10}$$

With this, a *stoichiometric flue gas-to-fuel ratio ($FFR_{st}$)* can be defined, like in equation 6.11:

$$FFR_{st} = \frac{\dot{m}_{fluegas}}{\dot{m}_{CH4}} = \frac{3.14}{0.123} = 25.5[-] \tag{6.11}$$

This results in the amount of fuel required to react with all the oxygen. Not all oxygen reacts, therefore boilers generally operate with 3 vol% oxygen in the exhaust. The amount of fuel required for this follows from the equivalence ratio $\phi$, which is a result of the oxygen content at the inlet and exhaust (equation 6.12):

$$\phi = \frac{O_{2,inlet}}{O_{2,inlet} - O_{2,excess}} = \frac{14.03}{14.03 - 3} = 1.27[-] \tag{6.12}$$

With the equivalence ratio, the flue gas-to-fuel ratio for 3 vol% oxygen in the exhaust can be calculated, by making use of formula 6.13

$$FFR_{3\%O2} = \phi * FFR_{st} = 1.27 * 25.5 = 32.4[-] \tag{6.13}$$

Finally, the maximum amount of methane that can be combusted, can be calculated. This follows from equation 6.14:

$$\dot{m}_{CH4,max} = \frac{\dot{m}_{fluegas}}{FFR_{3\%O2}} = \frac{3.14}{32.4} = 0.097[kg/s] \tag{6.14}$$

Considering this value as the design input of the burner, the dimensions of the geometry can be optimized to enable sufficient mixing.

### **6.4.3.** Geometrical considerations to improve mixing

To achieve sufficient mixing, injection of the fuel is done in three places. The precise locations are indicated in figure 6.7a & 6.7b by the numbers **1** (center injection), **2** (middle injection) and **3** (outer injection).

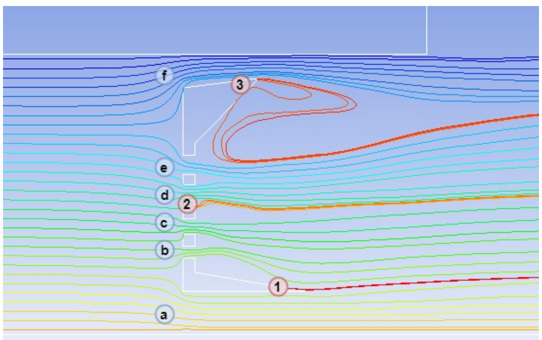


(a) Particle pathlines with fuel injections indicated with numbers **1** to **3**. Oxidizer is distributed over 6 areas, from **a** in the center to **f** at the duct wall.

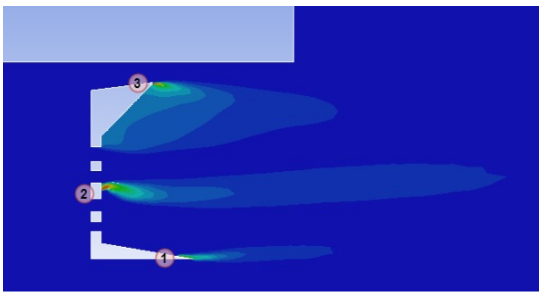


(b) Contour of the mean mixture fraction of the fuel & oxidizer. A fraction of nearly 1 means the mixture consists mostly of fuel. This can be observed near the injection areas (1 to 3) of the fuel (non-blue areas).

Figure 6.7: Injection locations for the 2D model.

The current design of the burner features several slits (**a** to **f** in figure 6.7a, A) over which the oxidizer is distributed before fuel is injected into the stream. Figure 6.7a B shows the effect this geometry has on mixing of the fuel and oxidizer. Within a short distance, the fuel is distributed very

Table 6.6: Distribution of the fuel- and oxidizer flow over the burner geometry.

| Injection point # | Fuel flow rate | % of fuel flow | Mixed with oxidizer flow | % of oxidizer flow area |
|---|---|---|---|---|
| 1 | 0.01 kg/s | 10 % | a & b | 11 % |
| 2 | 0.0435 kg/s | 45 % | c & d | 43 % |
| 3 | 0.0435 kg/s | 45 % | e & f | 46 % |

well over the flow domain. The dimensions of areas **a** to **f**, and the mass flow rates of injection holes **1** to **3** have been matched to achieve this mixing. This is shown in table 6.6.

Previous models showed that it was difficult to mix the fuel and oxidizer well near injection point **3**. Therefore, the geometry is designed to act as a bluff body and create a wake near that injection zone. This wake can be seen in figure 6.7a, where the flow near the duct wall rotates. This allows for better mixing of the fuel and oxidizer in that specific area.

Previous models also showed it was not possible to achieve decent mixing of fuel from injection point **1**, if area **a** (figure 6.7a) was not present. The current design has the burner at a certain distance away from the center of the duct, allowing the fuel to mix with an oxidizing stream from two directions, resulting in a short mixing length.

### 6.4.4. Results of the 2D CFD models

In figure 6.8a the temperature contour is shown. At the flue gas inlet, temperature is 973 K. Just downstream of the burner, combustion starts to take place. The contours of the flame can be derived from the hot area of the fluid zone, as this is where the combustion reaction takes place. Most of the reactions take place away from the burner, which means the burner remains relatively cool. This is most likely due to the oxidizer in the slits making sure the oxidizer-fuel mixture always moves in the flow direction, even just downstream of the burner.

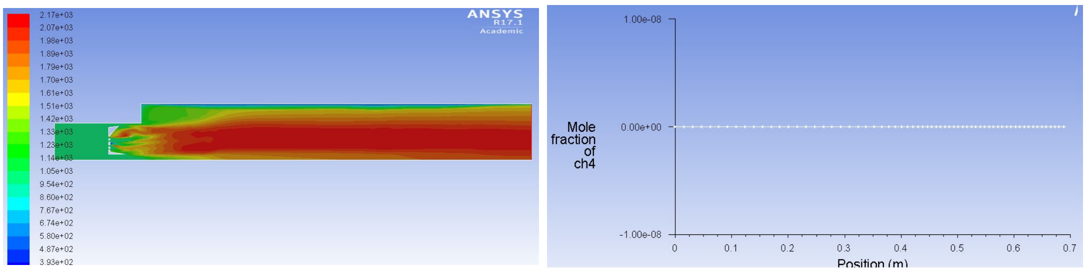


(a) Contour plot of the temperature (in K) of the fluid zone at maximum fuel injection.

(b) Concentration of methane over the height of the outlet.

Figure 6.8: Temperature contour and outlet fuel concentration of the 2D burner model.

The maximum temperature, following from the model, is around 2170 K. The right plot of figure 6.8b shows the methane fraction over the exhaust radius. There is no methane left at the exhaust, indicating that complete combustion takes place within the boiler.

In order to determine the complete operating range of the burner, a minimum fuel input has to be defined. Figure 6.9 indicates the temperature contours of the duct burner when fuel is injected in the center. At a fuel flow of 10 % of the total (0.0097 kg/s), figure 6.9 indicates that a short and high temperature flame (around 1900 K) is present. This is caused by a high local equivalence ratio (equation 6.12) which, with an ignition source, ensures the combustion reactions are most likely to occur.

The geometry makes sure the mixture is between the lower- and upper flammability limit so the combustion reactions can, even at low fuel injection rates. This results in an exhaust gas burner that can elevate the thermal operating range of the PowerBurner by 0.485-4.85 $MW_{th}$ with no methane left in the exhaust.

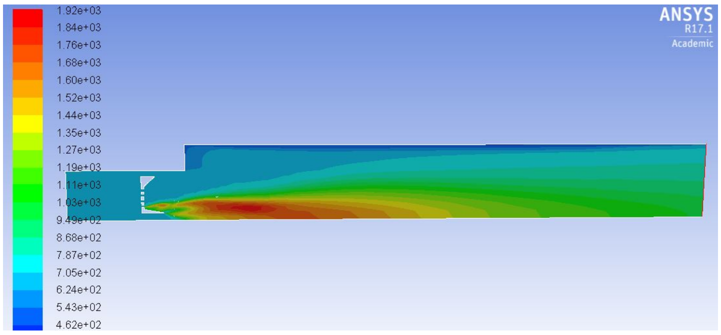


Figure 6.9: Contour of the temperature in K at minimum fuel injection through the center injection point.

## 6.5. From 2D To 3D design

The 2D model has not been revolved directly around the axis of symmetry, as indicated by **4** in figure 6.6, to translate it to 3D. Such a design would require the tubes, transporting and protecting the fuel- and ignition source, to cross the duct all the way to the middle. These would become very hot and difficult to replace. Also, the slits that were created to distribute the oxidizer flow would result in constructional difficulties.

Figure 6.10 shows the side view of the 3D model on the right, compared to the 2D axisymmetric model on the left. The 3D model also includes particular features which characterized the 2D model, like the offset of the burner from the central axis and the tilted upper part, which creates a circulating flow to improve mixing.

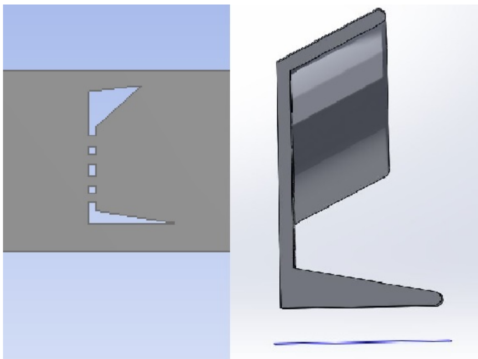

Figure 6.10: Translation of the 2D axisymmetric burner model (L) to a side view of the 3D model (R).

The fact that the 2D model has not been revolved around the axis of symmetry to create a 3D model is shown in figure 6.11. The upper and lower part of the burner allow for the burner to be connected to the duct easily. Also, pipes connected to the burner are directly in touch with the flue gas for only a short distance.

To achieve good mixing and complete combustion, the fuel injection and flue gas have been distributed over the duct, just like in the 2D model. The areas that were defined in figure 6.7a have been translated to the 3D design as shown in figure 6.12. In the right figure, red areas indicate fuel injection and blue areas the flue gas distribution. The amount of flue gas and fuel that mixes at each location is equal to that of the 2D model and is indicated in table 6.6.

### 6.5.1. 3D Combustion simulation

With a conceptual 3D design of the burner available, the design is used to create a 3D flow model in ANSYS Fluent. This is done in order verify the operating range, by checking if all methane has combusted at the exit. Also, this model is used to help determine whether the characteristics of the 3D design result in similar flow- and flame properties as the 2D design has due to its geometrical considerations (section 6.4.1).

The boundary conditions used for this model are shown in table 6.7, and the locations of each

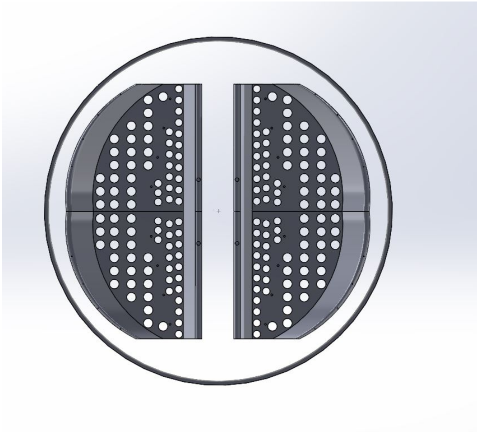

Figure 6.11: Front view of the exhaust gas burner placed inside a 910 mm diameter duct.

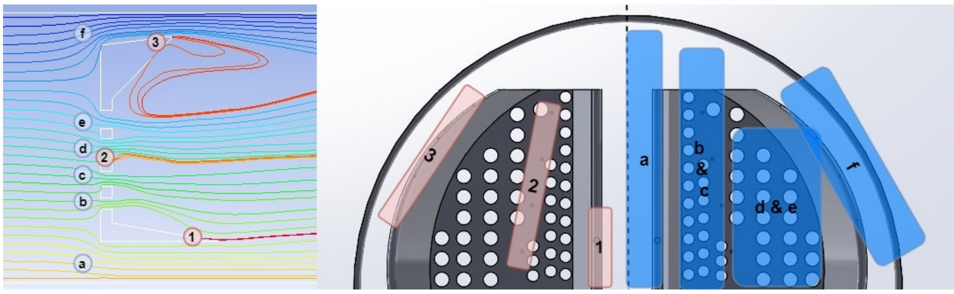


Figure 6.12: Translation of the flue gas- and fuel distribution over the burner from 2D (L) to 3D (R).

Table 6.7: Overview of the boundary conditions used in ANSYS Fluent at locations indicated in figure 6.13.

| **Boundary** | **# in figure 6.6** | **Type of B.C.** | **Value (if applicable)** | **Remarks** |
|---|---|---|---|---|
| Flue Gas Inlet | 1 | • Mass Flow Inlet | 0.785 kg/s | • Composition from table 6.4 |
| Burner Wall | 2 | Wall | - | • No-slip conditions for shear<br>• No heat transfer to burner |
| Flue Gas Outlet | 3 | Pressure Outlet | 0 barg | • To determine pressure loss over system |
| Lower Fluid Bound | 4 | Symmetry | - | • Mirroring plane parallel to side of burner part and fluid zone |
| Side Fluid Bound | 5 | Symmetry | - | • Mirroring plane parallel to top of burner and fluid zone |
| Fuel Inlet | (On burner wall) | Mass Flow Inlet | 0.00254 kg/s (min. load)<br>0.0254 kg/s (max. load) | • Locations are specified in figure 6.12 |
| Boiler wall | 6 | Wall | 450K | • Wall temperature for heat transfer<br>• No-slip conditions for shear |

boundary condition is indicated in figure 6.13. From this figure can be seen that only a quarter of the model is created. By making use of symmetry boundary conditions, the model (and results) can be mirrored in order to create the full duct- and burner as shown in figure 6.11. Due to the symmetry conditions, all inlet mass flow rates in this model are only a fourth of those supplied in table 6.5.

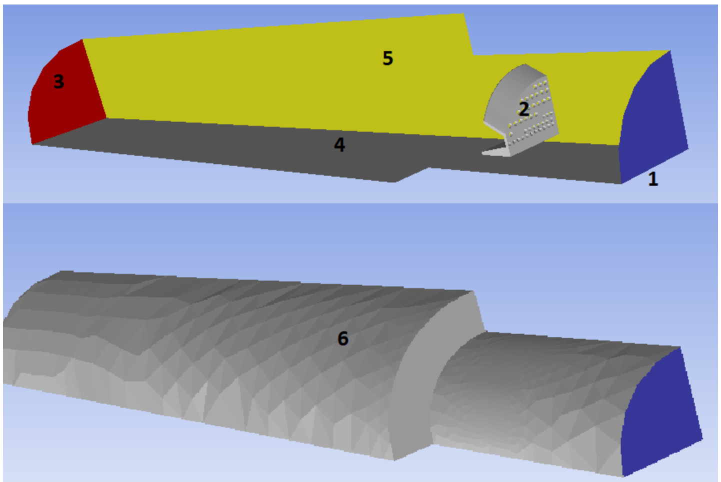


Figure 6.13: Indication of the location of boundary conditions used in a 3D CFD model of the burner design.

### Flame temperature and location

Figure 6.14a shows the temperature contours on both symmetry planes of the boiler. From this it can be seen that the maximum temperature that is achieved is very similar to that of the 2D model (2164 K max as opposed to 2170 K in figure 6.8a). The difference is less than 0.5 %, from which can be concluded that the local equivalence ratios, and thus the mixing, is very similar for the two models. The fact that all fuel is oxidized, is shown in figure 6.14b. It indicates all methane has reacted around 2 m into the boiler.

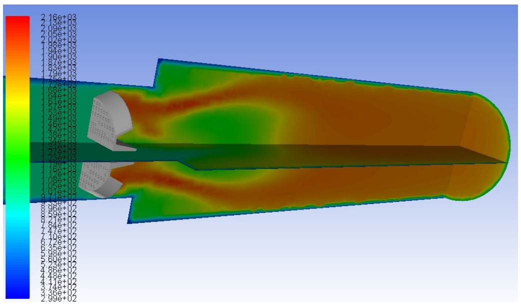

(a) Indication of the temperature contour in the 3D Fluent design. The maximum temperature reached is 2164 K.

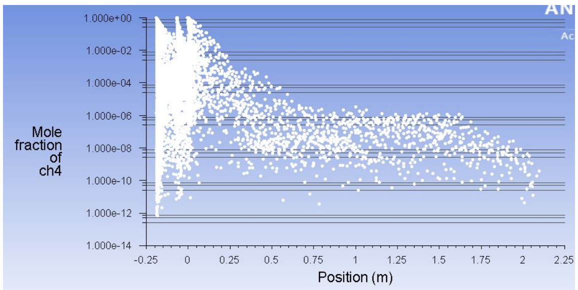


(b) Molar concentration of methane over the length of the boiler. No methane is present in the exhaust, which means all has reacted.

Figure 6.14: Flame temperature contour and fuel concentration of the 3D model at full load.

Figure 6.14a also shows a cold area in the center of the duct and that the temperature is very well distributed downstream of that area. This is due to the recirculation zone present in the center, which can be observed by the blue areas in figure 6.15a. This contour plot indicates the velocity in the z-direction, towards the boiler exhaust.

Wherever the contour is blue, the velocity is negative, which indicates the flow is recirculating. So, in figure 6.15a, two recirculating zones can be observed. But, from the center of the plane perpendicular to the one indicated in figure 6.15a follows that there is another area of recirculation. This is displayed in figure 6.15b. Recirculation zone one is of very high temperature (>1900 K), which can be observed from figure 6.14a. Therefore, combustion can take place in this zone and this could contribute to flame stability. Of the other two areas, the contribution to flame stability is not known as they result in relatively low temperature areas (<1400 K).

But, as the different planes provide different views on recirculation, it is very difficult to draw conclusions on whether or not the flame will be stable. Due to the fact that flame stability is unknown, the method of ignition cannot be determined yet. In the case of a non-stable flame, a pilot flame would be required for continuous ignition. Whereas for a stable flame, a single source of ignition like a spark

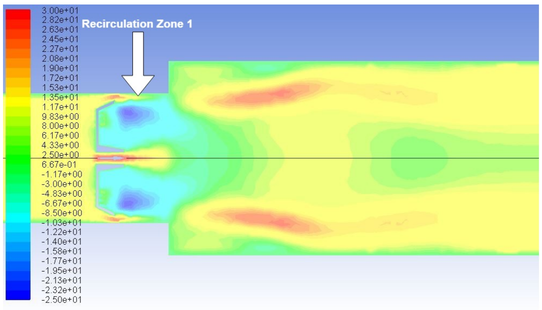


(a) Contour of the velocity in the Z-direction, on the XZ-plane. Recirculation zones are observed around the blue areas, where the velocity is negative.

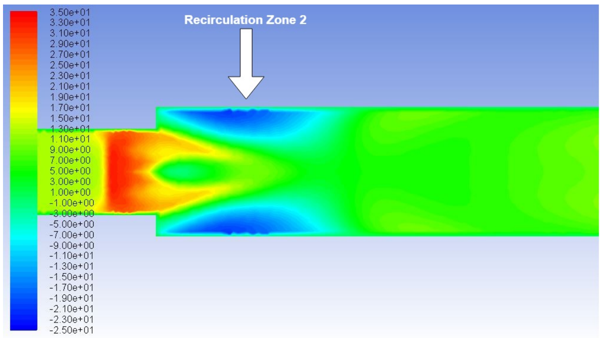


(b) Contour of the velocity in Z-direction, on the YZ-plane. Recirculation zones are observed around the blue areas, where the velocity is negative.

Figure 6.15: Recirculation zones in the 3D model as from velocity profiles over 2 planes..

plug, would be required. In that case, the flame would be self-sustaining due to autoignition.

Figure 6.16a indicates the temperature contour of the 3D model at the minimum fuel inlet (0.01 kg/s). This figure shows that at 10 % of the fuel input, a short, hot flame is created. Figure 6.16b shows that all methane has reacted at around 2.25 m inside the boiler.

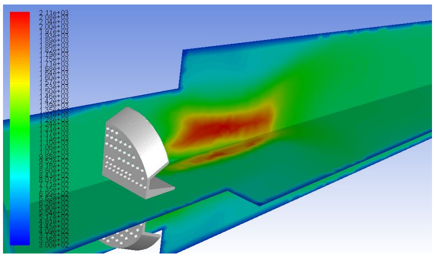

(a) Temperature contour inside the boiler at minimum load.

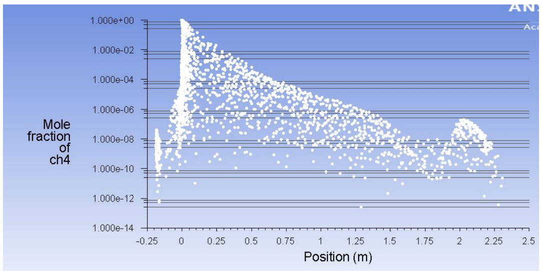


(b) Molar concentration of methane over the length of the boiler at minimum load.

Figure 6.16: Temperature contour and methane concentration over the boiler length at a minimum fuel input.

### 6.5.2. Model verification

For the 3D model, it is not possible to do a verification of the model results through grid refinement, as the amount of nodes is limited for the student licence of ANSYS Fluent, and this limit is almost reached in the first model. But, the 2D-axisymmetric results and those of the 3D model can be compared to formulate a conclusion on the accuracy of both models.

First of all, for the 2D model, the maximum flame temperature is 2170 K, whereas for the 3D model, this is 2164 K. As it is only 0.3 % lower, the local equivalence ratios, at which this occurs, are very similar.

The 2D model offers a similar recirculation zone near the tilted burner area (location 3 in figure 6.7a), compared to recirculation zone one in the 3D model (figure 6.15a).

## 6.6. Estimating $NO_x$ emissions

In this section an estimate of the $NO_x$ emissions is made by making use of the $NO_x$ model in ANSYS Fluent. Fluent offers the ability to determine the production of $NO_x$ through the methods which were elaborated earlier in this chapter.

It is assumed the natural gas supplied in the burner for supplementary firing contains no $NO_x$. Therefore, Fuel $NO_x$ is not taken into account. Due to the high temperatures, the prompt $NO_x$ rate is assumed to be very small compared to the Thermal $NO_x$ rate. In this case, only the thermal $NO_x$ rate is determined.

As the PowerBurner has produced $NO_x$ in the combustion chamber, a certain amount is present in the flue gas entering the secondary burner. These may react with hydrocarbons of the fuel, reducing the amount present in the exhaust. This is called reburn of $NO_x$, and is taken into account in Fluent, as well.

The PowerBurner is designed to emit < 50 mg/Nm$^3$ $NO_x$ (Artikel 3.10d Activiteitenbesluit milieubeheer) at 15 vol% oxygen in the exhaust, which can be translated to PPM with equation 6.15. In this equation, $C_{PPM}$ is the concentration of a certain species in PPM, $C_{mg/Nm^3}$ is the concentration in mg/Nm$^3$ and $M_w$ and $M_v$ are the molar weight- and volume of that species, in kg/kmol and m$^3$/kmol respectively. The molar weight depends on the composition of $NO_x$, which is assumed to be pure NO in this case.

$$C_{PPM} = C_{mg/Nm^3}\frac{M_v}{M_w} = 50\frac{22.4}{30} = 37.3PPM \tag{6.15}$$

This concentration of NO is assumed to be present in the exhaust of the PowerBurner and is included in the flue gas inlet boundary conditions for both the 2D and 3D model. For the Thermal $NO_x$ formation, partial equilibrium is assumed for the O and OH radicals[44]. The reburn fuel species is CH4. The $NO_x$ model is run post-processing.

This analysis results in a plot of the mole fraction of NO for both the 2D and 3D model at the maximum firing rate. If the secondary burner operates within the $NO_x$ limitations at this rate, it is able to run over the whole operating range within the limitations, as the rate is dominated by thermal $NO_x$ and the highest temperatures should be achieved at the maximum firing rate.

To determine the maximum allowable $NO_x$ concentration at the exhaust, the maximum concentration value is calculated to 3 vol% oxygen with equation 6.16. In this equation, $C_{x\%O_2}$ is the maximum allowable $NO_x$ concentration at x vol% $O_2$, while $O_{2,ref}$ and $O_{2,cur}$ are the reference and current oxygen vol% levels.

$$C_{3\%O_2} = C_{15\%O_2}\frac{20.9 - O_{2,ref}}{20.9 - O_{2,cur}} = 37.3\frac{20.9 - 3}{20.9 - 15} = 113.2PPM \tag{6.16}$$

### Results

For the 2D-model, the molar concentration of NO is plotted over the exhaust height in figure 6.17. An uneven distribution of the molar fraction of NO is observed. It ranges over the exhaust from 7E$^{-5}$ and 1.4E$^{-4}$, which is equal to a value of 70-140 PPM. The average concentration is around 100-110 PPM.

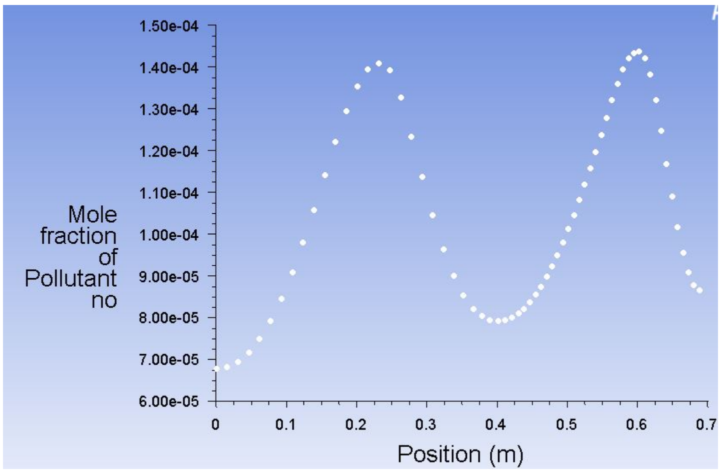


Figure 6.17: Molar concentration of NO over the boiler exhaust height of the 2D model.

For the 3D-model, a contour plot of the molar concentration over the exhaust of the boiler is indicated in figure 6.18a. In this figure, the molar concentration of NO ranges from 1.19E$^{-4}$ and 1.33E$^{-4}$, which is equal to a value of 119-133 PPM.

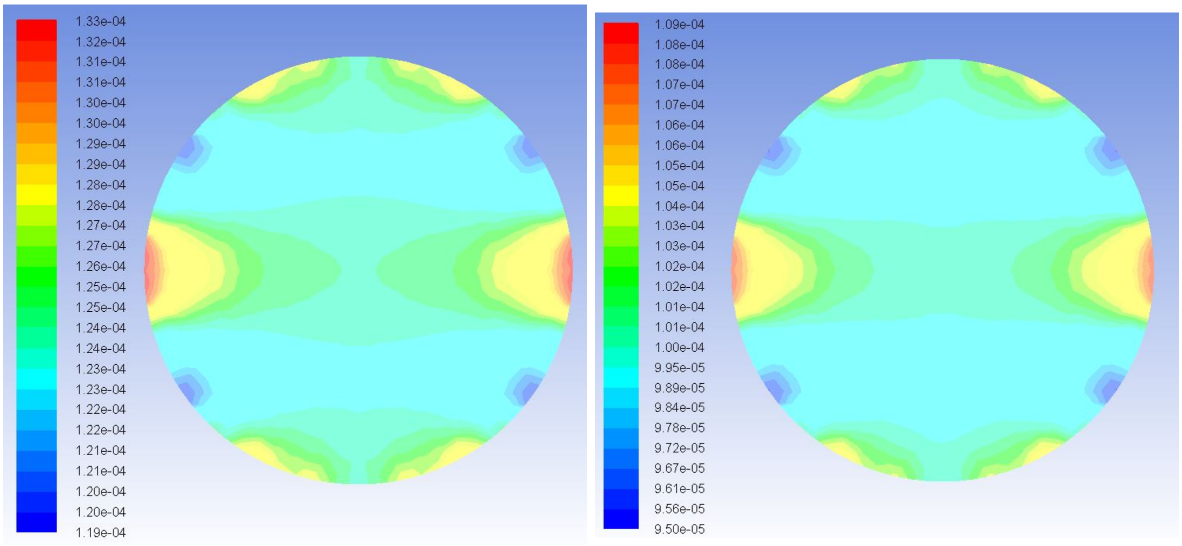


(a) Exhaust NO concentration at 50 mg/Nm³ inlet NO.

(b) Exhaust NO concentration at 25 mg/Nm³ inlet NO.

Figure 6.18: Contour plot of the molar concentration of NO over the boiler exhaust of the 3D model at varying inlet NO concentrations.

These values are calculated under the assumption that the PowerBurner has the maximum allowed NO in the exhaust (50 PPM at 15 vol% oxygen). If the PowerBurner would only contain half of the allowable NO in the exhaust, the burner might be able to operate more easily within the limits. For the 3D model, this is analyzed. The results (contour of molar NO concentration over the exhaust) are shown in figure 6.18b.

Figure 6.18b indicates a contour plot very similar to that in figure 6.18a but at a molar concentration of NO ranging from $9.5E^{-5}$ and $1.09E^{-4}$, which translates to a value of 95-109 PPM. This is a reduction of around 24 PPM at any location, which is almost the same amount by which the NO outlet concentration of the PowerBurner is lowered compared to the initial case.

In order to determine the amount of $NO_x$ the supplementary burner adds to the combustion products, an average flue gas density of 1.2 kg/Nm$^3$ is assumed. Under this assumption the exhaust burner increases the $NO_x$ flow by around 190 mg/s at full load, regardless of the inlet $NO_x$ concentration.

What finally has to be considered, is the fact that the $NO_x$ calculation in Fluent is a post-processing step. Therefore, it is very dependent on the parameters used in- and following from the Fluent model. Although the performance of the two models is very similar, it is not known how this would translate to $NO_x$ concentrations in reality.

## 6.7. Pressure loss

With the 2- and 3D design of the burner in ANSYS Fluent, an estimation of the static pressure losses can be made from the models. The static pressure drop following from Fluent over the 2D burner geometry is shown in figure 6.19, and for the 3D model in figure 6.20. Both show a reduction in static pressure over the geometry of the burner between the inlet and outlet of the flue gas.

The flue gas of the 2D model has a static pressure loss of about 2.5 mbar. The 3D model geometry incurs a static pressure drop of around 1.6 mbar. Both the 2.5 mbar and the 1.6 mbar pressure losses are close to the pressure losses of duct burners supplied by the manufacturers (figure 6.4a), which ranged from 2-7.5 mbar.

The fact that the 2D model has a pressure loss which is around 56% higher than that of the 3D burner can be explained for the largest part by the differences in geometries. The area of the burner perpendicular to the flow in the duct, is 26% larger for the 2D geometry than that of the 3D geometry. From the mass balance (equation 6.17), the average flow velocity now follows. In this equation, the areas for both geometries where the flow passes the burners are indicated with A, and V is the average flow velocity toward the outlet at the location of passage.

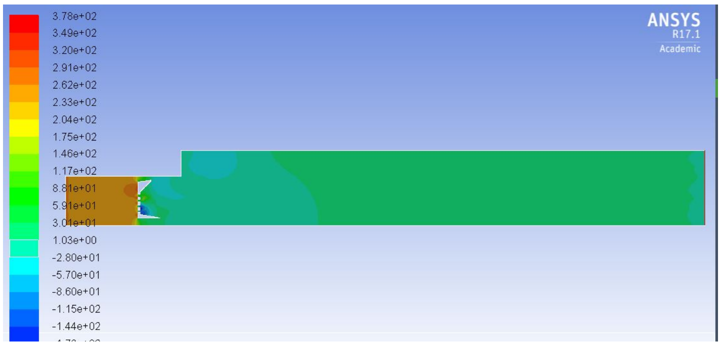


Figure 6.19: Static pressure [Pa] over the 2D burner model.

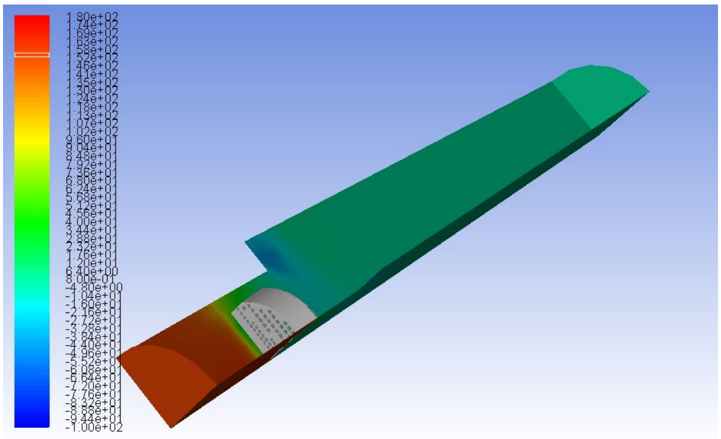

Figure 6.20: Static pressure [Pa] over the 3D burner model.

$$V_{2D} = \frac{A_{3D}}{A_{2D}} V_{3D} = 1.26 * V_{3D} \tag{6.17}$$

By using this value in the equation for static pressure loss (equation 6.18), it is shown that the larger burner area should result in an increase of the static pressure loss of 58%, which explains more than the 56 % difference between both pressure pressure losses. The 2% difference could be due to other differences in geometry.

$$\Delta P_{2D} = \frac{1}{2}\rho V_{2D}^2 = \frac{1}{2}\rho(1.26 * V_{3D})^2 = \mathbf{1.58}\frac{1}{2}\rho(V_{3D})^2 \tag{6.18}$$

From this it can be concluded that the current geometry, both in 2D- and 3D, most likely results in a static pressure loss similar to that of existing duct burners, which is lower than that of an Ultra-low $NO_x$- and Swirl Burner.

## 6.8. Conclusion

In this chapter, a conceptual design of a burner for supplementary firing of the PowerBurner-boiler setup, is presented. From a research of 3 different types of burners followed that a grid-type burner has the best performance in terms of a combination of pressure loss, $NO_x$ emissions and flame stability. Therefore, the design of the burner is based on a grid-type burner.

With the grid-type burner in mind, a 2D design is created (as explained in appendix E) and modelled in ANSYS Fluent to determine the performance of the flame in terms of complete combustion, $NO_x$ emissions, pressure losses and thermal operating range. The design has several characteristics, which affect the burner performance in terms of the aforementioned parameters:

1. 3 Fuel injection points which improves mixing and the operating range;

2. Slits in the burner geometry for the oxidizer to flow through, to improve mixing, the operating range, $NO_x$ emissions and keep the burner cool;
3. Gap between the burner and center of the duct, to improve mixing in the center of the duct and enable a low minimum thermal output of the burner;
4. Tilted geometry which creates a recirculated area behind the burner to improve mixing. This could also improve flame stability.

All these characteristics are implemented in a 2D axisymmetric geometry, which, in combination with an existing fire-tube boiler geometry, increase the thermal operating range by 0.485 to 4.85 MW. The location of each characteristic on the design is indicated in figure 6.21a. Over the entire operating range, complete combustion of the fuel takes place.

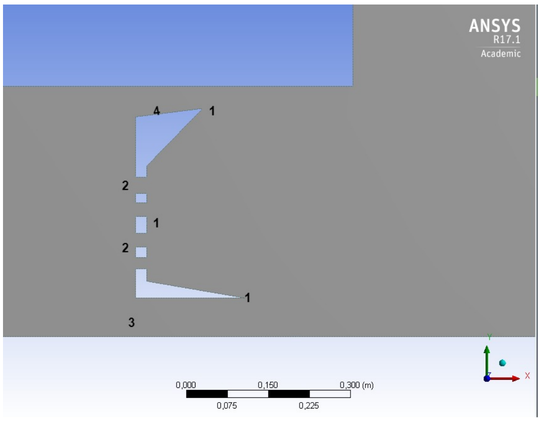


(a) Indication of the locations of geometry characteristics in the 2D design of the supplementary burner.

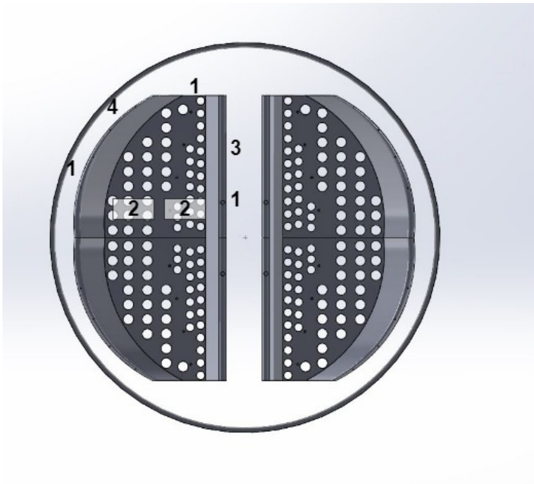


(b) Indication of the locations of geometry characteristics in the 3D design of the supplementary burner.

Figure 6.21: Location of the 4 design considerations in both models.

A translation from the 2D model to a 3D design, which incorporates these features, is made. This model serves as the conceptual design of the burner for supplementary-firing of the PowerBurner-boiler setup. The design was modeled in ANSYS Fluent, to determine its performance.

In terms of thermal capacity and combustion efficiency, both the 2D- and 3D model allow for complete combustion over an operating range of 0.485-4.85 MW, which is the required range from 10 % of the maximum load to a load which results in 3 vol% oxygen in the exhaust. As complete combustion occurs over this range, the required 99% combustion efficiency is met.

As a maximum allowable pressure loss, a loss of 25 mbar was defined. The 2D model showed a pressure loss of 2.5 mbar and the 3D model 1.6 mbar. The difference in pressure losses was explained by geometrical differences and the pressure loss requirement is met by this setup.

In terms of $NO_x$ emissions, the 2D model showed an average outlet NO concentration of 100-110 PPM, whereas according to the 3D model a volumetric outlet concentration of 109-133 PPM was present. These values are very close to the Dutch emission regulation for gas turbines of 113 PPM at 3 vol% oxygen but, as the accuracy of the $NO_x$ model is not known, no conclusions can be drawn on whether or not the current setup complies with the regulations.

The current results are achieved under the assumption that that the gas turbine outlet (or boiler inlet)already operates at its maximum allowable limit of NO (according to Dutch regulations). Reducing this value leads to an almost equal reduction in the boiler outlet NO concentration.

# 7
# Practical implementation

## 7.1. Introduction

With the conceptual design, operating range and pressure loss of the exhaust burner available, this chapter elaborates on the practical implementation of supplementary firing for the PowerBurner-boiler setup by analyzing two aspects: Part-load operation to reach lower thermal outputs and the location in which it would be economically viable to operate the supplementary-fired PowerBurner.

Regarding this, the questions that are answered in this section are: Which mode of operation is the most profitable for the supplementary-fired PowerBurner operating at part-load, and in which case would it be beneficial to operate the supplementary-fired PowerBurner? In the second question, the case is defined as a specific country and company size, which determines the price of electricity and gas.

The different modes of part-load operation will be discussed in the first section. The second section will provide a method to determine in which case supplementary firing should be implemented. Finally, conclusions will be drawn on the implementation of supplementary firing for the PowerBurner.

## 7.2. Shaft speed- or firing rate variation for part-load operation

Whenever the heat required from PowerBurner including supplementary firing is below the maximum possible heat output, there are three options to achieve the required heat output:

1. Reduce supplementary firing rate;
2. Operate the PowerBurner at part-load (reduced shaft speed);
3. A combination of both.

Each method has a different effect on the thermal- and electrical efficiencies of the PowerBurner-boiler setup. From figure 4.3a follows that, through reduction of the shaft speed, the electric efficiency is lowered. By reducing the supplementary firing rate, the thermal efficiency of the system is reduced, which can be observed in figure 4.7a. So, each method affects the performance in a specific way. This section aims to provide an analysis of which method is best from a thermodynamic and economic point of view.

### 7.2.1. Thermoflex analysis

For this analysis, an existing boiler is designed and connected to the PowerBurner in Thermoflex (appendix B) in order to simulate the effects of the three part-load methods. A *Viessmann Vitomax 300-HS* boiler with *type-200 economizer* is built in Thermoflex based data from the datasheet [11].

The first column of table 7.1 shows data of that boiler from the datasheet. The second column shows the characteristics of the modeled boiler in Thermoflex. There is a slight difference between the stack temperatures and efficiencies of both. The difference is very small and therefore the model will be used for this analysis.

Table 7.1: Verification of the Thermoflex model of a Viessmann Vitomax 300-HS with type 200 economizer from the datasheet [11].

| Parameter | Vitomax 300-HS Datasheet | Thermoflex model |
|---|---|---|
| **Fuel** | $CH_4$ | $CH_4$ |
| **Feedwater** | 102 °C | 102 °C |
| **Efficiency** | 95,4% | 95,3% |
| **Stack Temperature** | 109,5 °C | 109,7 °C |
| **Steam Production Rate** | 12 ton/hr | 12 ton/hr |
| **Pressure** | 10 bar | 10 bar |

To determine the effects of the part-load methods, the Thermoflex model will be operated in off-design mode. In this mode, the effects of the non-ideal operation of a gas turbine and boiler are taken into account. For the boiler, this includes the effect of the reduced mass flow on the heat transfer coefficient.

First, the secondary fuel flow is varied from 0% (no supplementary firing) to 100 % (max. supplementary firing rate). After that, the model is run at the maximum supplementary firing rate (at which 3 vol% oxygen is left in the exhaust), with the shaft speed varying from 28000 to 22000 RPM. From the model follows a certain electrical- and thermal output and a fuel requirement for every step. With this, the profitability can be calculated according to equation 5.3. The profitability is calculated at a price ratio of 2 and a gas price of 0.02 eur/kWh to simulate a Dutch case.

### 7.2.2. Effects of the part-load methods

In figure 7.1b, the results of this analysis from a thermodynamic point of view are observed. It indicates that, at any thermal output lower than the maximum, operating the supplementary-fired PowerBurner-boiler setup at varying shaft speeds always result in a higher thermal efficiency, but at a lower electrical efficiency. The opposite can be observed for the case in which the secondary burner firing rate is lowered.

Figure 7.1a shows the results from an economic point of view for a Dutch case. The *Variable firing rate* (blue dotted) line indicates the profitability compared to a conventional burner at a constant (maximum) shaft speed of 28.000 RPM and varying supplementary firing rates. The *Variable RPM* (red dashed) line shows the profitability compared to a conventional burner at constant maximum firing rates and varying PowerBurner shaft speeds for certain thermal outputs.

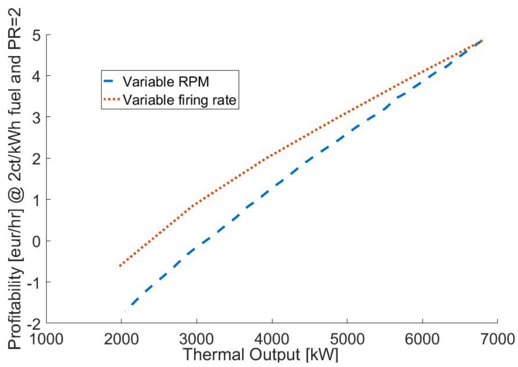


(a) Profitability at PR = 2 fuel price = 0.02 eur/kWh.

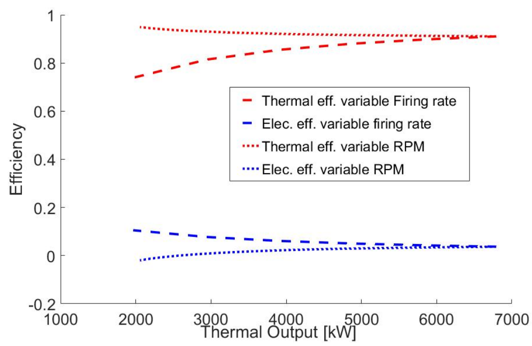


(b) Thermal- and electrical efficiencies.

Figure 7.1: Part-load performance through shaft-speed or secondary firing rate variation.

From this plot follows that at any thermal output (equal to- or larger than that of the PowerBurner), it is more profitable to achieve this rate by keeping the PowerBurner operating at its maximum shaft speed and lowering the supplementary firing rate, as opposed to using the maximum firing rate and lowering the shaft speed. This is for a price ratio of 2, however.

Both methods have different effects on the PowerBurner outputs, so what happens to the profitability at other price ratios? This is shown in figure 7.2. The maximum shaft speed and firing rate lines of figure 7.1a (price ratio = 2) can be observed as the combination of red lines in figure 7.2.

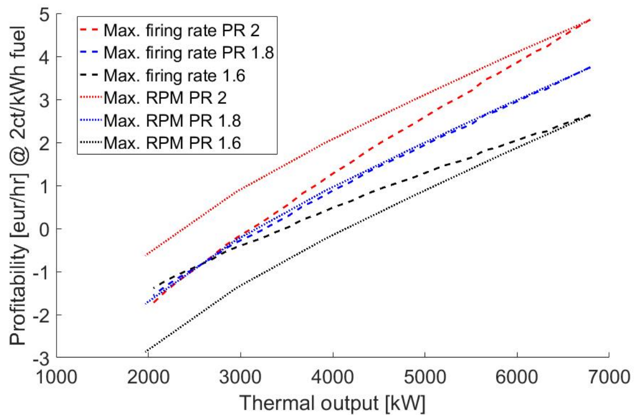


Figure 7.2: Profitability for the supplementary-fired PowerBurner at specific thermal outputs and varying price ratios with different part-load methods.

At a price ratio of 1.8 (blue lines), a turning point can be observed. Here, the profitability of varying either the shaft speed or the firing rate to reach different thermal outputs is almost equal. If the price ratio is lowered even further, the plot shows that it becomes more profitable to operate the PowerBurner at varying shaft speeds and keep the supplementary firing rate maximized. At low price ratios (<1.8), the increase in thermal efficiency apparently outweighs the decrease in electrical output in terms of profitability, as the revenue from electricity is relatively low. For the most profitability in this situation it is better to maximize thermal efficiency.

## 7.3. Application window for the supplementary-fired PowerBurner

From the previous section results that the profitability and ideal part-load operation of a PowerBurner with or without supplementary firing heavily depends on the price ratio. Therefore, this section will be dedicated to finding out in which case it is preferred to use the supplementary-fired PowerBurner over a regular burner or multiple PowerBurners.

As heat is the main product, comparisons will be made at equal thermal outputs. Different cases will be distinguished based on the price ratio (equation 5.2), as for different countries, different ratios apply. Finally, an analysis of the payback time for the supplementary-fired PowerBurner at different locations is made and compared to the payback time of employing several PowerBurners.

### 7.3.1. Profitability and depreciation of the system

Three methods are identified in this report to achieve a specific thermal output: Combustion with a regular burner to fire a boiler, a supplementary-fired PowerBurner-boiler system or multiple PowerBurner-boiler setups to achieve a specific thermal output. If the revenue of the electricity does not outweigh the extra fuel and investment costs of the PowerBurner, it is better to employ a regular burner. The option of multiple PowerBurner-boiler setups will be more profitable in a case where the price of electricity is very high compared to the price of fuel, as in this case, the revenue will outweigh the extra investment costs compared to a supplementary-fired system.

The common factor here, is the investment cost. So, in order to come to a decent comparison between these methods, the CAPEX will be taken into account through depreciation of the system. For this is assumed that a boiler is already available, and is thus not taken into account in the CAPEX. The profitability is affected in the following manner:

$$Prof_{net,method} = Prof_{method} - \frac{CAPEX_{method}}{Y_{method} * N_{op}} \tag{7.1}$$

In this equation, $\text{Prof}_{net,method}$ is the net profitability in $\frac{eur}{hr}$ of a certain method. $\text{Prof}_{method}$ is the profitability for a certain method according to equation 5.3, CAPEX$_{method}$ are the Capital Expenditures for that method and Y$_{method}$ and N$_{op}$ are the estimated years of operation and operational hours per year, respectively.

In order to perform this analysis, the price of the PowerBurner, burner and exhaust burner have to be estimated. The estimations are shown in table 7.2, along with the characteristics used for this analysis. The CAPEX required for a conventional burner and the exhaust gas burner are assumed to be equal and follow from an analysis of Dimian *et al.* [45].

Table 7.2: Characteristics to determine profitability limits of the supplementary-fired PowerBurner.

| **Type of system** | **Estimated CAPEX (Eur)** | **Years of Operation** | **Operational Hours (hr/year)** | **Thermal Efficiency (%)** | **Electrical Efficiency (%)** | **Fuel Input (kWh)** |
|---|---|---|---|---|---|---|
| **PowerBurner** | 300.000 | 10 | 8.000 | 75 | 10.5 | 2.660 |
| **PowerBurner (Sup. Fired)** | 335.000 | 10 | 8.000 | From model | From model | From model |
| **Burner** | 35.000 [45] | 10 | 8.000 | 95 | - | varying |

With the data from table 7.2, an upper and lower limit of the price ratio can be defined in terms of the thermal output. The lower limit indicates at which price ratio the profitability minus depreciation of the supplementary fired PowerBurner is equal to that of a regular burner. This is indicated as the lower limit, as it happens at low price ratios due to the thermal efficiency being maximized. This requires rewriting equations 7.1 and 5.3 as a function of the price ratio at equal thermal outputs:

$$\begin{aligned} Prof_{net,difference} = &((P_{el,pbsf} PR - \frac{Q_{thermal}}{\eta_{pbsf}})E_{fuel} - \frac{CAPEX_{pbsf}}{Y_{pbsf} N_{op}}) \\ &-((P_{el,burner} - \frac{Q_{thermal}}{\eta_{burner}})E_{fuel} - \frac{CAPEX_{burner}}{Y_{burner} N_{op}}) \end{aligned} \tag{7.2}$$

In this equation, P$_{elec,pbsf}$ and P$_{elec,burner}$ are the generated electrical power in kWh for the supplementary-fired- and regular burner or PowerBurner, respectively. Q$_{thermal}$ is the thermal output and $\eta$ is the thermal efficiency for each method. PR is the price ratio and E$_{fuel}$ is the fuel price in $\frac{euro}{kWh}$. Setting the difference in profitability to 0 at fixed certain thermal output will results in a specific price ratio at which this occurs. So the lower limit, with a profitability difference between the supplementary-fired PowerBurner and a regular burner of 0 is after some rewriting:

$$PR_{LL} = \frac{\frac{\frac{CAPEX_{pbsf}}{Y_{pbsf} N_{op}} - \frac{CAPEX_{burner}}{Y_{burner} N_{op}}}{E_{fuel}} + Q_{thermal}(\frac{1}{\eta_{pbsf}} - \frac{1}{\eta_{burner}})}{P_{el,pbsf}} \tag{7.3}$$

The upper limit is now defined as the price ratio at which the profitability difference between the supplementary-fired PowerBurner and an N$_{PB}$ amount of PowerBurners is 0. This is indicated as the upper limit, as it occurs at high price ratios, where the electrical output is maximized. The N$_{PB}$ factor indicate the amount of regular PowerBurners required to achieve an equal thermal output Q$_{thermal}$ as the supplementary-fired system. The CAPEX of such a system then also increases by N$_{PB}$. For this analysis it is assumed the capital expenditures for regular PowerBurners always vary linearly with the required thermal output. The upper limit is defined in equation 7.4.

$$PR_{UL} = \frac{\frac{\frac{CAPEX_{pbsf}}{Y_{pbsf} N_{op}} - \frac{N_{PB} CAPEX_{pb}}{Y_{pb} N_{op}}}{E_{fuel}} + Q_{thermal}(\frac{1}{\eta_{pbsf}} - \frac{1}{\eta_{pb}})}{P_{el,pbsf} - N_{Pb} * P_{el,pb}} \tag{7.4}$$

By calculating these limits at varying thermal outputs, the application window in which it is most beneficial to operate the supplementary-fired PowerBurner can be identified.

### 7.3.2. Results from the limiting cases

With the thermal and electrical outputs known from the Thermoflex models, the upper- and lower PR limits can be plotted as a function of the thermal outputs. The plot is shown in figure 7.3.

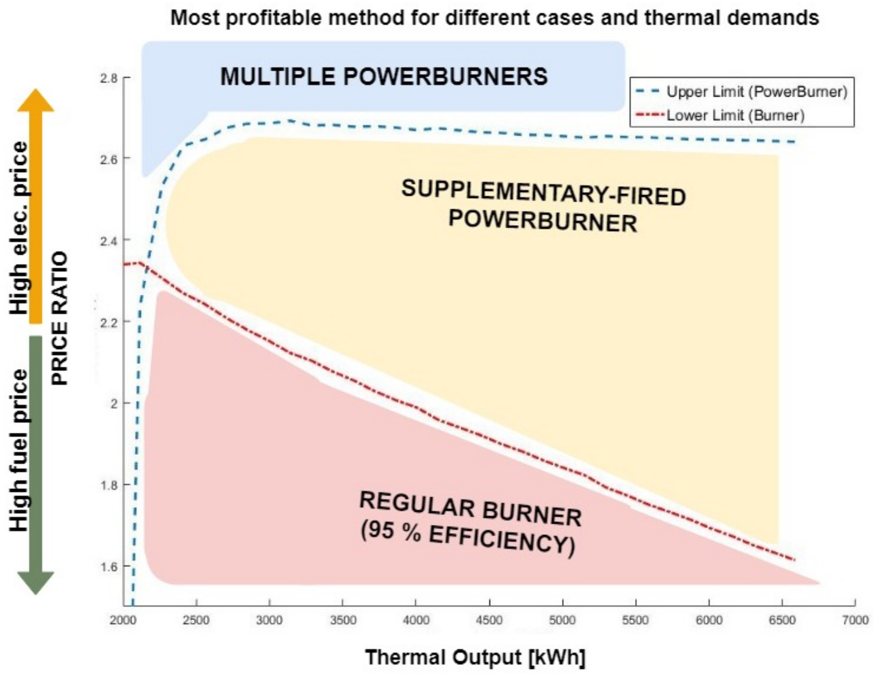


Figure 7.3: Upper- and lower limits of the price ratio at which the supplementary-fired PowerBurner has equal profitability to another method.

This figure shows which method is the most profitable to use at each combination of price ratio (subjected to a specific area) and required thermal output (subjected to a specific client), with the assumptions made in table 7.2. Three general cases can be distinguished. A specific combination of the price ratio and required thermal output is:

1. Below the Lower Limit;
2. Above the Upper Limit;
3. Between the Lower and Upper Limit.

If a certain case is *Below the Lower Limit*, it is most profitable to use a regular burner to generate the heat demand. As the price ratio is relatively low, the price of fuel is high compared to the electricity price. In this case, the extra investment costs plus lower thermal efficiency of a supplementary-fired PowerBurner outweighs the revenue from the generated electricity, and thus a regular burner should be used.

If a case is *Above the Upper Limit*, it is most profitable to use an $N_{pb}$ amount of PowerBurners to generate the heat required in any case. As the price ratio is high, the electricity is valuable compared to fuel. In this case, the revenue from the electricity of several gas turbines outweigh lower CAPEX and higher thermal efficiency of a single supplementary-fired PowerBurner-boiler setup.

If a case is *Between the Lower and Upper Limit*, it is most profitable to use supplementary-fired PowerBurner. The lower limit, at which this occurs, decreases with increasing thermal output. This is due to the fact that the thermal efficiency of the supplementary-fired PowerBurner increases at higher thermal outputs. At low thermal outputs, the area of price ratios in which it is advised to use an $N_{pb}$ amount of Powerburners increases rapidly. This is due to the assumption that the investment cost of these PowerBurners decrease linearly with the thermal output, while on the other hand, the investment costs of the supplementary-fired PowerBurner is fixed according to table 7.2.

With this figure and the price ratios as displayed for several EU countries in table 7.3, it is possible to determine whether or not the supplementary-fired PowerBurner is the best method to apply at a certain location. But, this does not take into account one other important aspect: The Payback time. As this usually determines whether or not a technology is implemented in the first place, the next section elaborates on that.

### 7.3.3. Payback time for the PowerBurner

The payback time (Simple Payout-time, SPOT) is mentioned in chapter 5 as the CAPEX divided by the profitability (compared to a 95 % efficient burner-boiler setup, equation 5.5). A similar comparison between the 3 methods is made as in the previous section, but as a burner has no positive SPOT, it is of no use to include the regular burner payback time in this comparison.

Therefore, one single limit is created at which the payback time of a supplementary-fired PowerBurner and employing N$_{pb}$ PowerBurners to reach a specific thermal demand, are compared. Equation 7.5 shows in which case the SPOT is equal for a supplementary-fired PowerBurner and a certain amount of PowerBurners required to reach a specific thermal output:

$$\frac{CAPEX_{pbsf}}{P_{elec,pbsf}PR - Q_{thermal}(\frac{1}{\eta_{pbsf}} - \frac{1}{\eta_{burner}})E_f} = \frac{N_{pb}CAPEX_{pb}}{N_{pb}P_{elec,pb}PR - Q_{thermal}(\frac{1}{\eta_{pb}} - \frac{1}{\eta_{burner}})E_f} \qquad (7.5)$$

In this equation, P$_{elec,pbsf}$ and P$_{elec,pb}$ are the generated electrical power in kWh for the supplementary-fired- and regular PowerBurner, respectively. Q$_{thermal}$ is the thermal output and $\eta$ is the thermal efficiency for each method. PR is the price ratio and E$_{fuel}$ is the fuel price in $\frac{euro}{kWh}$. Rewriting this to solve for the price ratio at equal thermal outputs results in equation 7.6.

$$PR = \frac{E_f Q_{thermal}((\frac{1}{\eta_{pb}} - \frac{1}{\eta_{burner}})\frac{CAPEX_{pbsf}}{N_{pb}CAPEX_{pb}} - (\frac{1}{\eta_{pbsf}} - \frac{1}{\eta_{burner}}))}{N_{pb}P_{elec,pb}\frac{CAPEX_{pbsf}}{N_{pb}CAPEX_{pb}} - P_{elec,pbsf}} \qquad (7.6)$$

With the data from Thermoflex, the price ratio, at which N$_{pb}$ PowerBurners and the supplementary-fired PowerBurners have an equal payback time can be calculated. This results in figure 7.4. If a combination of thermal output and price ratio results in a point below the line in this figure, it means the Simple Payout Time is shorter for the supplementary-fired PowerBurner. The SPOT for the supplementary-fired PowerBurner for different-sized companies at several locations have been indicated in the figure and table 7.3.

Table 7.3: Overview of 2017 price ratios and Simple Payout Time (SPOT) for different-sized industrial consumers of gas and electricity in the EU.

| Country | Company Size | Price ratio | SPOT 3 MW | SPOT 6 MW |
|---|---|---|---|---|
| Netherlands | S [33] | 3.14 | 5.6 | 4.1 |
| Netherlands | M [33] | 2.05 | 49 | 11 |
| Netherlands | L [33] | 2.05 | 51 | 12 |
| Belgium | S [33] | 3.7 | 4 | 3.1 |
| Belgium | L [33] | 2.3 | 18 | 8.2 |
| Germany | S [33] | 4.56 | 2.1 | 1.8 |
| Germany | L [33] | 2.83 | 7.2 | 4.6 |
| France | S [33] | 2.73 | 5.6 | 3.4 |
| France | L [33] | 1.73 | - | 14 |
| Italy | M [34, 35] | 5.6 | 1.6 | 1.5 |

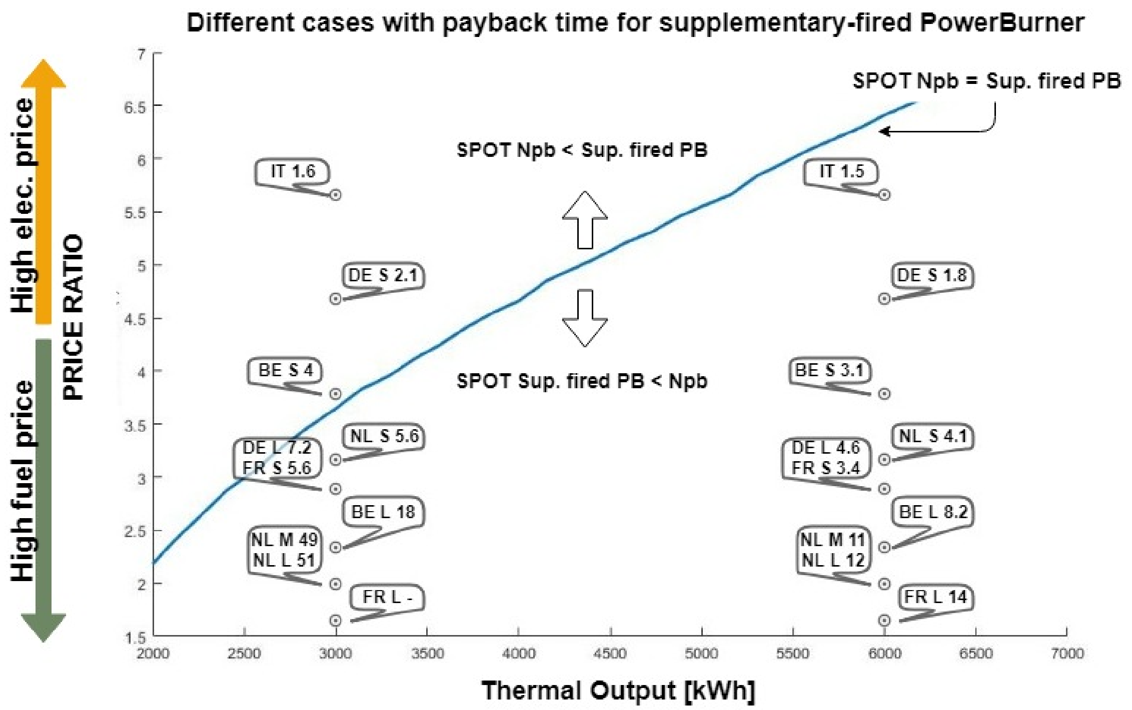


Figure 7.4: Payback time for different cases. Line indicates where supplementary-fired PowerBurner and $N_{pb}$ PowerBurners have equal SPOT.

## 7.4. Conclusion

In this chapter, the practical implementation of supplementary firing is elaborated upon by answering two questions: Which mode of operation is the most profitable for the supplementary-fired PowerBurner operating at part-load, and in which case would it be beneficial to operate the supplementary-fired PowerBurner?

The first question is answered with the use of a model of the PowerBurner and a commonly used boiler recreated in Thermoflex. The supplementary firing rate and shaft speed of the gas turbine have been varied separately, from which the thermal- and electrical output and fuel usage has been modeled. With these results, the profitability of the two methods have been compared at specific thermal outputs.

From this analysis resulted that with the supplementary-fired PowerBurner-boiler setup it was in most cases more profitable to operate the PowerBurner in part-load through maximizing the shaft speed while varying the supplementary firing rate. At a price ratio below 1.8 it becomes more profitable to operate at the maximum firing rate while varying the shaft speed to achieve a certain thermal output. From the cases which have been analyzed, this would only be a viable option for large-sized French based companies (table 7.3).

To determine in which case it would be economically beneficial to operate a supplementary-fired PowerBurner, this setup is compared with two others: A regular burner, which maximizes the thermal efficiency, and employing several PowerBurners to reach a certain thermal output, which maximizes the electric output.

The comparison showed that at high price ratios (>2.7), employing several PowerBurners is the most beneficial option in terms of profitability. At lower price ratios, it is sometimes more beneficial to employ a regular burner than a supplementary-fired PowerBurner depending on the thermal output. For the cases in between, the supplementary-fired PowerBurner is the most beneficial to employ in terms of profitability. These results have been captured in figure 7.1a.

A similar analysis is made on the payback time of the supplementary-fired PowerBurner. This is compared to the use of several PowerBurners to reach a specific thermal output. From this analysis followed that, at higher thermal outputs, the payback time of a supplementary-fired PowerBurner is generally lower. Only at lower thermal demands and high price ratios (for example small-sized Belgium-based businesses requiring 3 $MW_{th}$), payback time is better when employing multiple PowerBurners.

Reasonable payback times (< 5 years) for this system are generally applicable to smaller companies, as these have relatively high price ratios. Also, payback times are lower at higher thermal outputs. An overview the SPOT of different-sized companies at several locations in the EU can be found in figure 7.4.

# 8

# Conclusions & recommendations

The goal of this report was to identify, analyze and conceptualize methods to reduce the stack losses of the PowerBurner-boiler combination. This chapter contains an overview of the most important conclusions resulting from this research. Also, recommendations for future work on the subject are given.

## 8.1. Conclusion

In chapter 1, the following research question was defined:

- How can the stack losses of the PowerBurner-boiler combination be reduced, and what makes this a better alternative to a conventional burner?

From an analysis of the literature in chapter 3, four concepts were identified which could possibly improve the performance of a PowerBurner compared to a conventional burner for firing industrial installations. These concepts were: Steam injection, Flue gas recirculation, a boiler integrated in the combustion chamber: The Velox-type boiler and supplementary firing.

The system including a Velox-type boiler and supplementary firing were capable of achieving the best performance in terms of thermal capacity and -efficiency. The steam-injected system could achieve the highest electrical output, whereas flue gas recirculation allowed for the largest increase in total efficiency.

The supplementary-fired PowerBurner-boiler setup allowed for the largest operating range over which it was more profitable than a conventional burner. Also, it required the lowest CAPEX to be implemented at large thermal outputs. Therefore, supplementary firing was chosen to be the best performing method.

All aforementioned aspects result in the PowerBurner-boiler setup with supplementary firing being the best alternative to replace a conventional burner for the production of steam, as it allows for the largest thermal operating range and -efficiency, while requiring low costs and retaining enough electrical output in order for the system to be more profitable than a conventional burner over a large operating range.

In chapter 6, a conceptual design of the supplementary burner was developed. This design had to comply by a set of requirements which could directly affect the applicability of the burner. These were:

- An operating range with a maximum firing rate which results in 3 vol% oxygen in the exhaust and a minimum rate of at least 10% of the maximum firing rate.
- Over this operating range, a combustion efficiency of 99%;
- A maximum pressure loss over the burner of 25 mbar;
- A maximum emission of $NO_x$ of 50 mg/Nm$^3$ at 15 vol% oxygen.

From an analysis of burners of different manufacturers followed that a "grid-type burner" performed best in terms of these requirements. Based on the grid-type burner, a 2D-axisymmetric and 3D concept of the burner were developed by making use of the CFD tool ANSYS Fluent. Both models were able to burn 0.485-4.85 MW of fuel, of which the maximum results in 3 vol% oxygen in the exhaust and 100% combustion efficiency was achieved over the full operating range. The pressure loss of both models were in the range of 1-3 mbar, which was well below the requirement. Both models indicated $NO_x$ emissions at the maximum fuel input which were probably slightly higher than the required level, but the accuracy of these calculations was not known.

The following geometrical considerations of the 3D model resulted in the performance in terms of the requirements:

1. Distribution of fuel injection to improve mixing and the operating range;
2. Distribution of the oxidizer, matching with the fuel distribution, to improve mixing and keep the burner cool;
3. Gap between the burner and duct center, to improve mixing and enable a low minimum of the thermal operating range;
4. Tilted geometry near the duct wall to create a recirculation zone to improve mixing. This could improve flame stability.

The conceptual design of the supplementary burner, including the location of the geometrical considerations, is shown in figure 8.1.

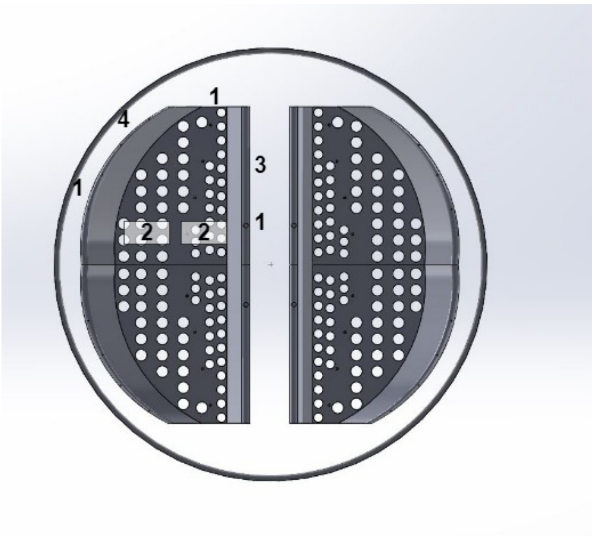


Figure 8.1: Design suggestion for the supplementary burner including locations of the geometrical considerations.

In chapter 7, aspects considering the practical implementation of the supplementary-fired PowerBurner have been analyzed. From this followed that, for part-load operation, it was generally more profitable to operate the gas turbine at the design shaft speed, while varying the supplementary firing rate to achieve a certain thermal output. Only in cases where the price of electricity was almost equal to the price of fuel, it was more profitable to achieve thermal outputs lower than the maximum by varying the shaft speed and keeping the secondary firing rate at a maximum.

In terms of profitability, it was most beneficial to employ several PowerBurners (without supplementary firing) in cases where the price of electricity was high compared to the price of fuel, as this maximizes the revenue from electrical power. At very low price ratios, it was often more beneficial to employ a regular burner than a supplementary-fired PowerBurner. This depends on the thermal output, however, as the output influences the supplementary firing thermal efficiency. For the cases in between, the supplementary-fired PowerBurner was the most beneficial to employ in terms of profitability. An overview of this is shown in figure 7.3.

In terms of payback time (SPOT), the supplementary-fired PowerBurner has been compared to the use of several PowerBurners to meet a specific thermal demand. At higher thermal outputs, the payback time of a supplementary-fired PowerBurner was generally lower. Reasonable payback times (<5 years) for this system are generally applicable to smaller-sized companies. Also, payback times are lower when higher thermal outputs are required. An overview the SPOT of different-sized companies at several locations in the EU can be found in figure 7.4.

## 8.2. Recommendations

This study showed how to select, design and implement a method to optimize a gas turbine like the PowerBurner, for combined heat- and power operation. Both the design proposal and aspects which have to be considered for the practical implementation of such a system, require some more work before the supplementary-firing concept can be implemented. Therefore, in this section, recommendations for future work are given.

### 8.2.1. Recommendations for the burner design

In order to define the true performance of the burner a prototype would have to be build and tested. The design, as proposed in chapter 6, was mostly based on the technical requirements. Some practical aspects like manufacturability, maintainability, material choice, type of ignition, supplementary equipment and connection to the duct are not considered. These aspects should be considered before the first prototype can be created. With the prototype available, the following process is recommended in order to come to a final design. This process is also depicted in figure 8.2.

#### From design proposal to final design

From this study the design proposal, 3D Fluent model and a set of design considerations are available. With this, a basic design can be created which can be turned into a working prototype. As from the models no conclusions could be drawn on flame stability, it is important to determine if the flame does not blow out or lift off from the burner. These are indications of an unstable flame.

Therefore, it is important to determine this before the burner is built. This could be checked through a more extensive CFD analysis. With this could also be determined which type of ignition would be required: A pilot flame if the flame is less stable, or a spark ignition source for a stable flame.

After that, it is important to split the testing process in three phases: One operating with ambient air, one operating at high temperature (973 K) ambient air and one with gas turbine flue gases. By creating an expectation of the high temperature test from the low temperature test results, severe damage to the high temperature- or gas turbine test setup can be prevented, by comparing the expectations to the structural limitations of these setups.

For the first testing phase, the results from the model (with ambient air) and prototype test are compared, to check if they correspond and are within expectation. If this is not the case, the model and prototype tests have to be analyzed to determine the reason. If it is the case, however, the results can be extrapolated to determine the expected outcome at high temperature ambient air.

This expectation and the results from the model (at high temperatures) and second testing phase result in a three-step verification of the results. If these do not correspond, it is again recommended to analyze the previous steps to determine why this is the case. If they do correspond, again, the results can be extrapolated to determine the expected outcome of the third testing phase, at gas turbine exhaust conditions.

Again, a three step verification of the results is formed by the extrapolation of the previous results, and the results of the model and testing at gas turbine conditions. If these do not correspond, it is suggested to analyze the results. If the results do correspond, they can be checked with the requirements for the supplementary burner. This will result in either accepting or rejecting the design of the current prototype as the final design. If it is rejected, the results can be used in a new basic design and another iteration of the process can be done.

### 8.2.2. Recommendations for determination of $NO_x$ emissions

The emissions of nitrogen oxides has been marked as a very important design constraint for the implementation of the supplementary-fired PowerBurner. From the models resulted that when operating at full load the emissions levels of NO (100-140 PPM) are close to the limit set by the Dutch government (50 mg/Nm$^3$ at 15 vol% oxygen or 113 PPM at 3 vol% oxygen). These values result from the analysis which assume the gas turbine is already emitting its maximum allowable rate of NO (50 mg/Nm$^3$ at 15 vol% oxygen), which is the worst case scenario.

From the models also followed that, if the oxidizer inlet concentration of NO is lowered, the NO concentration in the boiler exhaust will be lowered. So, in order to not preemptively eliminate any possible PowerBurner implementations due to the $NO_x$ level being too high, it is recommended to determine the PowerBurner exhaust compositions accurately.

On top of that, it is possible to make a more concluding remark on emissions, if the accuracy of the Fluent model is known. This could be determined by creating a 2D model of one of the burners, built by Innecs. As the actual $NO_x$ emissions of these burners are known, these can be compared to the results of the model to determine the model accuracy.

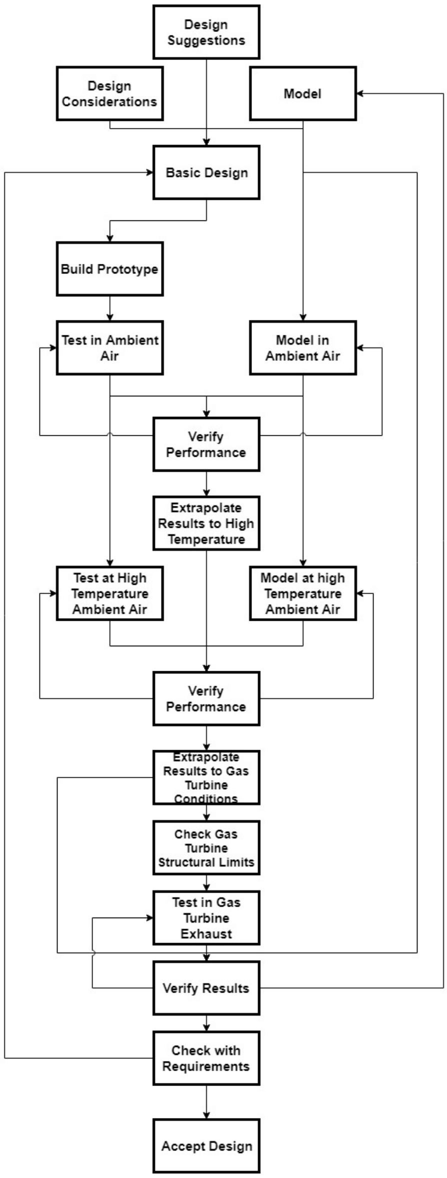


Figure 8.2: Recommendation for the design- and test process.

# A

# Electricity and gas prices in the Netherlands

In this chapter, the prices of electricity and gas in the Netherlands are elaborated to support the economical comparison between the different improvements to the PowerBurner. This is done by analyzing the components of which the prices consist and looking at how rates change when supply or demand of power or gas changes. Finally, the effect of selling electricity back to the grid on its price is elaborated.

## A.1. Components of electricity and gas prices

The prices of both electricity and gas are constantly changing and consist of different components, which account for factors like production or extraction of the energy source, transport and many more. There are three main parts in which the price can be split-up:

### A.1.1. Cost of delivery

In this part, the price for production and extraction (in the case of gas) is accounted for: This is the actual cost of gas or electrical power. Also, a fixed compensation for the supplier of energy is included.

### A.1.2. Cost of transportation

This part covers the price of transportation and the costs the network manager has by constructing and maintaining the grid. Also, the costs for the meter are accounted for in this part.

### A.1.3. Taxes

Finally, the price also includes taxes. For the Netherlands, this part generally is the largest one of the three. It consists of three parts. First one is the *energy taxes*, which are taxes with varying rates. These rates depend on the amount of kWh of electricity or cubic meter of gas consumed. This rate actually decreases with increasing consumption [12]. *Storage of Renewable Energy* is a part of the taxes which is used for the generation of renewable energy and is also depending on how much is consumed. Finally, the VAT (Value Added Taxes) has to be paid over all of the aforementioned sections, even the taxes, and is 21 % in the Netherlands.

Generally, the several parts of the prices are distributed like in figure A.1, but this depends on the amount of energy and gas which is consumed and several other factors.

## A.2. Price of electricity and gas based on supply and demand

As mentioned in this report, the PowerBurner is profitable whenever the yields from the produced electrical power outweigh costs of the extra fuel that is required compared to a burner, for a specified heat output. This heavily depends on the prices of gas and electricity.

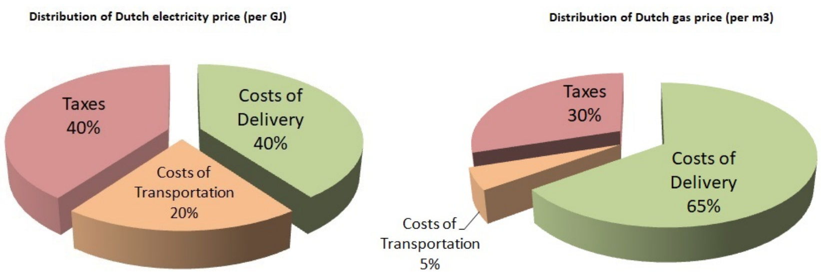


Figure A.1: Components of electricity prices (left) and gas prices (right) for consumers [9].

### A.2.1. Price based on consumption

Prices of electricity and gas depend heavily on the annual consumption of both. In this section, two prices for both gas and electricity are broken down in order to elaborate how what the effect of consumption on the price is. If output of the PowerBurner is considered, an estimate can be made of the amount of electricity and gas a company would consume. Estimates of the PowerBurner in- and outputs are found in table A.1.

Table A.1: Generalized production and consumption of a single PowerBurner

| Medium | Production/ Consumption | Annually | Annually |
|---|---|---|---|
| **Electricity** | 280 kWh | 2.240 MWh | 2.240.000 kWh |
| **Gas** | 2660 kWh | 76.6 TJ | 2.418.000 m$^3$ |

Now, based on table A.1, two prices for gas and electricity are selected. These are found in table A.2. The prices come from CBS [9] and taxes from Nuon [12]. Prices are based on the average price over 2017.

Table A.2: Electricity and gas prices based on annually consumed quantity for industrial users averaged over 2017[9, 12].

| Medium | Consumption | Total price (incl. Tax) | Delivery (ex. taxes) | Transportation (ex. taxes) | Taxes |
|---|---|---|---|---|---|
| **Electricity** | 2.000-20.000 MWh | 0,093 | 0,038 | 0,019 | 0,036 |
| **(€/kWh)** | 20.000-70.000 MWh | 0,069 | 0,026 | 0,016 | 0,027 |
| **Gas** | 10-100 TJ | 10,84 | 7,34 | 0,34 | 3,16 |
| **(€/GJ)** | 100-1.000 TJ | 8,13 | 5,18 | 0,36 | 2,59 |

A short example: If a company employs a single PowerBurner, which supplies half of the demanded electricity, the company would be charged the prices of the lower range for both electricity (2.240 MWh demand at 0,093 €/kWh) and gas (72 TJ demand at 10,84 €/GJ) (table A.2).

### A.2.2. Prices to- and from the grid

When electricity is generated locally, there are three possibilities for utilization: Use it directly, store it or sell it back to the grid. (Direct usage and storage are treated equally here, as they both aim to reduce the amount of electricity bought from the grid.) Utilization influences the value of the electricity, as electricity is sold back to the grid for a different price compared to what it was bought for. To explain this, three cases are distinguished:

1. All locally generated electricity is used (or stored) locally;
2. Part of the locally generated electricity is sold back to the grid, but the power supplied to the grid is lower than demand from the grid;

3. Local supply to the grid is larger than demand from the grid, the surplus is sold back to the grid.

In the first case, the electricity demand can be reduced by the amount that is generated. This means the full price of electricity can be saved, as less electrical power has to be bought from the grid. In the second case, part of the generated electricity is sold back to the grid. But, as more is supplied from the grid than sold back to the grid, most energy suppliers pay the costs of delivery plus taxes (see figures A.1 & A.2) for the amount that is sold to the grid[46]. In case three, where more electricity is supplied to the grid than taken from, in most cases only the costs of delivery are paid for the sold electricity. An overview for what happens to prices when generating power locally is found in figure A.2.

In this figure, the light areas indicate part of the demand or supply which is bought from- or sold to the grid. The colored area of the pie charts below indicates for each case which part of the price is retrieved when using or selling part of the electricity indicated with the circles in the bar chart.

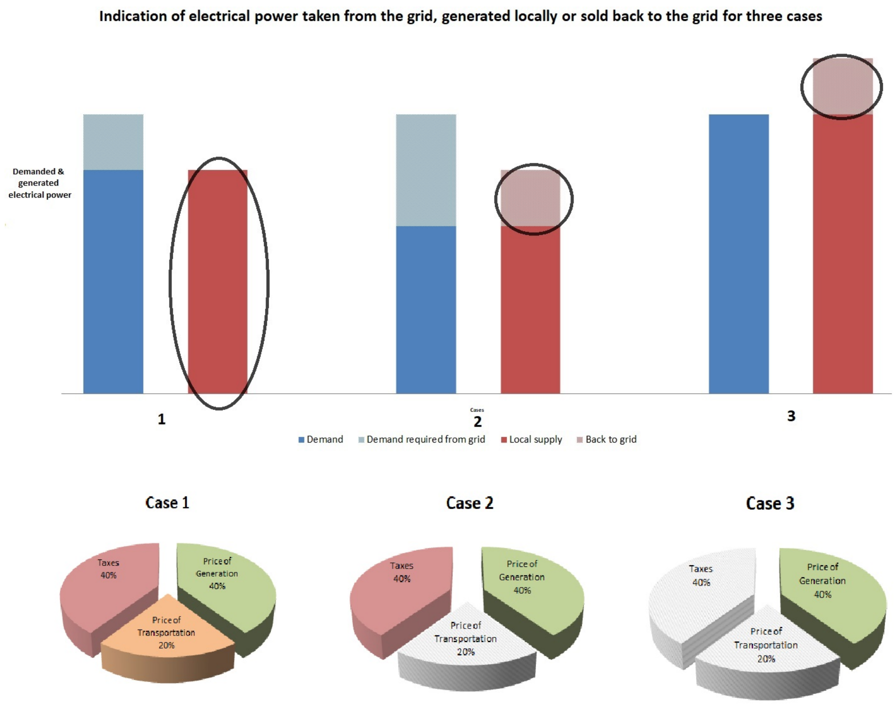


Figure A.2: Electricity demand (blue) and the locally generated supply (red).

From figure A.2 can be concluded that it is never more profitable to sell part of the electricity back to the grid when there is a possibility to use it locally, as the costs of transportation are not retrieved in this case. Also, it might be profitable to store locally generated energy, in order to reduce demand from the grid in the future. Selling the generated electricity straight away has much smaller yields.

For gas, it should be noted that if it is used to produce electricity, under certain conditions there is no need to pay taxes over the gas price (see figure A.1) in the Netherlands. One of these conditions is that the electrical efficiency of the system is at least 30%, which is something the PowerBurner does not reach currently.

# B

# Thermoflex models

In this appendix, the Thermoflex models that have been used throughout this report are elaborated. Thermoflex (https://www.thermoflow.com) is a piece of software can solve mass- and energy balances for a large set of components used in power plants (i.e. evaporators, compressors, gas turbines) by creating a closed loop of icons of such components. It can handle both design and off-design.

A total of 6 models have been created in Thermoflex and used for this report: The first is a basic model of the PowerBurner based on a design point specification supplied by Innecs. The next four models are all variations from the basic model with the implementation of the concepts that have been compared in chapter 4. The sixth model has been created for the analysis in chapter 7.

## B.1. Basic PowerBurner model including a boiler

The PowerBurner model on which all further models are based is shown in figure B.2. In this model, 15 different components can be distinguished by the number shown in bold. These are defined in table B.1. This table also shows the setting that has been used in Thermoflex for each component, if applicable. The numbers in figure B.2 that are supplied inside squares are stream numbers. Red streams are streams of air or flue gas, a yellow stream (5) consists of fuel and blue streams (13, 14, 17, 18) are composed of water and steam.

### B.1.1. Design point specification and Thermoflex inputs

For the basic Thermoflex models, data from the design point specification is used. These parameters are shown in table 4.1. The third column shows the PowerBurner data, as specified in the design point specification. The fourth column indicates the respective parameter in the Thermoflex model, which was either an input or calculated by the model. Column five indicates in which component number (of figure B.2) this parameter was defined, and the sixth column indicates the deviation of the Thermoflex parameter compared to the design point spec, for the parameters which were calculated by the model.

From the design point, all mass flows (except for fuel), bleeds and cooling flows could directly be used as inputs for the Thermoflex model. Local pressure losses from the specification are implemented in the model by the use of ducts. The compressor power consumption and turbine power output deviate around 0.1% and 0.0% from the design point, respectively. The net power output is around 0.5 % higher than the design point, which is due to slight variations in the auxiliary power consumption and electricity- and friction losses. All other Thermoflex output parameters deviate less than 0.7 % from the design point specification. From this can be concluded that the model is a very accurate representation of the PowerBurner as defined in the design point specification.

### B.1.2. Subsequent boiler for thermal output analysis

As the thermal energy from the PowerBurner is often used in a boiler, the thermal output cannot be defined as the heat released from cooling the flue gas down to ambient temperature. The thermal efficiency results from the pinch point of the boiler: A minimum temperature difference between the flue gas and water saturation temperature that enables enough heat transfer. So, in order to define

Table B.1: Overview of all components of figure B.2

| Component Number | Component Type | Remarks | Thermoflex Setting |
|---|---|---|---|
| 1 | Air inlet | - | Ambient Air |
| 2 | Fuel inlet | Groningen Gas (LHV 38041 kJ/kg) | - |
| 3 | Compressor | - | Design |
| 4 | Combustion Chamber | - | Specify Outlet Temperature |
| 5 | Turbine | - | Design |
| 6 | - | - | - |
| 7 | Duct | Defines pressure loss | - |
| 8 | Duct | Defines pressure loss | - |
| 9 | Air/gas outlet | Bleed outlet | Ambient |
| 10 | Air/gas splitter | Splits main flow & bleed & turbine cooling flow | Throttle 1st outlet (to 9) |
| 11 | Air/gas outlet | Stack outlet | Ambient |
| 12 | Duct | Defines pressure loss | - |
| 13 | Evaporator | Part of Boiler | Pinch temperature difference |
| 14 | Superheater | Part of Boiler | - |
| 15 | Economizer | Part of Boiler | No water-side recirculation |
| 16 | Water inlet | Boiler feedwater inlet | Subcooled liquid |
| 17 | Water outlet | Outlet of superheated steam | - |
| 18 | Gas/air mixer | Mixes main gas flow w/ turbine cooling flow | Throttle 1st inlet (from 10) |

the true performance (in terms of thermal efficiency) of the four concepts in chapter 4, a boiler has been modelled in Thermoflex at the exhaust of the PowerBurner.

The boiler consists of an economizer, evaporator and superheater, and operates at a water/steam pressure of 10 bar. The fixed temperatures and parameters that define the boiler performance are shown in table B.2. This table shows the temperatures that are used to include the effect of the pinch point on the thermal efficiency of the different concepts.

Table B.2: Temperatures of the water/steam streams (at 10 bara) of the boiler model.

| Boiler Component | Inlet Temperature | Outlet Temperature | Performance Defined By |
|---|---|---|---|
| **Economizer** | 368.2 K | 443.9 K | Outlet Subcooling (10 K) |
| **Evaporator** | 443.9 K | 453.9 K | Pinch Temperature (20 K) |
| **Superheater** | 453.9 K | 523.2 K | Outlet Temperature (523.2 K) |

### B.1.3. Off-design operation

The parameters used in the basic model act as the ”Thermodynamic Design”: Characteristics at which the components are designed to run. An example of this is the shaft speed of the single-shaft Power-Burner: In the ”Thermodynamic Design”, the shaft speed for normal operation is used. When this design is specified, Thermoflex offers the ability to operate (part of) the system in off-design. The effect of varying a parameter will be relative to the deviation of that parameter from the design point. An example: If in Thermodynamic design the static pressure loss of a duct is defined, in off-design, the duct will apply a lower pressure loss to the stream if the stream velocity is reduced. This is due to the fact that the static pressure loss scales with the stream velocity in the following manner:

$$\Delta P_{static} \sim 0.5 \rho v^2 \tag{B.1}$$

In order to simulate the performance of a compressor or turbine in off-design, a map is required for both. Basic maps can be generated within Thermoflex and scale with the pressure ratio, mass flow and isentropic efficiency defined in the Thermodynamic Design. These maps are shown in figure B.1. For each model will be indicated whether or not parts have been operated in off-design.

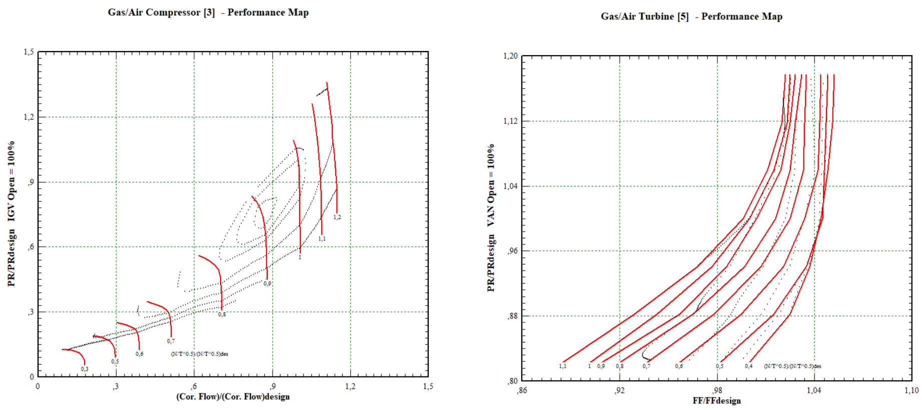


Figure B.1: Basic compressor- and turbine maps generated in Thermoflex and used for off-design operation in certain models.

As there is no actual performance data known of the PowerBurner at part-load operation, it is assumed that running the basic thermodynamic model in off-design in Thermoflex accurately represents the PowerBurner in part-load operation.

## B.2. PowerBurner models including 4 concepts.

In this section, the Thermoflex models are shown for the four concepts (steam Injection, flue gas recirculation, the Velox-type boiler and supplementary firing) which are compared in chapter 4. For each concept explained in chapter 4, a parameter is varied in the model to analyze its effect on 3 parameters: The electrical power output, fuel usage and steam production rate. These are used for the comparison of the concepts in that chapter.

### B.2.1. Steam injection

In order to apply steam injection to the PowerBurner, a splitter is added to the steam exhaust of the superheater. This splitter can be identified with number 11 in figure B.3. This component will split the flow in 2 directions: Towards the steam outlet like in the basic model, or towards the combustion chamber where it is to be injected. The extra component that is used is shown in table B.3.

Table B.3: Extra components used in the Thermoflex model of the PowerBurner for steam injection.

| Component Number | Component Type | Remarks | Thermoflex Setting |
|---|---|---|---|
| 11 | Splitter | Performance set by injection rate of combustor (4) | - |

In the combustion chamber component the mass flow of steam that is to be injected can be specified. This is the parameter that will be varied to determine how the thermal- and electrical output and fuel input are influenced. As steam injection is to be applied to the current PowerBurner setup, every component is set to off-design mode to analyze the effect on the existing components.

### B.2.2. Flue gas recirculation

In order to enable flue gas recirculation in the basic cycle, a couple of enhancements have to be made. First of all, an air/gas specification is added which can be identified by number 20 in figure B.4.

This component will split the exhaust gas from the turbine into a part that is recirculated back to the compressor , and part that will be released to the surrounding area. The part of the exhaust gas that flows back to the compressor is mixed with fresh air in the duct balancing mixer labeled with number 19. This component defines the mass flow. All new components of the flue gas recirculated system are indicated in table B.4.

Table B.4: Extra components used in the Thermoflex model of the PowerBurner for flue gas recirculation.

| **Component Number** | **Component Type** | **Remarks** | **Thermoflex Setting** |
|---|---|---|---|
| 19 | Duct balancing mixer | Fixed outlet massflow | Design by flow fraction |
| 20 | Gas/air specification | | Gas source set by network |

The recirculation ratio is regulated through duct balancing mixer 19 by varying the flow fraction from the first inlet. To determine the amount of flue gas that is to be added, the mass flow rate after mixer 19 is fixed a value equal to the air inlet of the base model. With this, setting the flow fraction to the first inlet of mixer 19 fixes the flow fraction of exhaust gas at specification and the mass flow of air from gas/air inlet 1.

To determine the effect of flue gas recirculation on the current PowerBurner setup, everything but duct balancing mixture 19 (figure B.4) can be put in off-design mode as the mixture fraction is defined in this component, and it fixes its thermodynamic design at a certain recirculation ratio.

### B.2.3. Velox-type boiler

As the Velox-type boiler is a boiler incorporated within the combustion chamber, figure B.5 shows that the basic cycle has been extended with an evaporator (19) and a superheater (11), which together form that Velox boiler. Furthermore, a splitter (20) is added, which splits the feedwater flow towards the economizer of the boiler at the exhaust and the Velox boiler. An extra water outlet (21) is added, which is the outlet for the steam from the Velox boiler. All these components are shown in table B.5.

Table B.5: Extra components used in the Thermoflex model of the PowerBurner to include a Velox-type boiler.

| **Component Number** | **Component Type** | **Remarks** | **Thermoflex Setting** |
|---|---|---|---|
| 11 | Superheater | - | Steam outlet temperature |
| 19 | Evaporator | Pinch point = TiT | Pinch temperature difference |
| 20 | Splitter | - | - |
| 21 | Water outlet | - | - |

The superheater (19) is added to enable the production of steam with properties equal to the superheater of the other boiler (14). The Velox boiler allows for more fuel to be combusted, resulting in a higher flue gas temperature. This is then cooled in that boiler to meet the turbine inlet temperature requirements of the PowerBurner.

In the basic model this was done by fixing the outlet temperature of the combustor (4). With this setup it is done by fixing the flue gas outlet temperature of evaporator 19 at the TiT. This temperature is determined by the pinch point of that evaporator. As water to the Velox boiler is directly supplied from the feedwater inlet (16), the required pinch point of evaporator 19 can be determined with equation B.2.

$$\Delta T_{pinch,19} = TiT_5 - T_{feedwater,16} \tag{B.2}$$

If the outlet temperature of combustor 4 is now raised above the level of the basic model, heat has to be taken away in the Velox boiler to ensure the pinch point is reached. Splitter 20 will always direct enough water to the Velox boiler to enable this heat transfer. The steam rate (and thermal output) of the system will be the sum of the mass flows of outlets 17 and 21.

The Velox boiler allows for more fuel to be combusted which results in more mass flow over the turbine (5). To simulate this effect, the whole system is run in off-design mode except for the Velox boiler itself. The size and heat transfer properties of this boiler are not defined initially. Therefore, by operating components 11 and 19 in thermodynamic design mode, their thermodynamic properties will be fixed for the amount of heat that is transferred in the current state.

### B.2.4. Supplementary firing

With supplementary firing, the leftover oxygen in the exhaust is used in another combustion stage before the products enter the boiler. To determine the effect of this system on the PowerBurner, a duct burner (11) and fuel inlet (19) have been added to the basic model. These components are shown in figure B.6 and table B.6.

Table B.6: Extra components used in the Thermoflex model of the PowerBurner to include supplementary firing boiler.

| Component Number | Component Type | Remarks | Thermoflex Setting |
|---|---|---|---|
| 11 | Horizontal Duct Burner | - | Specify fuel flow<br>Minimum allowed oxygen content (vol%) |
| 19 | Fuel inlet | Flow determined by duct burner | - |

The mass flow from the fuel inlet (19) is determined by setting the desired fuel flow in the duct burner (11). Furthermore, the maximum allowed fuel flow can be fixed by setting the "Minimum allowed volumetric oxygen concentration" in the settings for the duct burner. Furthermore, after defining the thermodynamic design (with no supplementary firing), the whole system can be put to off-design to analyze the effects of the raised mass flow rate and temperature in the boiler, as well as the change in pressure due to the added burner.

## B.3. Thermoflex model of the PowerBurner including the Viessmann 300 HS Boiler

For the analysis done in 7, the boiler in the basic Thermoflex model has been replaced with a model of the Viessmann Vitomax 300 HS boiler with type-200 economizer. Of this boiler, a datasheet was available [11] which has been used to determine certain properties of the boiler. As the goal of that section is to determine the performance of a supplementary-fired PowerBurner in combination with an actual boiler, the burner is included as well.

The upper part of figure B.7 shows the basic model of the PowerBurner from figure B.2, without the boiler section. Following the stream from duct 12 in the direction of stream 7 the model includes a duct burner (11) with fuel inlet (19) which operates like in figure B.6. After stream 12, an outflow switch (24) is present. Such a switch is open in either direction 1 or 2, indicated with the red number. This switch determines whether the flue gases from the PowerBurner flow through the boiler(direction 2) or flow directly to the stack (air/gas outlet 25/ direction 1) according to the rules in B.3.

If the flue gas from the PowerBurner does not go through the boiler, the flue gas from combustion chamber 20 will. This combustion chamber takes air and fuel from air- and fuel inlets 17 and 22 respectively. If the flue gas of the PowerBurner goes through the boiler, the flue gas from combustion chamber 20 goes to the stack at outlet 26. From switch 16, either of the flue gas flows go through an economizer (14) and evaporator (21) and ends up in the stack at air outlet 15. On the other side of the boiler, feedwater enters through water inlet 6 and steam leaves through water outlet 13. All changed components compared to the basic model are shown in B.7.

$$\begin{aligned}\textbf{Switch 16 Direction 1} = OPEN \Longrightarrow \textbf{Switch 24 Direction 2} = OPEN\ \&\ \textbf{Switch 23 Direction 2} = OPEN \\ \textbf{Switch 16 Direction 2} = OPEN \Longrightarrow \textbf{Switch 24 Direction 1} = OPEN\ \&\ \textbf{Switch 23 Direction 1} = OPEN\end{aligned} \tag{B.3}$$

The setup of this Thermoflex model with 3 switches has a very specific reason: It allows for a thermodynamic design of the boiler by making use of data from the Viessmann Datasheet[11]. Combustor 20 simulates an actual burner used for the boiler. So, in the thermodynamic design, the boiler gets the flue gas from combustor 20, which fixes the overall heat transfer coefficient and other properties at a specific mass flow.

From table 7.1 follows that the outputs of the model in thermodynamic design are very similar to the data supplied by the datasheet. From this can be concluded that the thermodynamic properties of the boiler are an accurate representation of the thermodynamic properties in reality, and changing the flue gas input should result in a realistic simulation of the off-design characteristics of the boiler. Now that the thermodynamic design of the system is fixed, every component can be set to off-design. By opening switch 16, direction 1, the (supplementary-fired) PowerBurner flue gas will start transferring heat in the boiler, resulting in an accurate simulation of the thermal output.

With the static pressure drop of the boiler known from the datasheet, and the pressure loss over the duct burner known from CFD calculations of chapter 6, these losses are included in the Thermodynamic design. So, the effect of these losses on the PowerBurner performance are included in this model, as well.

Table B.7: Overview of the extra components added to the basic PowerBurner model for the analysis done in 7.

| **Component Number** | **Component Type** | **Remarks** | **Thermoflex Setting** |
|---|---|---|---|
| 6 | Feedwater inlet | - | Subcooled liquid |
| 11 | Duct Burner | - | Specify fuel flow<br>Minimum oxygen vol% content |
| 13 | Steam outlet | - | - |
| 14 | Evaporator | Input based on datasheet | Design steam production<br>(in Thermodynamic design) |
| 15 | Air/gas outlet | - | Ambient |
| 16 | Inflow switch | - | Node 2 (Thermodynamic Design)<br>Node 1 (Off-design) |
| 17 | Air inlet | For thermodynamic design<br>of Boiler | Ambient |
| 19 | Fuel inlet | For supplementary firing<br>Mass flow set by 11 | - |
| 20 | Combustor | Input based on datasheet | Specify fuel flow |
| 21 | Economiser | Input based on datasheet | Outlet subcooling |
| 22 | Fuel inlet | Input based on 20 | - |
| 23 | Outflow switch | Fixed by 16 | - |
| 24 | Outflow switch | Fixed by 16 | - |
| 25 | Air/gas outlet | PowerBurner<br>flue gas stack | Ambient |
| 26 | Air/gas outlet | Combustor 20<br>flue gas stack | Ambient |

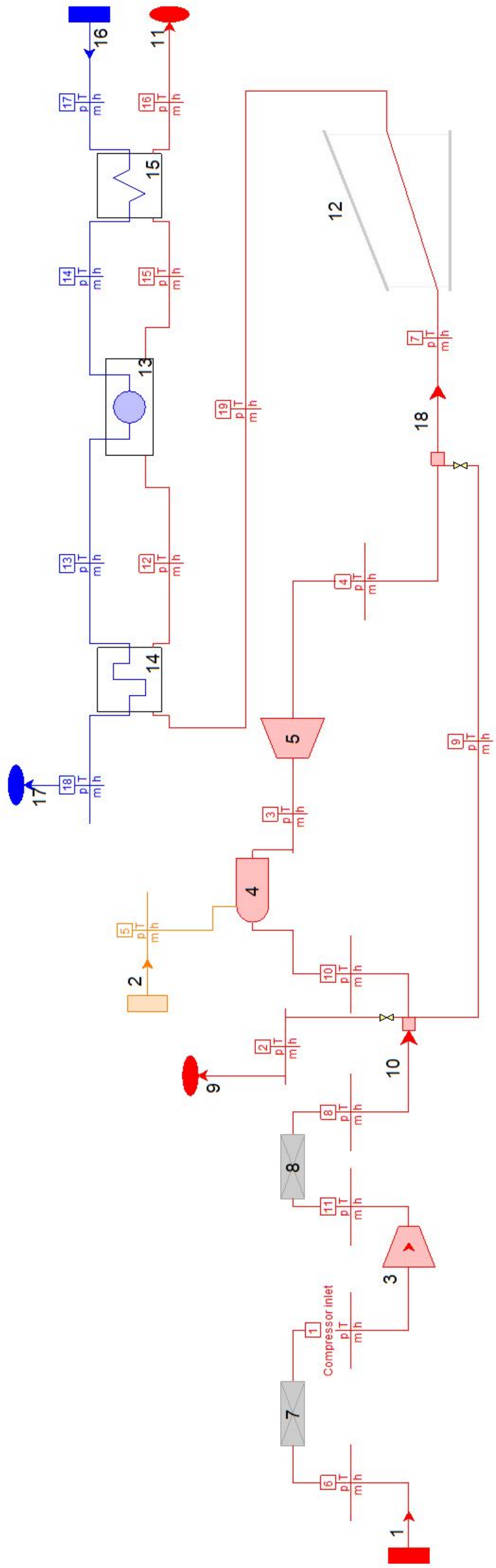


Figure B.2: Basic Thermoflex model of the PowerBurner, including a boiler connected to the exhaust.

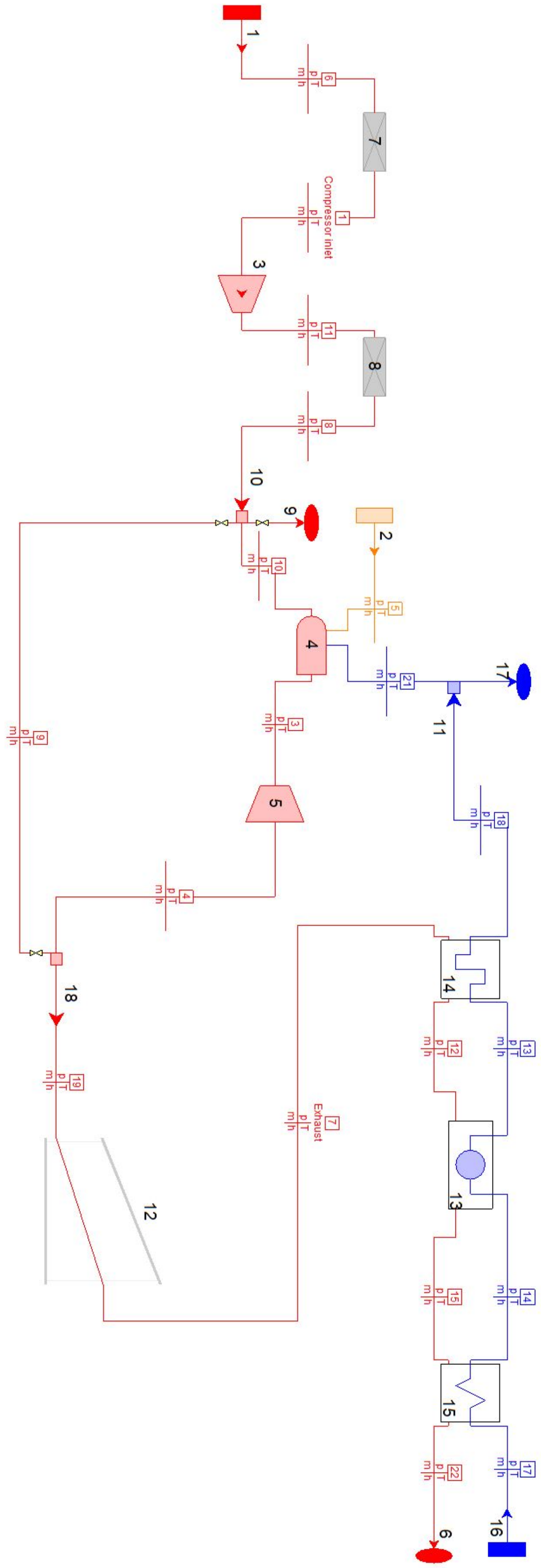


Figure B.3: Thermoflex model of the PowerBurner including steam injection and a boiler connected to the exhaust.

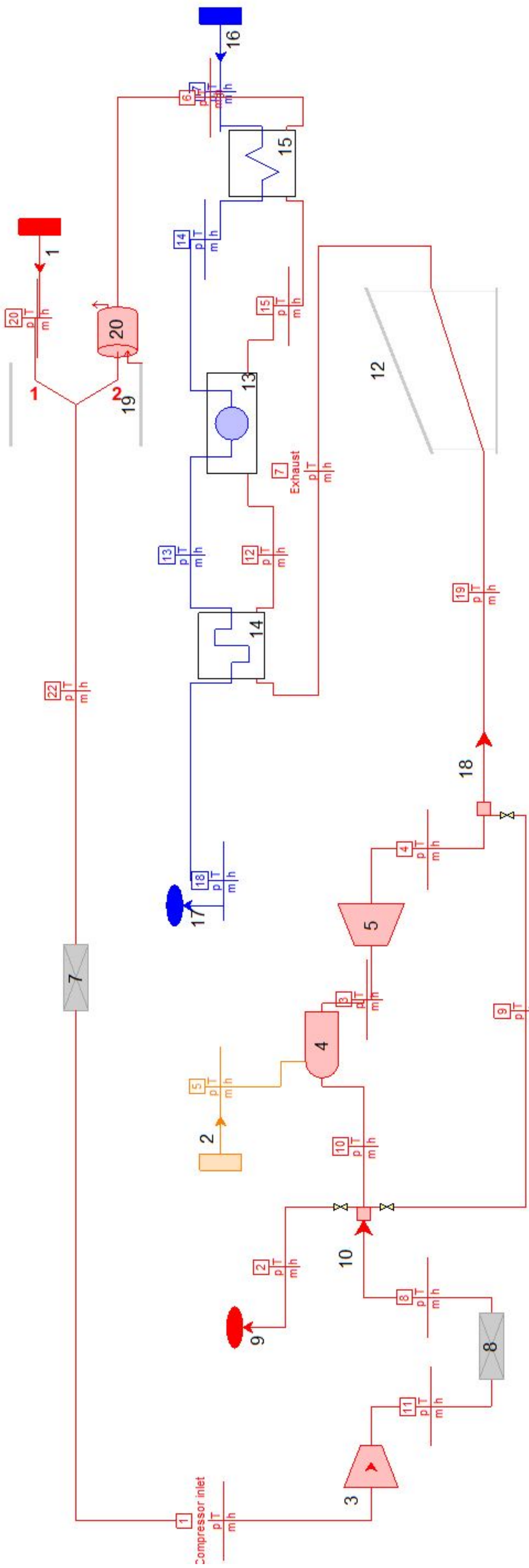


Figure B.4: Thermoflex model of the PowerBurner including flue-gas recirculation and a boiler connected to the exhaust.

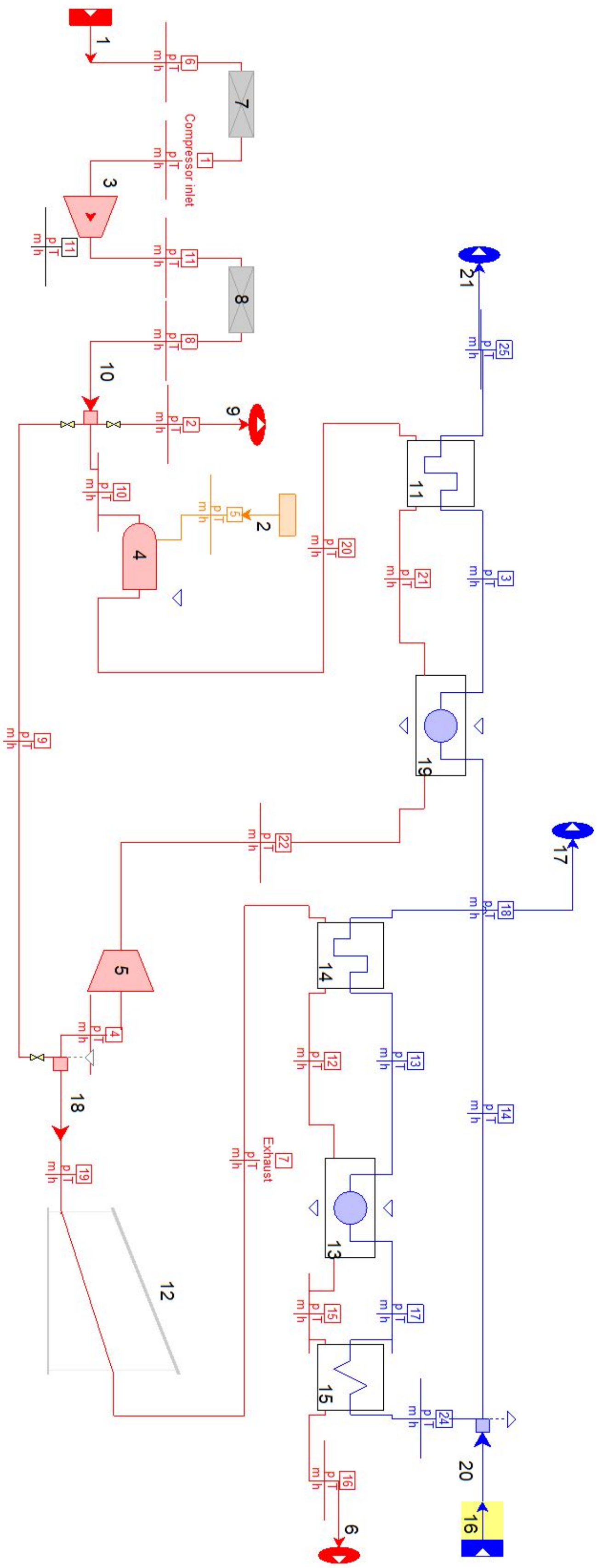


Figure B.5: Thermoflex model of the PowerBurner including the Velox-type boiler after the combustion chamber and a regular boiler connected to the exhaust.

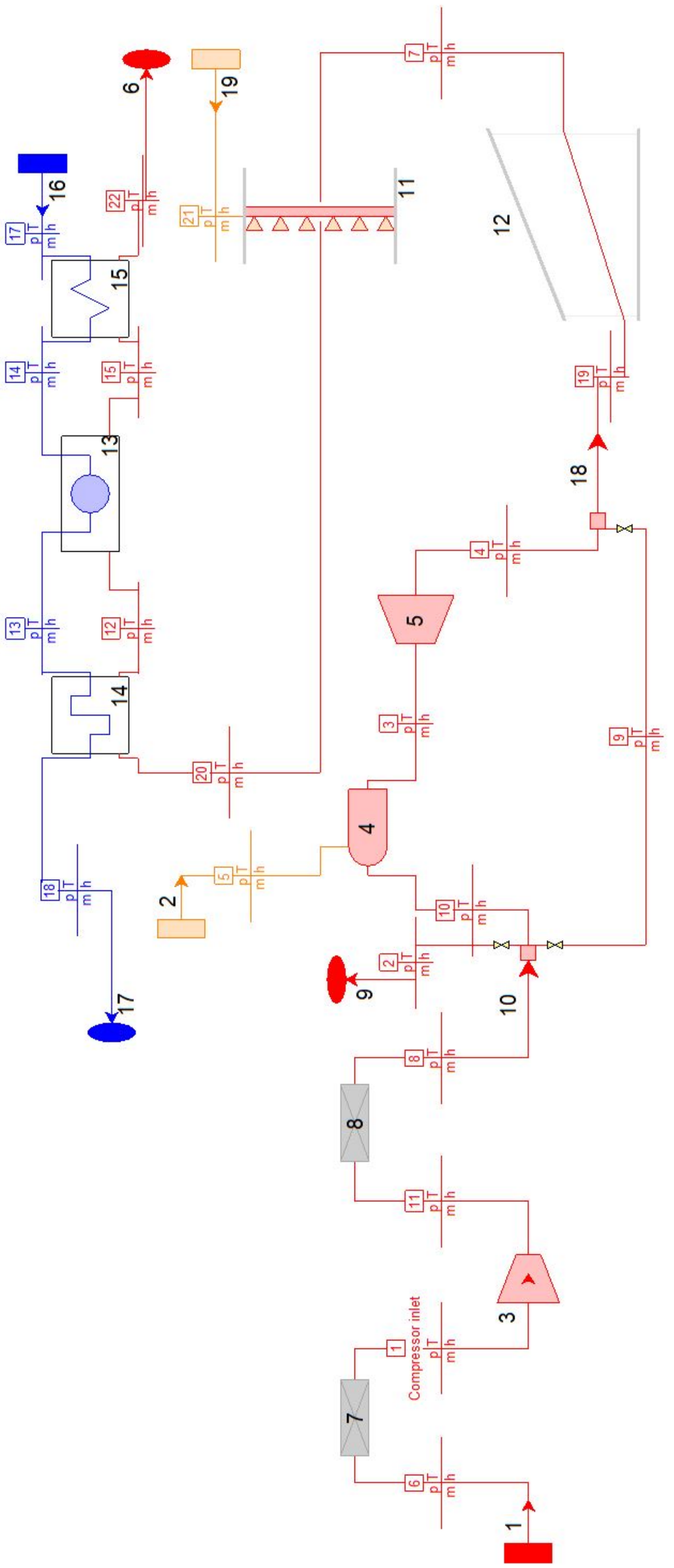


Figure B.6: Thermoflex model of the PowerBurner including supplementary firing of the exhaust gases before the flue gas enters the boiler.

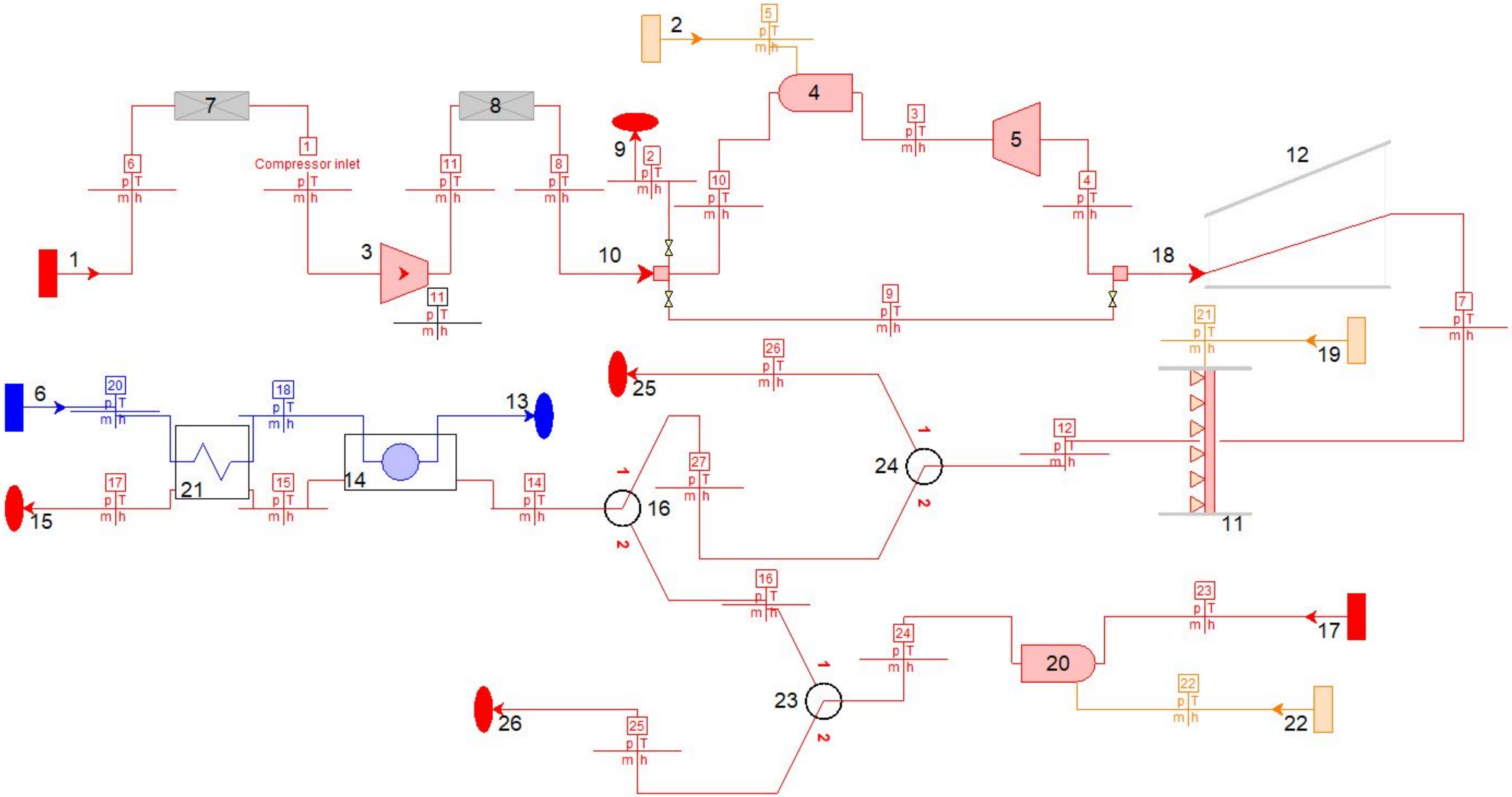


Figure B.7: Thermoflex model of the PowerBurner including supplementary firing and a model of the Viessmann boiler compromised of two flue gas inlets: One from a combustion chamber to determine the thermodynamic design, and one from the PowerBurner/exhaust gas burner outlet.

# C

# Sizing of the Velox-type boiler

This section will elaborate on the sizing of a Velox-type boiler (which is to be implemented in the combustion chamber of the PowerBurner. This is done in order to make a preliminary estimation of the size and equipment cost. Sizing and cost estimation will be done based on methods supplied by Towler and Sinnott [10] for the design of shell & tube heat exchangers, boilers, condensers and more. For this, results from the Thermoflex model will be used to base the design on. The equipment design method is shown in figure C.1.

From here on, each step in the design process of C.1 will be followed and elaborated:

### Step 1 & 2: Specification, Duty and Physical Properties

The size of the Velox-type boiler will be based on the PowerBurner with a 3 vol% $O_2$-content in the exhaust. This allows the system to have a very large operating range in terms of thermal output. The air flow towards the combustion chamber is set by the compressor. The fuel that is used in the calculations is Groningen Gas (GG), with a composition as shown in C.1.

Table C.1: Composition and properties of Groningen Gas in mol%.

| **Substance** | **Composition (mol%)** |
|---|---|
| CH4 | 81.41 |
| C2H6 | 2.86 |
| C3H8 | 0.38 |
| C4H10 | 0.14 |
| C5H12 | 0.04 |
| N2 | 14.26 |
| O2 | 0.01 |
| CO2 | 0.9 |
| **Fuel Properties** | |
| LHV [kJ/kg] | 38041 |
| AFR (@3vol% $O_2$) | 14.98 |
| fuel flow [kg/s] | 0.2 |

From this follows the flame temperature at the specified exhaust oxygen content. As the Turbine Inlet Temperature is limited at 1173 K, the duty of the heat exchanger can now be calculated. The duty, along with the properties of both fluids along the gas- and water paths are shown in table C.2. Fouling factors have been estimated from Towler and Sinnott [10], for flue gas and oil-free steam.

### Step 3: Assume Overall Coefficient

The overall heat transfer coefficient $U_{o,ass}$ is assumed based on a flue gas-steam heater based on Towler and Sinnott [10], table 19.1. The value is assumed to be:

$$U_{o,ass} = 100[W/m^2K] \tag{C.1}$$

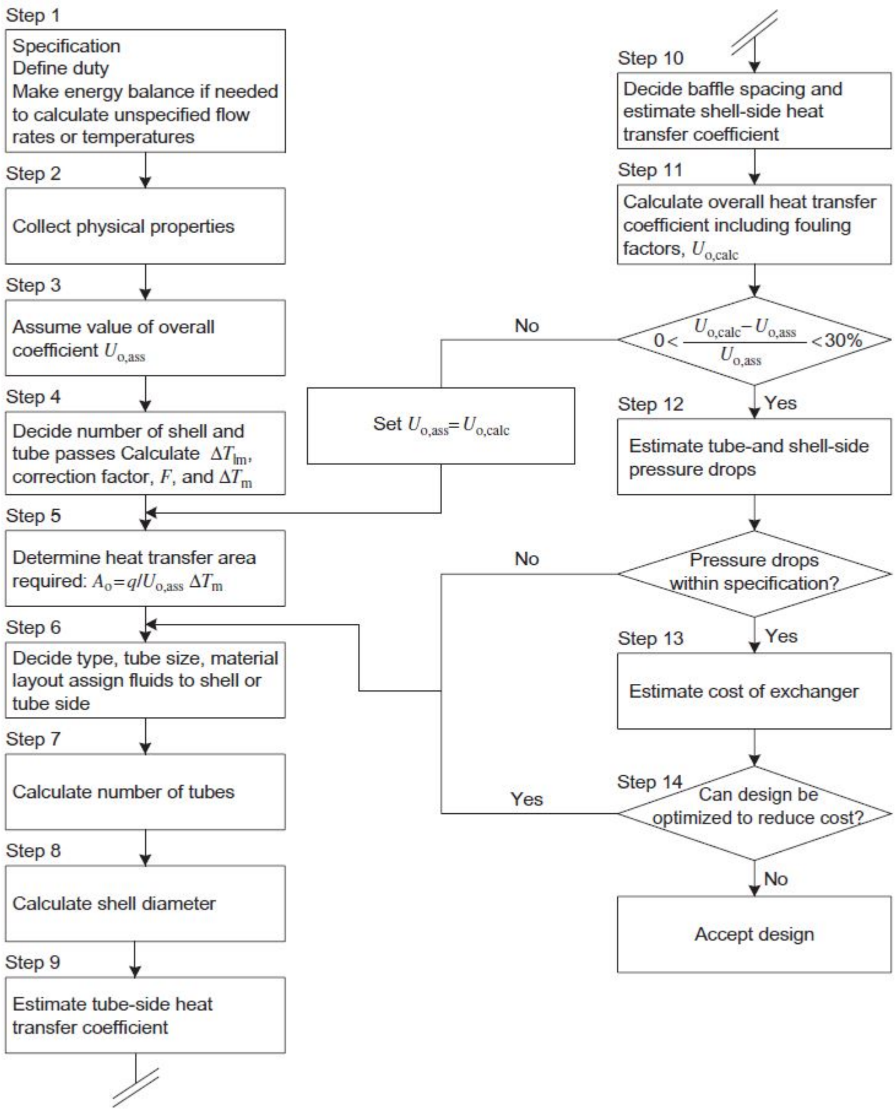


Figure C.1: Design procedure for heat exchangers[10].

Table C.2: Properties and duty of the gas- and steam paths of the Velox-type Boiler.

| Gas Path | Property | Steam Path |
|---|---|---|
| 2220 | Inlet Temperature [K] | 368 |
| 1173 | Outlet Temperature [K] | 368 |
| 3.18 | Pressure [bar] | 10 |
| 1.40 | Average Cp [kJ/kgK] | 4.2 |
| 5.003 | Duty [MW] | 5.003 |
| 3.25 | Mass flow [kg/s] | 2.2 |
| 0.71 | avg Density [kg/m$^3$] | 966 |
| 54.7 | avg Viscosity [$\mu$Pa.s] | 226.5 |
| 97 | avg Thermal Cond. [mW/mK] | 680 |
| 0.0003 | Fouling Factor [m$^2$K/W] | 0.00016 |

### Step 4: Decide number of shell and tube passes and calculate $\Delta T_{LM}$

For the easiest connection between the combustion chamber and the turbine, a single shell- and tube pass will be assumed at first. Because of this, the flow is assumed to be strictly counter-current, so the logarithmic mean temperature difference will not require a temperature correction factor and becomes:

$$\Delta T_{LM} = \frac{(2291-368)-(1173-368)}{ln\frac{2220-368}{1173-368}} = 1283[K] \tag{C.2}$$

### Step 5: Determine the required heat transfer area

The required heat transfer area for the current setup becomes:

$$A_o = \frac{Q}{U_{O,ass} * \Delta T_{LM}} = \frac{5.003 * 10^3}{100 * 1283} = 39[m^2] \tag{C.3}$$

### Step 6 & 7: Determine tube size, number and velocity

As the flue gas is also under pressure, it is beneficial to let this flow on the shell-side [30]. Steam flows on the tube-side. A square tube arrangement will be used for reduced pressure drop. For the tube sizing, standard dimensions will be used. The results are shown in table C.3.

Table C.3: Standard tube dimensions, with resulting number of tubes and steam velocity.

| **Property** | **Value** |
|---|---|
| Outside tube diam. [mm] | 19 |
| wall thickness [mm] | 2.1 |
| Tube length [m] | 2.44 |
| Tube pitch [mm] | 1.25*outside diam. |
| Single Tube Area [$m^2$] | 0.146 |
| Number of Tubes | 268 |
| Tube Velocity [m/s] | 2 |

The steam velocity is very low initially. Therefore, the amount of tube passes is changed to 4, which increases the flow velocity by a factor 4. On top of that, a recirculation ratio of 10 is applied on the steam-side. This results in a velocity of 2 m/s.

### Step 8: Bundle and shell diameter

The diameter from the tube bundle follows the following equation, with $N_t$ and $d_0$ the number of tubes and tube outside diameter, respectively. $K_1$ and $n_1$ are constants depending on the amount of tube passes and pitch arrangement of the tubes.

$$D_b = d_0 * (\frac{N_t}{K_1})^{\frac{1}{n_1}} \tag{C.4}$$

For a four-pass square-tube tube setup, the results are displayed in table C.4. For the amount of clearance, a pull-through floating head-type heat exchanger is chosen, as this type can handle high temperature differentials[10].

Table C.4: Results from equation C.4 for a four-pass squared-tube arrangement

| **Property** | **Value** |
|---|---|
| $K_1$ | 0.158 |
| $n_1$ | 2.263 |
| Bundle diameter $D_b$ [mm] | 937 |
| Shell-bundle clearance [mm] | 95 |
| Inside shell diameter [mm] | 1032 |

### Step 9: Tube-side Heat Transfer Coefficient

With the presently known parameters, the actual heat transfer coefficient for the flue gas on the tube side can be calculated. This follows from the following equation:

$$h_i = j_h \frac{k_f}{d_0} RePR^{0.33} = Nu \frac{k_f}{d_i} \tag{C.5}$$

In this equation, the factor for viscosity correction is neglected. $j_h$ is here the heat transfer factor, which follows from figure 19.23 of Towler and Sinnott [10]. The Reynolds- and Prandtl number can be calculated from the aforementioned data. $k_f$ is the thermal conductivity and $d_0$ is the inner tube diameter. The parameters and results are shown in table C.5.

Table C.5: Parameters and results for calculating the tube-side heat transfer coefficient.

| Property | Value |
|---|---|
| Re | $9.5*10^4$ |
| Pr | 1.85 |
| Nu | 463.6 |
| $L/d_0$ | 168.9 |
| $j_h$ | 4 |
| $h_i$ [W/m²K] | $2.1*10^4$ |

### Step 10: Shell-side heat transfer

The shell area is results in the following flow area and -velocity (table C.6).

Table C.6: Dimensions and flow velocity of flue gas on the shell side.

| Property | Value |
|---|---|
| Shell-side flow area [mm²] | 213127 |
| Shell-side flow velocity [m/s] | 21.6 |

As with equation C.5, the properties of the stream and heat transfer coefficient can now be calculated. Results are displayed in table C.7.

Table C.7: Parameters and results for calculating the shell-side heat transfer coefficient.

| Property | Value |
|---|---|
| Re | 5230.2 |
| Pr | 0.777 |
| Nu | 174.1 |
| $j_h$ | 0.007 |
| $h_o$ [W/m²K] | 174 |

### Step 11: Determination of the overall heat transfer coefficient

The overall heat transfer coefficient follows from the next equation:

$$\frac{1}{U_0} = \frac{1}{h_0} + \frac{1}{h_{od}} + \frac{d_o}{d_i}\left(\frac{1}{h_{id}} + \frac{1}{h_i}\right) + \frac{d_o ln\frac{d_o}{d_i}}{k_w} \tag{C.6}$$

Most of these values have been calculated in the previous section. Table C.8 indicates the values used and the final result of the overall heat transfer coefficient. For the determination of the tube material thermal conductivity ($k_w$), Hastelloy-C267 is chosen, as this material should be able to withstand temperatures over 1300 K.

Now, the difference between the assumed and calculated overall heat transfer coefficient can be calculated, this follows from figure C.1:

$$\frac{U_{o,ass} - U_{o,calc}}{U_{o,ass}} = \frac{121.2 - 100}{100} = 21.2\% \tag{C.7}$$

This is within the 30 % deviation limit suggested by Towler and Sinnott [10]. Therefore, the assumed overall heat transfer coefficient can be accepted, as well as the dimensioning and total tube surface area.

Table C.8: Parameters used in equation C.6 to determine the overall heat transfer coefficient $U_0$.

| **Property** | **Value** | **Description** |
|---|---|---|
| $h_o$ | 174 | Shell heat transfer coefficient [W/m$^2$K] |
| $h_{do}$ | 6250 | Shell coefficient due to fouling [W/m$^2$K] |
| $d_o$ | 19 | Tube outside diameter [mm] |
| $d_i$ | 14.8 | Tube inside diameter [mm] |
| $h_i$ | 21381 | Tube heat transfer coefficient [W/m$^2$K] |
| $h_{di}$ | 3300 | Tube coefficient due to fouling [W/m$^2$K] |
| $k_w$ | 26 | Tube Thermal conductivity [W/mK] |
| **$U_0$** | **121.2** | **Total heat transfer coefficient [W/m$^2$K]** |

### Step 13: Boiler Cost Estimation

In Towler and Sinnott [10], a method is supplied to estimate the costs of parts of a process plants, including boilers and other heat transfer equipment. Such a cost estimation could help in the choice of concepts applied to the PowerBurner. The method is based on a correlation between the price and a certain size parameter. This size parameter can be the steam production rate for a boiler, or the area of heat transfer for heat exchangers, for example. The price can be estimated from the following equation:

$$C_e = a + bS^n \tag{C.8}$$

In this equation, $C_e$ is the Purchased equipment cost on a U.S. Gulf Coast basis from January 2010. In table C.9, the factors a, b, S and n are indicated for different pieces of equipment, along with the estimated price. The price will also be corrected, for 3 factors: Location, time and material.

The price estimation from equation C.8 is based on U.S. Gulf Coast prices. For the Netherlands, a factor ($f_c$) of 1.138 can be applied for the conversion rate to Euro. The second factor corrects for the change in value over time, by making use of the CEPCI-value (Chemical Engineering Plant Cost Index). Finally, a correction factor for material will be applied, as the standard carbon steel cannot be used due to the very high temperatures. As mentioned, a Hastelloy-C alloy would fit. This would induce a correction factor ($f_m$) of 1.55 compared to basic carbon steel. The corrected price will follow from equation C.9.

$$C_{cor} = C_e * f_c * \frac{CEPCI_{2018}}{CEPCI_{2010}} * f_m = C_e * 1.138 * \frac{567.5}{532.9} * 1.55 = C_e * 1.88 \tag{C.9}$$

Estimation of the cost becomes:

Table C.9: Cost estimation of a Packaged Boiler and Floating-head shell- and tube heat exchanger. A correction factor of 1.88 is applied to the $C_e$ price.

| **Property** | **Packaged Boiler** | **Floating Head Shell & Tube** |
|---|---|---|
| a | 124,000 | 32,000 |
| b | 10 | 70 |
| S | 2.2<br>Steam rate [kg/s] | 39<br>Area [m$^2$] |
| n | 1 | 1.2 |
| $C_e$ | €199,600 | €38,817 |
| **$C_{cor}$** | €375,248 | €72,975 |

In table C.9, the costs have been estimated for both a packaged boiler and a floating-head shell-and tube heat exchanger, as the Velox-type boiler has similarities with either. It has to operate with high pressures and temperatures, as a boiler, while the flow path is designed like a shell-and tube heat exchanger. The price of the Velox-type boiler would lie somewhere between the two values of table C.9. Therefore, an cost estimation of €100,000-300,000 for the Velox-boiler seems reasonable based on these estimations

# D

# Burner comparison table

Table D.1: Burners from different manufacturers with $NO_x$ emissions and pressure losses, according to the manufacturer.

| | Burner Type | | | | | |
|---|---|---|---|---|---|---|
| Manufacturer | Grid | Swirl | Ultra-low Nox | Pressure Loss | Nox Emission | Source |
| Mehldau-Steinfath | | x | | 15 mbar | - | website |
| INNECS (concept) | | x | | 20 mbar | 10 ppm | - |
| Maxon | x | | | 2 mbar | - | website |
| | | x | | 15 mbar | - | website |
| Saacke | x | | | 1,5 mbar | < 22 ppm | website |
| | | x | | 27-36 mbar | 22-86 ppm | |
| Forney | x | | | 7,5 mbar | 29 ppm | website |
| Zeeco | x | | | - | 26 ppm | website |
| Eclipse | x | | | 7,5 mbar | - | website |
| Cleaver Brooks | x | | | - | 7 ppm | website |
| | | x | | - | 30 ppm | website |
| Fives | x | | | - | - | website |
| Venairflam | x | | | 1-3 mbar | - | website |
| Alzeta | | | x | - | <3 ppm | website |
| Weishaupt | | | x | - | <15 ppm | website |
| Burnertech | | | x | - | <20 ppm | website |
| worgas | | | x | - | - | website |

# E

# Design process of the 2D burner geometry

In this section, the design process of the 2D geometry, as used in chapter 6, will be elaborated. Although many more iterations were made, the four main steps in the process are shown. The following models are axisymmetric (revolved around the axis of symmetry for 3D) and make use of the maximum fuel input which should result in an exhaust oxygen content of 3 vol%. If all fuel is oxidized in this case, at lower loads it should be able to do so, as well.

## E.1. Basic duct burner geometry

The geometry of the very first model is based on existing geometries of duct burners The aim was to create a geometry which would induce a wake right after the fuel injection. This wake would then ensure the oxidizer and fuel mixed well. The first geometry is shown in figure E.1, along with the temperature contour which was created with the combustion process. The geometry includes fuel injection in the middle section near the symmetry axis, where the low temperature zone is present.

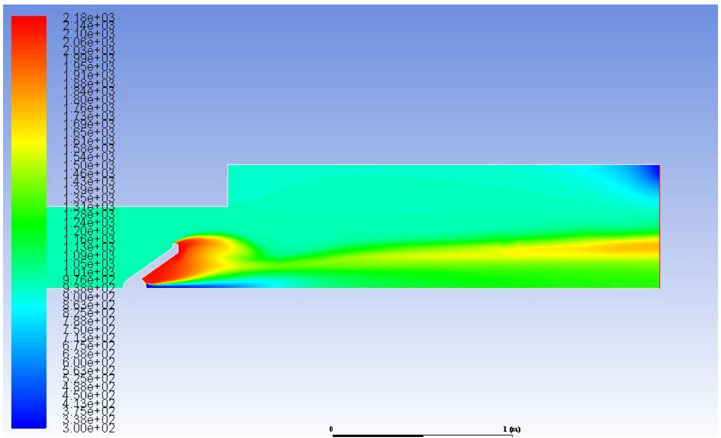

Figure E.1: Temperature contour of the first geometry. Temperatures are shown in K.

In this figure, two high-temperature areas can be distinguished: One attached to the burner geometry and one small area near the boiler exhaust. The first area will heat up parts of the burner. As the high-temperature areas are located where the combustion reactions take place, it would seem there is still fuel left near the exhaust. This indicates the flame is not stable, and as the high temperature zones are so far apart, the fuel and oxidizer are probably not mixing well.

This is supported by figure E.2, in which the concentration of methane over the height of the burner outlet is shown. There is still methane present, so the combustion reaction did not have the opportunity to completely take place. Methane is mostly present in the middle of the duct (r=0), which indicates that there is not enough oxygen in that area for the combustion reaction to take place.

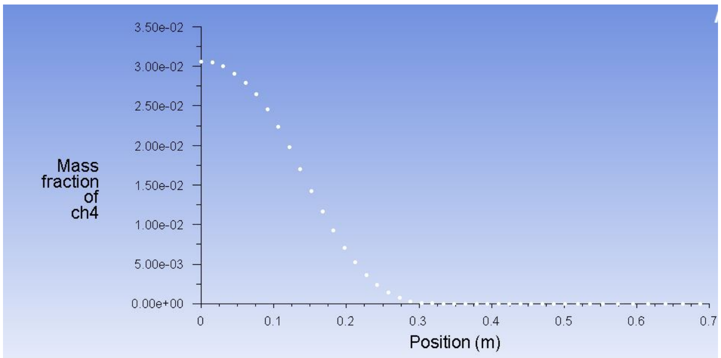


Figure E.2: Methane concentration at the boiler exhaust in the first step of the burner design.

What can be concluded from these figures is that the first burner geometry has to be improved on 3 aspects: Flame stability, mixing and location of the flame to prevent the burner from overheating.

## E.2. First design iteration

To improve the aspects mentioned in the previous section, the second burner iteration included a hole in the geometry. This hole is supposed to improve mixing in the center of the duct. Figure E.3 indicates the methane concentration over the length of the boiler. From this can be seen that the methane concentration again does not reach 0 at the outlet.

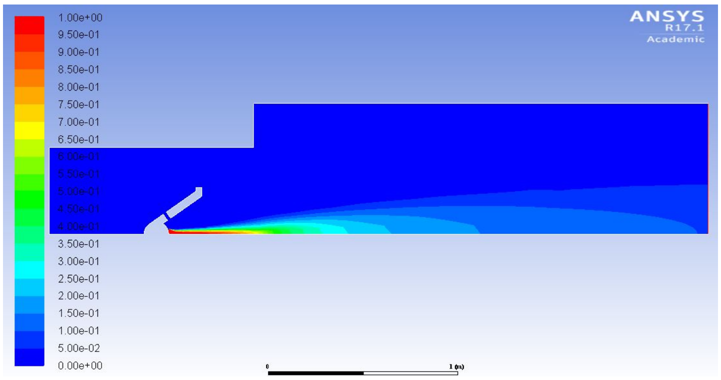


Figure E.3: Methane molar concentration over the length of the boiler, after the first design iteration.

## E.3. Second design iteration

For the third iteration, instead of adding more oxidizer to the center, the fuel injection point was split-up in 2 sections: One in the middle and one on the outer section of the burner, close to the boiler wall. The new geometry and the temperature contour resulting from this geometry is displayed in figure E.4. The geometry includes fuel injection in the middle section near the symmetry axis and at the outer part of the geometry, near the boiler wall. Here, the high-temperature zone is much more evenly spread over the length of the boiler.

Figure E.5 shows the concentration of methane at the boiler outlet of this iteration. Again, there is methane present, but it is reduced by an order of $10^3$. From this can be concluded that spreading the injection zones over the boiler radius improves the mixing.

With this design, the mixing of fuel and oxidizer is done almost sufficiently due to the combination of spreading the fuel, addition of zones where oxidizer flows through the geometry and the shape which should incur a recirculation zone. This geometry could provide difficulties in creating a stable flame at lower loads, however. This is taken care of in the final iteration.

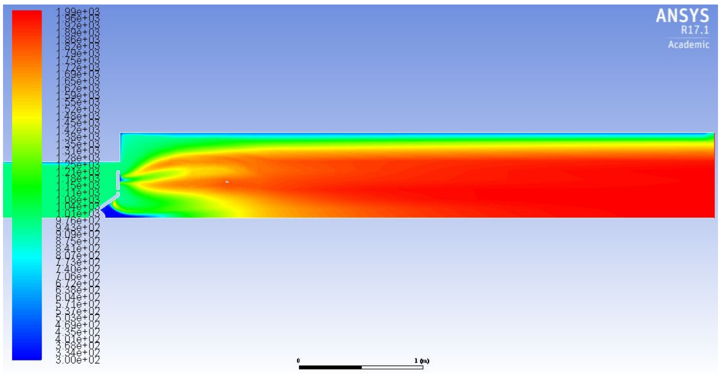


Figure E.4: Temperature contour of the third iteration. Temperatures are shown in K.

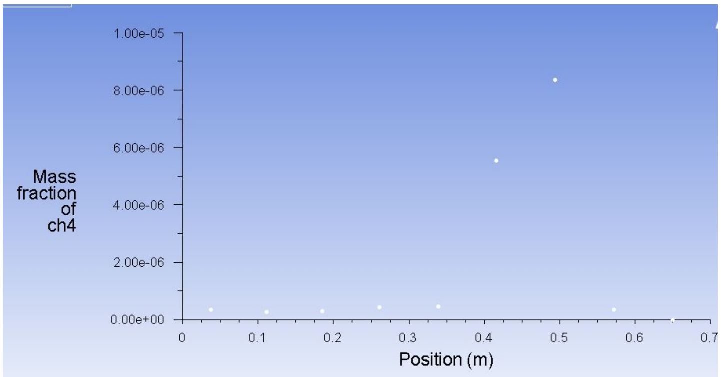


Figure E.5: Methane concentration at the boiler exhaust in the third iteration of the burner design.

## E.4. Final design iteration

The final iteration takes care of the lower load problem by setting the geometry off from the central axis. Injecting part of the fuel at the lower side of the burner should result in decent mixing, as the oxidizer mixes with the fuel both from below and above the injection point. This effect is shown in figure E.6. The geometry includes fuel injection in the middle section, in the middle of the burner and at the edge near the boiler wall. A high-temperature area occurs around the central axis close to the burner, unlike figure E.4, where this zone is further downstream of the burner.

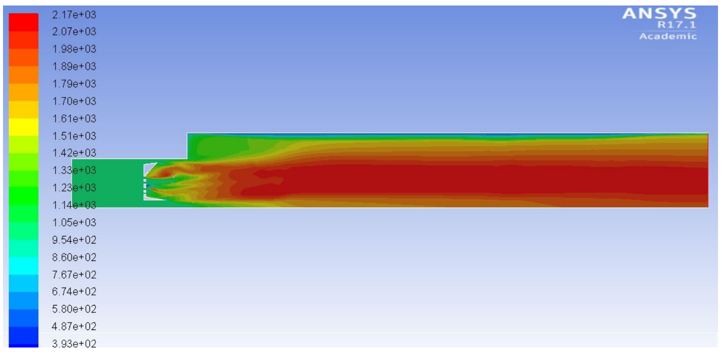


Figure E.6: Final design with the resulting temperature contour. Temperatures are shown in K.

The design features several slits over the height of the burner. These slits are present to improve mixing and to make sure the high-temperature areas do not touch the geometry. The size of these slits have been adjusted so each injection zone gets an amount of oxidizer which matches the fraction of fuel injected in that area. Further details on this are provided in chapter 6.

From the left figure of figure E.7 follows that the methane concentration for this geometry is reduced to 0 over the exhaust, so all fuel has reacted. The right figure shows the oxygen concentration over the exhaust. Oxygen is not distributed evenly, but an average of around 3 vol% can be distinguished, which is according to the amount of fuel supplied.

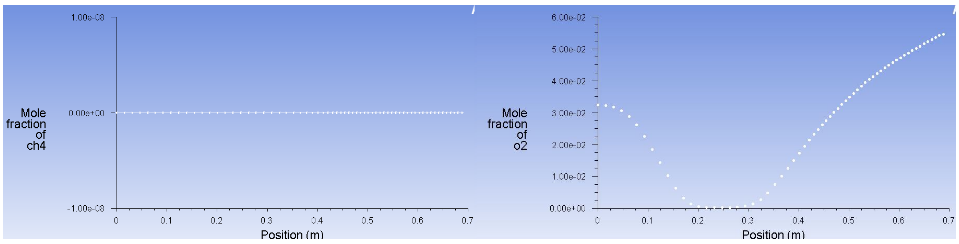


Figure E.7: Methane concentration at the boiler exhaust in the final iteration of the burner design.

# Bibliography


[1] ASME, *The World's first Gas Turbine Set – GT NEUCHÂTEL- A Historic Mechanical Engineering Landmark*, Tech. Rep. (Alstom, Baden (CH), 2007).

[2] P. Naggar, *What is the difference between a centrifugal compressor and a screw compressor?* (2017).

[3] M. Boyce, *Gas Turbine Engineering Handbook*, 4th ed. (Elsevier Ltd, 2012) pp. 3–15.

[4] E. A. Baskharone, *Principles of Turbomachinery in Air-Breathing Engines* (Cambridge University Press, Cambridge, 2006).

[5] O. A. El Masry, *ME332 Operation and Management of Power Plants: Cogeneration & Combined cycles,* (2015).

[6] K. Smołka and S. Dykas, *The performance of a steam-gas power unit of a velox-type cycle,* Journal of Power Technologies **97**, 343 (2017).

[7] A. H. Lefebvre and D. R. Ballal, *Gas Turbine Combustion: Alternative Fuels and Emissions* (CRS Press, 2010).

[8] I. Glassman, R. A. Yetter, and N. G. Glumac, *Combustion* (Academic Press, 2015).

[9] CBS, *Aardgas en electriciteit, gemiddelde prijzen van eindgebruikers,* (2018).

[10] G. Towler and R. Sinnott, *Chemical Engineering Design*, 2nd ed. (Elsevier, 2013) pp. 1047–1250.

[11] Viessmann Werke GmbH&Co KG, *Viessmann Vitomax 300-HS Type M95A Datasheet,* (2013).

[12] Nuon, *Tarieven energiebelasting 2017,* (2017).

[13] C. R. Branan, *Boilers,* in *Rules of Thumb for Chemical Engineers* (Elsevier, 2015) 4th ed., Chap. 21, pp. 371–386.

[14] C. L. Dym, *Engineering Design: A project-Based Introduction* (Wileys, 2013) pp. 16–24.

[15] H. R. Sankey, *Thomas Hawksley Lecture: Heat Engines,* Proceedings of the Institution of Mechanical Engineers **93**, 703 (1917).

[16] Innecs Power Systems BV, *Innecs PowerBurner specifications,* (2018).

[17] H. Saravanamuttoo, G. Roger, H. Cohen, and P. Straznicky, *Combined Cycle and Cogeneration Schemes,* in *Gas Turbine Theory* (Pearson Education Limited, Harlow, 2009) 6th ed., pp. 89–94.

[18] W. De Paepe, M. M. Carrerro, S. Bram, A. Parente, and F. Contino, *Advanced Humidified Gas Turbine Cycle Concepts Applied to Micro Gas Turbine Applications for Optimal Waste Heat Recovery,* Energy Procedia **105**, 1712 (2017).

[19] S. Dodo, S. Nakano, T. Inoue, M. Ichinose, M. Yagi, K. Tsubouchi, K. Yamaguchi, and Y. Hayasaka, *Development of an Advanced Microturbine System Using Humid Air Turbine Cycle,* in *Volume 6: Turbo Expo 2004* (ASME, 2004) pp. 167–174.

[20] M. S. Sahith, G. Giridhara, and R. S. Kumar, *Development and analysis of thermal barrier coatings on gas turbine blades - A Review,* Materials Today: Proceedings **5**, 2746 (2018).

[21] C. Soares, *Microturbines: Applications for Distributed Energy systems* (Elsevier, 2007) pp. 3–121.

[22] Y. S. Najjar, *Enhancement of performance of gas turbine engines by inlet air cooling and cogeneration system,* Applied Thermal Engineering **16**, 163 (1996).

[23] B. Dawoud, Y. H. Zurigat, and J. Bortmany, *Thermodynamic assessment of power requirements and impact of different gas-turbine inlet air cooling techniques at two different locations in Oman,* Applied Thermal Engineering **25**, 1579 (2005).

[24] J. Kaikko and J. Backman, *Technical and economic performance analysis for a microturbine in combined heat and power generation,* Energy **32**, 378 (2007).

[25] P. van der Meer, *Small gas turbine combined cycles: a system comparison of natural gas and biogas fired cogeneration plants*, Tech. Rep. (Delft University of Technology, 2011).

[26] H. Li, G. Haugen, M. Ditaranto, D. Berstad, and K. Jordal, *Impacts of exhaust gas recirculation (EGR) on the natural gas combined cycle integrated with chemical absorption CO2capture technology,* Energy Procedia **4**, 1411 (2011).

[27] F. Sander, R. Carroni, S. Rofka, and E. Benz, *Flue Gas Recirculation in a Gas Turbine: Impact on Performance and Operational Behavior,* in *Volume 4: Cycle Innovations; Fans and Blowers; Industrial and Cogeneration; Manufacturing Materials and Metallurgy; Marine; Oil and Gas Applications* (ASME, Vancouver, 2011) pp. 123–132.

[28] F. Guethe, M. d. l. Cruz Garcia, and A. Burdet, *Flue Gas Recirculation in Gas Turbine: Investigation of Combustion Reactivity and NOx emission,* Proceedings of ASME Turbo Expo 2009, June 8-12, 2009, Orlando, Florida, USA , 1 (2009).

[29] The Institute of Energy, R. M. Davies, D. P. Graham, and B. Strugnell, *EMISSION CHARACTERISTICS OF SUPPLEMENTARY FIRING WITH NATURAL GAS IN TURBINE EXHAUSTS,* The Institute of Energy's Second International Conference on Combustion & Emissions Control , 249 (1995).

[30] S. Dykas, K. Smolka, and S. Rulik, *A comparative analysis of the performance of a steam-gas system of a velox-type cycle and a gas-steam power station ...* in *4th International Conference on Contemporary Problems of Thermal Engineering*, September (2016).

[31] G. Towler and R. Sinnott, *Chemical Engineering Design*, 1975 (Elsevier, 2013) pp. 307–354.

[32] J. E. Edwards, *Design and Rating Shell and Tube Heat Exchangers,* Chemical Engineering , 30 (2008).

[33] J. W. Velthuijsen, *Vergelijking van gas- en elektriciteitsprijzen 2017*, Tech. Rep. (Ministerie van Economische Zaken en Klimaat, 2018).

[34] Eurostat, *Electricity Prices for non-household consumers,* (2018).

[35] Eurostat, *Gas Prices for non-household consumers,* (2018).

[36] J. P. Longwell, E. E. Frost, and M. A. Weiss, *Flame Stability in Bluff Body Recirculation Zones,* Journal of industrial and engineering chemistry **45**, 1629 (1953).

[37] A. K. Gupta, D. G. Lilley, and N. Syred, *Swirl Flows* (Abacus Press, Tunbridge Wells, 1984).

[38] INPROHEAT, *Duct Burners,* (2012).

[39] Weishaupt, *Ultra-low-NOx PLN-version gas burners (up to 2500 kW),* (2017).

[40] Mehldau und Steinfath Feuerungstechnik GmbH, *Duct Burners,* (2012).

[41] L. Ziani, A. Chaker, K. Chetehouna, A. Malek, and B. Mahmah, *Numerical simulations of non-premixed turbulent combustion of CH4–H2 mixtures using the PDF approach,* International Journal of Hydrogen Energy **38**, 8597 (2013).

[42] A. Frassoldati, S. Frigerio, E. Colombo, F. Inzoli, and T. Faravelli, *Determination of NOx emissions from strong swirling confined flames with an integrated CFD-based procedure,* Chemical Engineering Science **60**, 2851 (2005).

[43] T.-H. Shih, W. W. Liou, A. Shabbir, Z. Yang, and J. Zhu, *A new kt Eddy Viscosity Model for high-Reynolds number Turbulent Flows,* Compurers Fluids **24**, 227 (1995).

[44] A. Khelil, H. Naji, L. Loukarfi, and G. Mompean, *Prediction of a high swirled natural gas diffusion flame using a PDF model,* Fuel **88**, 374 (2009).

[45] A. C. Dimian, C. S. Bildea, and A. A. Kiss, *Computer Aided Chemical Engineering*, Vol. 35 (Elsevier B.V., 2014) pp. 717–755.

[46] Minder.nl, *Terugleververgoeding Zakelijke Energieleveranciers,* (2017).